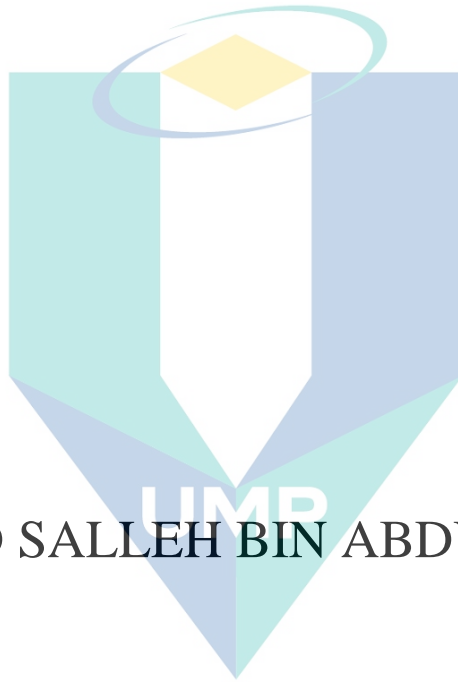


NANO METAL ADDITIVE ENHANCED
MAGNETORHEOLOGICAL FLUID
BASED ON RHEOLOGICAL AND
THERMOPHYSICAL PROPERTIES



MOHD SALLEH BIN ABDUL RAHIM

اونيورسيتي مليسيا قهغ

UNIVERSITI MALAYSIA PAHANG

DOCTOR OF PHILOSOPHY

UNIVERSITI MALAYSIA PAHANG

UNIVERSITI MALAYSIA PAHANG

DECLARATION OF THESIS AND COPYRIGHT

Author's Full Name : MOHD SALLEH BIN ABDUL RAHIM

Date of Birth : 02 DECEMBER 1986

Title : NANO METAL ADDITIVE ENHANCED
MAGNETORHEOLOGICAL FLUID BASED ON
RHEOLOGICAL AND THERMOPHYSICAL
PROPERTIES

Academic Session : SEM II 2019/2020

I declare that this thesis is classified as:

- CONFIDENTIAL (Contains confidential information under the Official Secret Act 1997)*
- RESTRICTED (Contains restricted information as specified by the organization where research was done)*
- OPEN ACCESS I agree that my thesis to be published as online open access (Full Text)

I acknowledge that Universiti Malaysia Pahang reserves the following rights:

1. The Thesis is the Property of Universiti Malaysia Pahang
2. The Library of Universiti Malaysia Pahang has the right to make copies of the thesis for the purpose of research only.
3. The Library has the right to make copies of the thesis for academic exchange.

Certified by:

(Student's Signature)

861202-33-5277

New IC/Passport Number
Date:

(Supervisor's Signature)

DR. IZWAN BIN ISMAIL

Name of Supervisor
Date:

NOTE : * If the thesis is CONFIDENTIAL or RESTRICTED, please attach a thesis declaration letter.

SUPERVISOR'S DECLARATION

I hereby declare that I have checked this thesis and in my opinion, this thesis is adequate in terms of scope and quality for the award of the degree of Doctor of Philosophy.

(Supervisor's Signature)

Full Name : DR. IZWAN BIN ISMAIL

Position : SENIOR LECTURER

Date :



UMP

اونيورسيتي ملايسيا قهغ

UNIVERSITI MALAYSIA PAHANG



STUDENT'S DECLARATION

I hereby declare that the work in this thesis is based on my original work except for quotations and citations which have been duly acknowledged. I also declare that it has not been previously or concurrently submitted for any other degree at Universiti Malaysia Pahang or any other institutions.

(Student's Signature)

Full Name : MOHD SALLEH BIN ABDUL RAHIM

ID Number : PMF14003

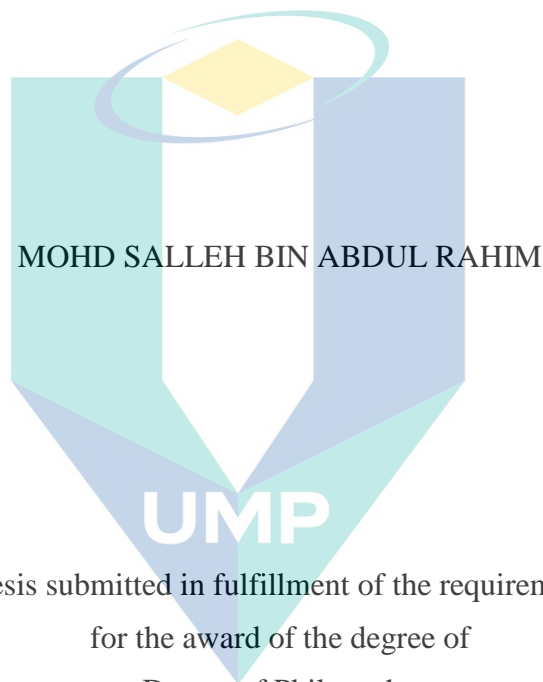
Date :

UMP

اونيورسيتي ملايسيا قهغ

UNIVERSITI MALAYSIA PAHANG

NANO METAL ADDITIVE ENHANCED
MAGNETORHEOLOGICAL FLUID
BASED ON RHEOLOGICAL AND
THERMOPHYSICAL PROPERTIES



Thesis submitted in fulfillment of the requirements
for the award of the degree of
Doctor of Philosophy

اونيورسيتي مليسيا قهغ

UNIVERSITI MALAYSIA PAHANG

Faculty of Manufacturing & Mechatronic Engineering Technology

UNIVERSITI MALAYSIA PAHANG

AUGUST 2020

ACKNOWLEDGEMENTS

Alhamdulillah, all praises to Allah for giving me the strength, capability, and perseverance to complete this thesis. It was all due to His blessings and guidance that I was able to finish this thesis. It would also not have been possible to complete this journey without the help and support of countless people around me throughout the years.

First and foremost, I would like to express my sincere gratitude to my supervisor, Dr. Izwan Ismail for his continuous support of my PhD study and related research, for his patience, motivation, and immense knowledge. His guidance helped me in all the time of research and writing of this thesis. I could not have imagined having a better advisor and mentor. He has been a true inspiration and has unfailingly led me through both good and tough times while completing my study. Thank you for not giving up on me and guiding me throughout this entire process.

My heartfelt thanks go to Assoc. Prof. Dr. Wan Azmi Wan Hamzah who has provided me with knowledge and guidance. He has given me unlimited access to his laboratory and equipments to conduct my research. Without his precious support, it would not have been possible for me to conduct this research. For me, he is a true example of how to become a great researcher. A special thanks to the staff and colleagues in Faculty of Manufacturing & Mechatronic Engineering Technology who have provided me with good amenities, technical, and financial assistance during my studies.

My highest appreciation extends to MyBrain15 for providing me with full scholarship to further my study, Yayasan Pahang Grant for the assistance of registration as a PhD student, and RAGS grant (RDU131409) for the allowance while I was the research assistant. These financial aids have facilitated me in paying the tuition fees, conference fees, purchasing of materials and instruments, travelling expenses, and much more.

I am extremely grateful to my loving parents, Dato' Indera Haji Abdul Rahim Mohd Ali and Datin Indera Hajah Yong Faridah Omar who have supported me in all these years. My mother always prays for my success while my father constantly pushed me forward and created positive pressure for me to finish my studies. I am also grateful to my siblings; Along, Angah, Acik, Kakteh, Imah, and Adik. They were incredibly accommodating from the very beginning by understanding my needs and commitments and I could not have asked for more than that.

Much love and recognition are due to my wife, Dr. Rosliza Mohd Salim, for supporting me over the years as I completed my study. She constantly provided unwavering support and sacrificed a lot to help me continue this journey. She is truly a devoted wife and my shining light, and I could not be who I am today without her. I also thank my children, Aisyah and Aiman as my source of motivation all this while. Their love and presence gave me the will and strength to complete this research and I truly hope that one day, this journey will be an inspiration to them.

ABSTRAK

Sifat terkawal reologi melalui medan magnet luar menjadikan bahan magnetoreologi berguna dalam banyak aplikasi seperti brek dan klac. Walau bagaimanapun, prestasi bendalir magnetoreologi terjejas oleh penjana haba disebabkan keadaan kendalian dan geseran zarah. Haba tersebut perlu dilesapkan dengan menghasilkan bendalir magnetoreologi dengan peningkatan keberaliran haba. Kajian ini bertujuan untuk membangunkan bendalir magnetoreologi stabil dengan penambahan logam nano untuk peningkatan keberaliran haba dan untuk menilai kesan penambahan logam nano dalam bendalir magnetoreologi ke atas gerak balas magnetoreologi. Bahan bagi kajian ini adalah bendalir magnetoreologi dengan penambahan logam nano dan silika berwasap. Bahan-bahan tersebut disediakan dengan kepekatan tertentu bagi komponen yang disarankan dengan penggunaan kaedah dua-langkah. 10 sampel telah dibangunkan di bawah tiga kategori iaitu MRF, MRF-Cu, dan MRF-Al. Eksperimen direka berasaskan model **D-optimal** tergabung untuk tatarajah campuran dengan sasaran untuk mengoptimalkan konfigurasi bendalir magnetoreologi bagi nisbah pemendapan tinggi dan keberaliran haba tinggi. Kajian dimulakan dengan siasatan nisbah pemendapan melalui kaedah pengamatan visual. Pemendapan sampel yang telah disintesis diperhatikan dengan memeriksa mendapan selama 28 hari. Kemudian, kajian diikuti dengan siasatan keberaliran haba dalam ketiadaan dan kehadiran medan magnet. Siasatan dijalankan oleh penganalisis sifat haba dan oleh sebuah modul berasaskan kaedah plat-panas terkawal. Modul telah dibangunkan disebabkan had penganalisis sifat haba dalam mengukur keberaliran haba di bawah medan magnet. Berikutnya, kajian dimuktamadkan dengan penentuan gerak balas magnetoreologi dalam kehadiran medan magnet. Gerak balas reologi dijalankan oleh reometer dan gerak balas pemagnetan dijalankan oleh magnetometer gegaran sampel. Hasil daripada setiap siasatan dibandingkan dengan MRF-132DG yang komersial. Daripada siasatan nisbah pemendapan, sampel dengan 5% aluminium merekodkan peningkatan tertinggi pada 14% disebabkan zarah aluminium yang berketumpatan rendah dan penambahan silika berwasap. Daripada siasatan keberaliran haba, keberaliran haba tertinggi tanpa medan magnet direkod pada $0.902 \text{ W/m}\cdot\text{K}$ daripada sampel yang mempunyai 5% tembaga disebabkan nilai keberaliran haba yang tinggi bagi bahan tembaga dan saiz zarah. Peningkatan daripada sampel tersebut adalah 153%. Dengan menggunakan modul yang dibangunkan, sampel menunjukkan peningkatan daripada $0.925 \text{ W/m}\cdot\text{K}$ tanpa medan magnet kepada $1.102 \text{ W/m}\cdot\text{K}$ dengan medan magnet. Hasil tersebut adalah daripada kesan pembentukan struktur berantai zarah apabila mengalami pemagnetan. Sampel tersebut mempunyai peningkatan tertinggi sebanyak 137% disebabkan kepekatan maksimum tembaga. Akhirnya, daripada penentuan gerak balas magnetoreologi, sampel dengan 5% tembaga menunjukkan tegasan ricih tertinggi (90.3 kPa) dalam kehadiran medan magnet dengan peningkatan 276% disebabkan bilangan rantai zarah yang lebih tinggi. Sampel merekodkan pemagnetan (30.98 emu) dan tepuan magnet tertinggi dengan peningkatan 71%. Penambahan zarah tembaga nano telah menghindarkan pembentukan zarah terkumpul daripada zarah magnetik dengan membentuk gemawan di sekeliling setiap zarah magnetik dan menyebabkan ikatan yang lebih kuat di antara zarah. Penemuan-penemuan dalam kerja ini memberi hasil yang menggalakkan dalam peningkatan sifat bendalir magnetoreologi. Dengan dengan tatarajah komponen bendalir magnetoreologi yang optimum, penambahan bahan tambah logam nano telah meningkatkan nisbah pemendapan, keberaliran haba, dan gerak balas magnetoreologi. Maka, bendalir magnetoreologi ditambah logam nano adalah sesuai digunakan untuk peningkatan prestasi bagi aplikasi bersuhu yang dinaikkan. Adalah dicadangkan bahawa kebolehpnyuraian semula oleh bendalir magnetoreologi ditambah logam nano dikaji pada masa akan datang.

ABSTRACT

Controllable rheological properties through external magnetic field makes magnetorheological materials useful in many applications such as brakes and clutches. However, the performance of magnetorheological fluid is affected by heat generation due to operating condition and particle friction. The heat must be dissipated by producing magnetorheological fluid with enhanced thermal conductivity. This study aims to develop stabilized nano metal added magnetorheological fluid for enhanced thermal conductivity and to evaluate the effects of nano metal added magnetorheological fluid on magnetorheological response. The materials for this study were the nano metal added magnetorheological fluid with fumed silica additive. The materials were prepared with specific concentration of suggested components by using two-step method. 10 samples were developed under three different categories namely MRF, MRF-Cu, and MRF-Al. Experiments were designed based on combined D-optimal model for mixture design with the target to optimize the configuration of magnetorheological fluid for high sedimentation ratio and high thermal conductivity. The study started with investigation of sedimentation ratio through visual observation method. Sedimentation of synthesized samples was observed by inspecting the sediment for 28 days. Then, the study followed with investigation of thermal conductivity in the absence and the presence of magnetic field. The investigation was conducted by thermal properties analyzer and by a module that was based on guarded hot-plate method. The module was developed due to the limitations of thermal properties analyzer in measuring thermal conductivity under magnetic field. Next, the study was finalized with determination of magnetorheological response in the presence of magnetic field. The rheological response was conducted by rheometer and the magnetization response was conducted by vibrating sample magnetometer. The results from every investigation were compared with the commercial MRF-132DG. From the sedimentation ratio investigation, the sample with 5% aluminum recorded the highest enhancement at 14% due to the low density of aluminum particles and the addition of fumed silica. From the thermal conductivity investigation, the highest thermal conductivity without magnetic field was recorded at 0.902 W/m·K from the sample with 5% copper due to the high thermal conductivity value of copper material and its particle size. The enhancement from the sample was 153%. By using the developed module, the sample showed an increase from 0.925 W/m·K without magnetic field to 1.102 W/m·K with magnetic field. The result was from the effect of the chain-like structures formed by the particles when experiencing magnetization. The sample has the highest enhancement at 137% due to the maximum concentration of copper. Finally, from the magnetorheological response determination, the sample with 5% copper demonstrated the highest shear stress (90.3 kPa) in the presence of magnetic field with 276% enhancement due to the higher number of particle chains. The sample recorded the highest magnetization (30.98 emu) and magnetic saturation with 71% enhancement. The addition of copper nanoparticles has avoided the formation of aggregates from magnetic particles by forming clouds around each magnetic particle and resulted to stronger bonds between the particles. The findings in this work provided encouraging results of enhanced magnetorheological fluid properties. With optimized configuration of magnetorheological fluid components, the addition of nano metal additive has enhanced the sedimentation ratio, thermal conductivity, and magnetorheological responses. Hence, nano metal added magnetorheological fluid is suitable to be used for improved performance in elevated temperature applications. It is recommended that redispersibility of the nano metal added magnetorheological fluid is investigated in the future.

TABLE OF CONTENT

DECLARATION

TITLE PAGE

ACKNOWLEDGEMENTS **ii**

ABSTRAK **iii**

ABSTRACT **iv**

TABLE OF CONTENT **v**

LIST OF TABLES **viii**

LIST OF FIGURES **ix**

LIST OF SYMBOLS **xii**

LIST OF ABBREVIATIONS **xiii**

CHAPTER 1 INTRODUCTION **1**

1.1 Background 1

1.2 Problem Statement 2

1.3 Objectives of Study 3

1.4 Scope of Study 4

1.5 Contribution of Study 5

1.6 Overview of Thesis 5

CHAPTER 2 LITERATURE REVIEW **7**

2.1 Introduction 7

2.2 MR Fluid and Its Applications 8

2.3 Challenges in MR Fluid 12

2.4 Development of MR Fluid 14

2.4.1 Magnetic Particles 15

2.4.2 Suitability of Carrier Fluid 17

| | | |
|---|---|-----------|
| 2.4.3 | Additives for Sedimentation Improvement | 18 |
| 2.4.4 | Synthesis of MR Fluid | 22 |
| 2.5 | Thermal Conductivity of MR Fluid | 24 |
| 2.5.1 | Factors Affecting Thermal Conductivity | 24 |
| 2.5.2 | Thermal Conductivity Models | 29 |
| 2.5.3 | Characterization of Thermal Conductivity | 30 |
| 2.6 | Magnetorheological Response of MR Fluid | 34 |
| 2.7 | Summary | 37 |
| CHAPTER 3 METHODOLOGY | | 39 |
| 3.1 | Introduction | 39 |
| 3.2 | Development of MR Fluid | 41 |
| 3.2.1 | Morphology of Particles | 42 |
| 3.2.2 | Experimental Design | 43 |
| 3.2.3 | Synthesis of MR Fluid | 47 |
| 3.3 | Investigation of Sedimentation Ratio | 49 |
| 3.4 | Investigation of Thermal Conductivity in the Absence of Magnetic Field | 50 |
| 3.5 | Investigation of Thermal Conductivity in the Presence of Magnetic Field | 53 |
| 3.5.1 | Operation of Guarded Hot-Plate Module | 56 |
| 3.5.2 | Validity and Reliability of Guarded Hot-Plate Module | 59 |
| 3.6 | Determination of Magnetorheological Response | 62 |
| 3.6.1 | Rheological Response | 62 |
| 3.6.2 | Magnetization Response | 64 |
| 3.7 | Summary | 65 |
| CHAPTER 4 RESULTS AND DISCUSSION | | 67 |
| 4.1 | Introduction | 67 |

| | | |
|-----------------------------|---|------------|
| 4.2 | Effect of Sedimentation Ratio | 68 |
| 4.3 | Thermal Conductivity Behavior in the Absence of Magnetic Field | 74 |
| 4.4 | Mixture Optimization by Design of Experiment | 79 |
| 4.5 | Thermal Conductivity Behavior in the Presence of Magnetic Field | 80 |
| 4.6 | Magnetorheological Response of MR Fluid | 83 |
| | 4.6.1 Rheological Response | 83 |
| | 4.6.2 Magnetization Response | 87 |
| 4.7 | Summary | 88 |
| CHAPTER 5 CONCLUSION | | 90 |
| 5.1 | Summary of Findings | 90 |
| 5.2 | Recommendation for Future Works | 91 |
| REFERENCES | | 92 |
| LIST OF PUBLICATIONS | | 104 |
| APPENDICES | | 105 |
| Appendix A | Thermal conductivity of MR fluid samples by thermal properties analyzer instrument | 106 |
| Appendix B | Viscosity and shear stress against shear rate of MRF-Cu samples | 107 |
| Appendix C | Thermal conductivity of MRF-Cu samples against MRF-132DG in the presence of magnetic field at higher temperatures | 111 |

LIST OF TABLES

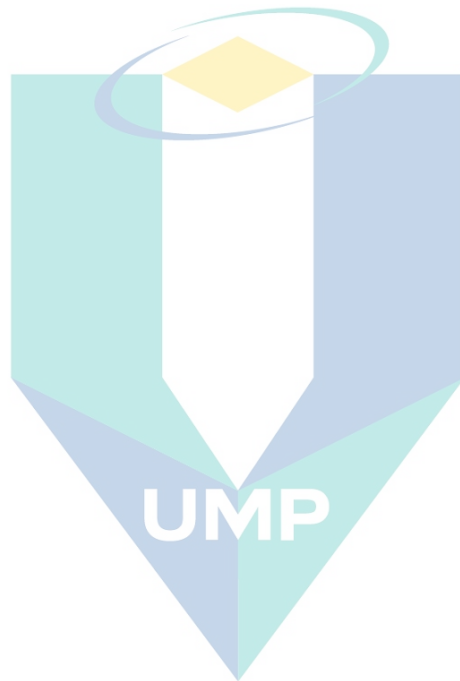
| | | |
|------------|---|----|
| Table 2.1 | Several applications of MR fluid in an elevated temperature environment | 11 |
| Table 2.2 | Different magnetic materials used in MR fluid | 16 |
| Table 2.3 | Several types of carrier fluid used in MR fluid | 17 |
| Table 2.4 | Several approaches to overcome the sedimentation problem in MR fluid | 19 |
| Table 2.5 | Thermophysical properties of metal particles at 300 K | 29 |
| Table 2.6 | Previous literature of using the THW method to measure thermal conductivity | 32 |
| Table 3.1 | Concentration range of MR fluid components | 44 |
| Table 3.2 | Composition of MR fluid samples | 45 |
| Table 3.3 | Optimization of MR fluid mixture with high sedimentation ratio and thermal conductivity properties | 46 |
| Table 3.4 | Composition of nano metal added MR fluid samples | 47 |
| Table 3.5 | Composition of MR fluid samples for sedimentation ratio analysis | 50 |
| Table 3.6 | Composition of MR fluid samples for thermal conductivity analysis in the absence of magnetic field | 51 |
| Table 3.7 | Determination of the required power for the GHP module | 59 |
| Table 3.8 | Thermal conductivity of MRF-132DG across different temperatures by thermal properties analyzer and GHP module | 60 |
| Table 3.9 | Actual thermal conductivity of MRF-132DG by GHP module | 60 |
| Table 3.10 | Thermal conductivity measurements of MRF-Cu5 sample in the absence of magnetic field | 61 |
| Table 4.1 | Sedimentation ratio of MR fluid samples | 69 |
| Table 4.2 | Apparent thermal conductivity of MR fluid samples in the absence of magnetic field | 75 |
| Table 4.3 | Optimal composition solutions by combined D-optimal model | 79 |
| Table 4.4 | Input parameters for thermal conductivity calculation in the presence of magnetic field | 81 |

LIST OF FIGURES

| | | |
|-------------|---|----|
| Figure 2.1 | Distribution of magnetic particles in MR fluid (a) without magnetic field and (b) with magnetic field | 8 |
| Figure 2.2 | General working modes of MR fluid. (a) valve mode; (b) direct-shear mode; (c) squeeze mode | 9 |
| Figure 2.3 | A schematic diagram of a large-scale semi-active damper | 10 |
| Figure 2.4 | Typical structure of a disc-type MR brake | 11 |
| Figure 2.5 | Schematic drawing of a two-way liquid cooling MR clutch | 12 |
| Figure 2.6 | Total torque vs coil current before and after long-term service in liquid cooling MR clutch | 13 |
| Figure 2.7 | Temperature effect on torque transmission in MR brake | 14 |
| Figure 2.8 | Schematic formulation of iron penta-carbonyl [Fe(CO) ₅] | 17 |
| Figure 2.9 | Magnetisation curves of bare CIP (solid line) and coated CIP (dashed line) particles | 20 |
| Figure 2.10 | Sedimentation ratio for MR fluid without SiO ₂ and MR fluid with SiO ₂ | 21 |
| Figure 2.11 | Shear stress as a function of shear rate of MR fluids with hydrophilic SiO ₂ (closed symbol) and MR fluids with hydrophobic SiO ₂ (open symbol) | 22 |
| Figure 2.12 | Schematic of MR effect comprising magnetic particles and nanoparticles | 22 |
| Figure 2.13 | Thermal conductivity vs magnetic field for different concentrations of CIP | 25 |
| Figure 2.14 | Thermal conductivity of MR fluids with different concentration of magnetic particles | 26 |
| Figure 2.15 | Effect of different particle sizes in Al ₂ O ₃ /water nanofluid to thermal conductivity ratio at 30 °C | 27 |
| Figure 2.16 | Temperature effect for 80 nm Cu nanofluid | 27 |
| Figure 2.17 | Thermal conductivity ratio of Cu and CNT nanofluids as a function of sedimentation time | 28 |
| Figure 2.18 | Schematic of a transient hot-wire (THW) experimental setup R_w | 31 |
| Figure 2.19 | Schematic of the transient hot-square measurement setup | 32 |
| Figure 2.20 | Schematic of the absolute technique for measuring thermal conductivity | 33 |
| Figure 2.21 | Shear viscosity versus shear rate of MR fluids | 35 |
| Figure 2.22 | Magnetic yield stress versus magnetic induction of MRF-J01 | 36 |
| Figure 2.23 | M-H curve for a ferromagnetic material | 37 |
| Figure 3.1 | Methodology flow chart | 40 |

| | | |
|-------------|---|----|
| Figure 3.2 | MR fluid components comprised of (a) CIP, (b), HO, (c) Cu, (d), Al, and (e) SiO ₂ | 42 |
| Figure 3.3 | SEM image of (a) CIP and FESEM images of (b) Cu, (c) Al, and (d) SiO ₂ | 43 |
| Figure 3.4 | Two-step method of synthesizing MR fluid | 48 |
| Figure 3.5 | Sedimentation measurement of MR fluid sample | 49 |
| Figure 3.6 | Thermal conductivity measurement of MR fluid with its (a) general setup, (b) close-up view in thermal bath, and (c) recorded thermal conductivity value by thermal properties analyzer instrument | 52 |
| Figure 3.7 | Actual and schematic diagrams of GHP module | 54 |
| Figure 3.8 | Measurement of magnetic flux density on magnet gap | 56 |
| Figure 3.9 | Arrangement of the GHP module operation | 56 |
| Figure 3.10 | Layers of material in PTFE cap | 57 |
| Figure 3.11 | Rheological characterization by (a) MCR302 rheometer and (b) its schematic figure | 63 |
| Figure 3.12 | Viscosity and shear stress of MR fluid sample | 64 |
| Figure 3.13 | Magnetic characterization by (a) Lakeshore 7404 vibrating sample magnetometer with (b) the close-up view of MR fluid sample location | 65 |
| Figure 4.1 | Sedimentation comparison of MR fluid samples taken when immediately after mixed and on day 14 th | 68 |
| Figure 4.2 | Sedimentation ratio of MR fluids at different concentration of CIP | 70 |
| Figure 4.3 | Sedimentation ratio of MR fluids at different concentration of SiO ₂ | 71 |
| Figure 4.4 | Sedimentation ratio of MR fluids at different concentration of Cu | 72 |
| Figure 4.5 | Sedimentation ratio of MR fluids at different concentration of Al | 73 |
| Figure 4.6 | Sedimentation ratio of MR fluids and the commercial MRF-132DG | 74 |
| Figure 4.7 | Comparison of experimental results with thermal conductivity models as a function of CIP concentration | 76 |
| Figure 4.8 | Thermal conductivity of MR fluids at different concentration of metal additive | 77 |
| Figure 4.9 | Thermal conductivity of MRF-Cu samples against MRF-132DG | 78 |
| Figure 4.10 | Thermal conductivity of MRF-Al samples against MRF-132DG | 79 |
| Figure 4.11 | Comparison of thermal conductivity by GHP module in the absence and the presence of magnetic field | 82 |
| Figure 4.12 | Thermal conductivity of MRF-Cu samples against MRF-132DG in the presence of magnetic field at 30 °C | 82 |
| Figure 4.13 | Shear viscosity of MRF-Cu samples under different shear rates in the absence of magnetic field | 84 |

| | | |
|-------------|---|----|
| Figure 4.14 | Shear viscosity of MRF-Cu samples under different shear rates in the presence of magnetic field | 84 |
| Figure 4.15 | Shear stress of MRF-Cu samples under different shear rates in the absence of magnetic field | 85 |
| Figure 4.16 | Shear stress of MRF-Cu samples under different magnetic fields | 86 |
| Figure 4.17 | Magnetic properties of MR fluid samples under different magnetic flux density | 87 |



اونيورسيتي ملايسيا قهغ

UNIVERSITI MALAYSIA PAHANG

LIST OF SYMBOLS

| | |
|------------|--|
| k | Thermal conductivity |
| α | Thermal diffusivity |
| ρ | Density |
| c_p | Specific heat |
| k_c | Thermal conductivity of carrier fluid |
| k_p | Thermal conductivity of solid particles |
| ϕ | Solid volume fraction |
| q | Heat flux per unit length |
| A | Cross-sectional area of the sample |
| ΔT | Temperature difference between thermocouples |
| τ | Yield stress |
| τ_o | Yield stress caused by an applied magnetic field |
| H | Magnetic field strength |
| η | Plastic viscosity |
| γ | Shear rate |
| τ_m | Magnetic yield stress |
| J | Current density |
| μ | Magnetic permeability |
| μ_r | Relative magnetic permeability |
| V | Voltage |
| I | Current |

اونیورسیتی ملیسیا قہق

UNIVERSITI MALAYSIA PAHANG

LIST OF ABBREVIATIONS

| | |
|---------------------|---|
| Al | Aluminum |
| CIP | Carbonyl iron particle |
| CNT | Carbon nanotubes |
| Cu | Copper |
| DOE | Design of experiment |
| ER | Electrorheological |
| Fe(CO) ₅ | Iron penta-carbonyl |
| FESEM | Field emission scanning electron microscopy |
| GHP | Guarded hot-plate |
| HO | Hydraulic oil |
| MR | Magnetorheological |
| NdFeB | Neodymium-Iron-Boron |
| PDMS | Polydimethylsiloxane |
| PMMA | Polymethyl methacrylate |
| PTFE | Polytetrafluoroethylene |
| SEM | Scanning electron microscopy |
| SiO ₂ | Fumed silica |
| THW | Transient hot-wire |
| vol% | Volume concentration percentage |
| VSM | Vibrating sample magnetometer |
| wt% | Weight concentration percentage |

اونيور سيني مليسيا قهغ

UNIVERSITI MALAYSIA PAHANG

CHAPTER 1

INTRODUCTION

1.1 Background

Magnetorheological (MR) fluids are smart materials made of magnetic particles in a carrier fluid that have the ability to rapidly change their flow characteristics due to viscosity increase in the presence of an applied magnetic field (Dorosti, Ghatee, & Norouzi, 2020). Generally, there are three components in MR fluid namely carrier fluid, magnetic particles, and additives (Wang et al., 2020). The composition of these three components determines the MR behavior of the MR fluid since the change of one of the components will lead to the change of fluid properties. Viscosity, shear stress, and magnetization are several of the major properties that determine the performance of MR fluid (Plachy et al., 2018).

MR fluid has unique characteristics such as adjustable viscosity, rapid response time, and high dynamic flow strength. These characteristics enable wide applications like shock absorbers, suspension systems, and optical finishing (Xiao, Lu, Zeng, & Bi, 2016). Another significant implementation of MR fluid is in the domain of thermal engineering where the insight of heat transfer is crucial especially in elevated temperature applications. Hence, many researchers (Diaz-Bleis, Vales-Pinzón, Freile-Peigrín, & Alvarado-Gil, 2014; Forero-Sandoval, Vega-Flick, Alvarado-Gil, & Medina-Esquivel, 2017; Yildirim & Genc, 2013) are beginning to pay major attention in developing MR fluid with improved heat transfer rate for elevated temperature applications.

Due to the direct relationship of heat transfer rate and thermal conductivity, enhancing the thermal conductivity of MR fluid will dissipate heat in MR devices at a higher rate (Maroofi & Hashemabadi, 2019). Several studies (Reinecke, Shan, Suabedissen, & Cherkasova, 2008; Yildirim & Genc, 2013) were found on the enhancement of thermal conductivity in MR fluid through different approaches. Reinecke et al. (2008) investigated the behavior of the thermal conductivity in MR fluid and found

that the thermal conductivity of the MR fluid increased by almost 100% in the presence of magnetic field. Later on, an experimental study was conducted by Yildirim and Genc (2013) to understand the thermal conductivity behavior of MR fluid in diverse temperature ranges. They found that the enhancement ratio of thermal conductivity for the MR fluid was approximately 134% in the presence of magnetic field for the temperature interval between 50-100 °C.

There were also other studies (Diaz-Bleis et al., 2014; Forero-Sandoval et al., 2017) conducted to enhance the thermal conductivity of MR fluid. Diaz-Bleis et al. (2014) focused on improving the thermal conductivity by varying the concentration of magnetic particles while Forero-Sandoval et al. (2017) worked on varying magnetic field strengths. However, there is a lack of interest on the effects of materials properties composition to the thermal conductivity of MR fluid. Therefore, significant research needs to be conducted to define the effects. By enhancing this property, their importance in heat dissipation of MR devices and the potential of new applications can be explored.

1.2 Problem Statement

Recent advancements in thermal systems require higher efficiencies of heat dissipation. MR devices that are designed for such application must adapt to this situation for technological sustainability. MR fluid in MR devices which is functioned as a damping material is subjected to heat generation due to the mutual frictions among the magnetic particles (Bossis, Kuzhir, Lopez-Lopez, Meunier, & Magnet, 2013). Besides frictions, there is another heat generation problem of MR fluid which is coming from outside of the device itself. For example, MR clutches and brakes operated at elevated temperature. MR clutches and brakes usually operate between 30-70 °C in ambient temperature (Wang, Hou, & Tian, 2013).

Another source of heat generation is magnetization induction by high current inside the magnetic coils. The generated heat increases the MR fluid temperature. The rising temperature of MR fluid has caused the reduction of shear stress either under the excitation of magnetic field or without the excitation of magnetic field (Wang, Zi, Zeng, Hou, & Meng, 2014). As a result, MR devices such as tunable dampers, clutches, and brakes experienced adverse effects on their performance. Oxidation of magnetic particles in the MR fluid is another problem that rose from the elevation of MR fluid temperature.

These situations, consequently affected the magnetization of the particles and performance of the MR devices (Wang, Zi, Zeng, Xie, & Hou, 2015).

Previous studies indicate enhancing the thermal conductivity property of MR fluid will help to solve such issue (Diaz-Bleis et al., 2014; Forero-Sandoval et al., 2017; Zhou, Zhang, & Shao, 2016). There are three methods to enhance the thermal conductivity of MR fluid. The first method is by increasing the magnetic field strength (Forero-Sandoval et al., 2017). However, this method often requires electrical current increment that leads to elevated temperature. The second method is by increasing the concentration of magnetic particles (Diaz-Bleis et al., 2014). This method might reduce the sedimentation ratio, but can be solved by having an appropriate composition of MR fluid components (Cheng, Zhang, Liu, Ma, & Wereley, 2016). Low sedimentation ratio caused the reduction of thermal conductivity of MR fluid (Jana, Salehi-Khojin, & Zhong, 2007).

The third method is by including high thermal conductivity metal nanoparticles as an additive to MR fluid. The nano-sized additive provides high specific surface area that encourages heat transfer of the particle-liquid interface (Xie et al., 2002). Cu and Al are the possible candidates of metal nanoparticles that possess high thermal conductivity property (Sattler, 2010). To address these issues, a study has to be carried systematically in achieving efficient heat dissipation system. Such research will provide new knowledge of synthesizing the stabilized MR fluid with nano metal additive.

1.3 Objectives of Study

There are three objectives involved in this study:

- i. To synthesize MR fluid with nano metal additive for high sedimentation ratio property
- ii. To analyze MR fluid with nano metal additive for enhanced thermophysical property in the absence and the presence of magnetic field
- iii. To evaluate the effects of MR fluid with nano metal additive on shear stress and magnetization responses in the presence of magnetic field

1.4 Scope of Study

The research objectives were set to provide new insight on enhancing the thermal conductivity of MR fluid at highest possible sedimentation ratio. This target was achieved through research scopes as given in the following list.

- i. Developing an optimal composition of MR fluid components for high sedimentation ratio and thermal conductivity. The MR fluid components involved were the carbonyl iron particles (CIP), hydraulic oil (HO), fumed silica (SiO_2), and metal additives. The metal additive is a major approach to achieve the enhanced thermal conductivity property, while the SiO_2 is to induce particle buoyancy for high sedimentation ratio. Based on the established theory of MR fluid mixture (Kumbhar, Patil, & Sawant, 2015; Yildirim & Genc, 2013), the two-step method was employed to synthesize the MR fluid. Volume concentration of each component was set at 20-40% for CIP, 50-75% for HO, 0-5% for SiO_2 , and 0-5% for metal additives.
- ii. Samples were subjected to a measurement of sedimentation ratio and to a measurement of thermal conductivity in the absence and the presence of magnetic field. The thermal conductivity was measured by using thermal properties analyzer instrument and guarded hot-plate (GHP) module. The GHP module involves a newly modified established method that allows measurement in the presence of magnetic field.
- iii. The GHP module was developed with a solid state heater as the heat source and two N52 grade permanent magnets as the magnetic field source. Thermal conductivity was measured in parallel direction with magnetic flux. Fourier's law of heat conduction equation was used to calculate the thermal conductivity.
- iv. Samples were subjected to a measurement of magnetorheological response in the presence of magnetic field. The rheological response was measured by using rotational rheometer while the magnetic response was measured by using vibrating sample magnetometer (VSM).
- v. Evaluating the effects of metal additive on rheological response by using rotational rheometer under $0.1\text{-}100\text{ s}^{-1}$ of shear rate and $0\text{-}0.4\text{ T}$ of magnetic field

strength; and magnetization response by VSM up to 1.2 T of magnetic field strength.

1.5 Contribution of Study

There are four main contributions involved in this study:

- i. A new formulation of MR fluid with nano metal additive was developed with high sedimentation ratio property and improved thermophysical (thermal conductivity) property. This contribution provides a potential candidate of MR material for elevated temperature applications such as MR brake and MR clutch.
- ii. An approach to identify the best composition of MR fluid components through the combined D-optimal design of experiment model was introduced. This approach is new in the field of MR fluid synthesization.
- iii. A new module to measure the thermal conductivity of MR fluid in the presence of magnetic field was developed. The module involves a newly modified established method that enables the study of thermal conductivity behavior of MR fluid in a parallel direction with the magnetic flux.
- iv. The MR response of the developed MR fluid with nano metal additive was enhanced with high shear stress and magnetization. This contribution provides a good platform for the MR fluid to become a new competitor in the market that offers good MR performance.

1.6 Overview of Thesis

This thesis is comprised of five chapters. It contains an introductory chapter which gives a brief overview of MR fluid. This chapter is also included with previous research findings, problem statement, objectives, scopes, and contributions. The second chapter is the literature review which presents the general overview of MR fluid, applications, and development of MR fluid. Previous literature on the thermal conductivity of MR fluid and the performance of MR fluid in terms of magnetorheological response are also discussed in this chapter.

The following chapter is the methodology that elaborates on the selection manner of component materials, characterization method, design of experiments (DOE) method, and synthesis process of nano metal added MR fluid. The method of measuring sedimentation ratio of MR fluid is also explained. Besides, this section describes the investigation of thermal conductivity in the absence and the presence of magnetic field, and the determination of magnetorheological response, namely rheological and magnetization responses.

Next, results and discussion is the chapter that discusses the effect of sedimentation ratio of nano metal added MR fluid. The chapter continues with the discussion on the thermal conductivity behavior of nano metal added MR fluid in the absence and the presence of magnetic field. The chapter closes with the results and discussion of magnetorheological response of nano metal added MR fluid.

Finally, the thesis ends with the conclusion chapter that summarizes the optimized MR fluid development with the inclusion of nano metal additive. This section also concludes on the findings of thermal conductivity property which is the integral part of this research. The magnetorheological performance of the optimized MR fluid in the presence of magnetic field is concluded.

اونيورسيتي ملايسيا قهغ

UNIVERSITI MALAYSIA PAHANG

CHAPTER 2

LITERATURE REVIEW

2.1 Introduction

This chapter presents the literature review on the study of nano metal additive enhanced MR fluid. The chapter starts with the definition of MR fluid and its characteristics. MR fluid is explained by its general working modes in MR devices. Several applications that are related to elevated temperature are included. The chapter continues with the development of MR fluid where each component that makes an MR fluid is explained in terms of its functions, materials, and characteristics. Studies of additives for improving sedimentation problem in MR fluid are considered. After that, two general methods of synthesis are presented.

Then, the chapter focuses on the thermal conductivity of MR fluid. In this section, several factors that affected the thermal conductivity of MR fluid are highlighted. The identified factors are essential to the current study in developing MR fluid for elevated temperature environment. The section continues with the most significant theoretical models in predicting the thermal conductivity of MR fluid. These models are used to compare with the experimental values of MR fluid samples. The last section is on the characterization of thermal conductivity property in which two methods of characterizing the property in the absence and the presence of magnetic field are presented.

Finally, the chapter ends with the MR response of MR fluid in the presence of magnetic field. The MR response of MR fluid is focused on the viscosity and shear stress properties under rheological response as well as magnetization and magnetic saturation properties under magnetization response. The chapter ends with the summary that highlights the scope and boundaries of the parameters to be used in this study.

2.2 MR Fluid and Its Applications

Magnetorheological fluid is a suspension that possesses alterable rheological properties in magnetic field presence (Acharya, Tak, Singh, & Kumar, 2020). Consisting of magnetic particles, the MR fluid has the ability to rapidly change its fluid flow in the presence of an applied magnetic field. The magnetic fluid is also termed as smart material because it can be handled easily and its rheological behaviors can be controlled reversibly by external magnetic field (Chae, Piao, Maity, & Choi, 2015).

As shown in Figure 2.1(a), the magnetic particles are randomly distributed in the absence of external magnetic field and the MR fluid behaves similarly to a Newtonian fluid (Cruze et al., 2018). When a certain amount of magnetic field strength is imposed, the magnetic particles formed a chain-like structure in the field direction as in Figure 2.1(b) due to an induced magnetic dipole-dipole interaction. Thus, during this process, their rheological properties like yield stress and apparent viscosity are being rapidly altered (Park, Fang, Zhang, & Choi, 2010).

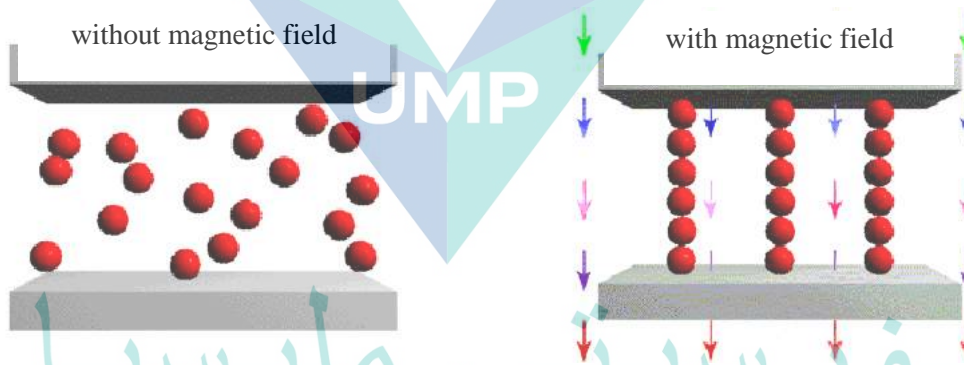


Figure 2.1 Distribution of magnetic particles in MR fluid (a) without magnetic field and (b) with magnetic field

Source: Cruze et al. (2018)

Jacob Rabinow worked for the US National Bureau of Standards and was the first who introduced MR fluid in the 1940s. At the same time, Willis Winslow was working on a competitive technology called electrorheological (ER) fluid. There are some similarities between the two different technologies. However, the ER fluid depends on an electrostatic field and requires thousands of volts and some milliamperes while the MR fluid depends on magnetic field and normally requires between 2 to 24 V and some amperes (Olabi & Grunwald, 2007).

As shown in Figure 2.2, MR fluid generally has three working modes namely valve mode, direct-shear mode, and squeeze mode (Yaojung, Quang-Anh, & Zhengyang, 2015). In all cases, MR fluid is placed between two surfaces or plates but having different working modes. These working modes are governed by the arrangement of magnets to generate magnetic fields.

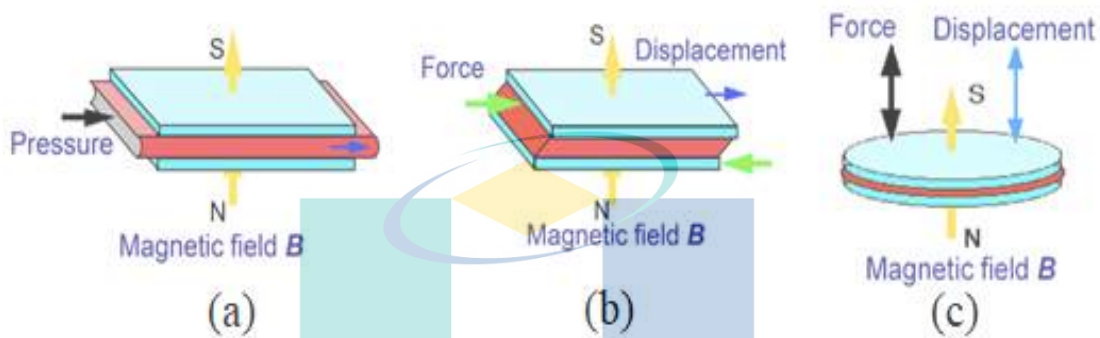


Figure 2.2 General working modes of MR fluid. (a) valve mode; (b) direct-shear mode; (c) squeeze mode

Source: Yaojung et al. (2015)

In the valve mode as in Figure 2.2 (a), a flow of MR fluid between stationary plates is created by pressure drop. The applied magnetic field is perpendicular to the direction of the flow to alter the viscosity of the fluid and therefore, the flow rate of the MR fluid can be controlled. Dampers and shock absorbers are the examples of a valve mode application. Figure 2.2 (b) shows the direct-shear mode in which one plate rotates or slides and the other is in stationary while the applied magnetic field is perpendicular to the plates. By this mode, the shear force from the moving plate can be characterized by shear properties and can be controlled by the magnetic field. The applications that operate by this mode are clutches and brakes. Meanwhile, in Figure 2.2 (c), the squeeze mode is when one of the plates is applied with force in the same direction with the magnetic field. With the distance between the two plates can be increased or decreased depending on the magnetic field strength, the MR fluid can be applied with static or dynamic loading. One of the applications that operate in squeeze mode is a vibration damper.

A linear MR damper in a seat suspension system for heavy-duty vehicles was developed and commercialized (Carlson, Catanzarite, & Clair, 1996). The controllable MR damper operated in valve mode has a magnetic coil integrated into the piston of the

damper that generates magnetic field and regulates the MR fluid flow resistance within the damper (Olabi & Grunwald, 2007). This application has become a catalyst for a variety of semi-active control schemes. A semi-active damper is considered to be more economical, compact, and functionally simple as they require only a variable damper and a few sensors to achieve adequate performance (Dixit & Buckner, 2005). A large-scale MR damper in building structures for seismic vibration control was also developed and a schematic diagram of the damper is shown in Figure 2.3 (Jiang & Christenson, 2012). The operation of the semi-active damper is based on abrupt changes in the rheological properties of MR suspension in magnetic field (Bica, Liu, & Choi, 2013).

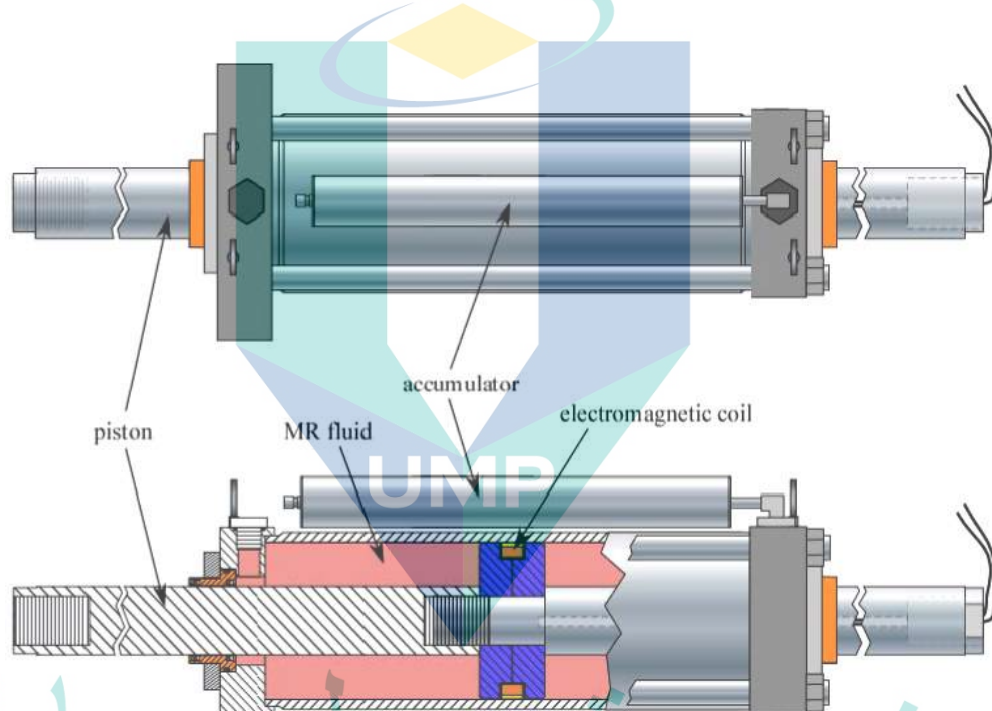


Figure 2.3 A schematic diagram of a large-scale semi-active damper

Source: Jiang and Christenson (2012)

In 2003, one of the first prototypes of MR brake operated in direct-shear mode was built with the focus is to design and fabricate a high-efficiency MR brake in terms of transmittable torque and long term stability (Li & Du, 2003). Figure 2.4 shows a typical structure of a disc-type MR brake (Farjoud, Vahdati, & Fah, 2008). The principle of MR brake is to acquire an accurate control of the braking torque with no moving parts by simply regulating the current in the coils. The magnetic flux path passes through the chassis and the rotating disk and the fluid is sheared between these elements. The braking force depends on the yield stress of the fluid and thus, making the system controllable (Spaggiari, 2012).

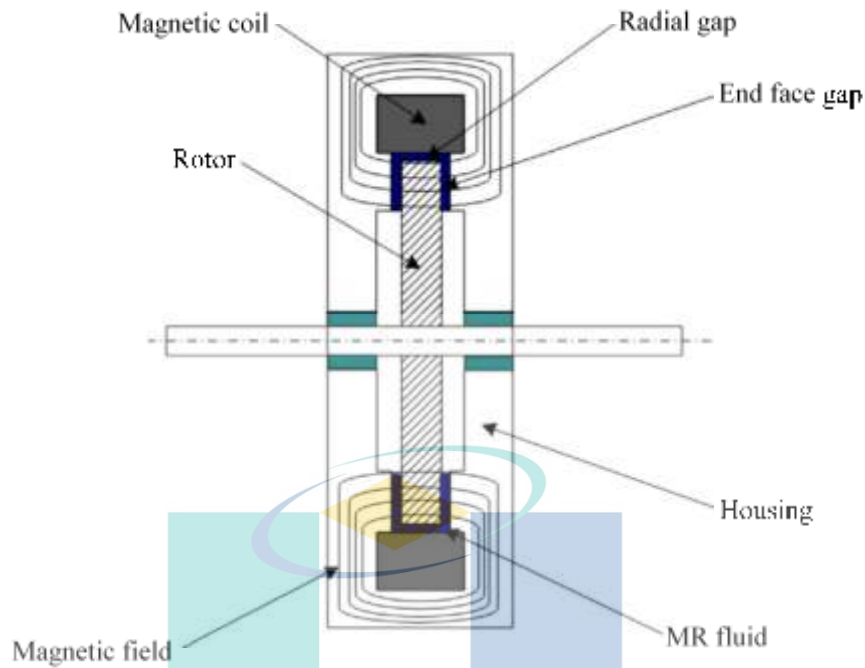


Figure 2.4 Typical structure of a disc-type MR brake
Source: Farjoud et al. (2008)

Another significant implementation of MR fluid is in the domain of thermal engineering where the insight of heat transfer is crucial especially in elevated temperature applications. Such an environment could negatively impact the performance, accuracy and service life of the applications (Wang, Zi, et al., 2015). Hence, many researchers are beginning to pay major attention in developing MR fluid applications concerning to elevated temperature. Several notable development works of such purpose were summarized in Table 2.1. The applications involved are such as damper, brake, transmission, and clutch.

Table 2.1 Several applications of MR fluid in an elevated temperature environment

| No. | Applications | References |
|-----|--------------|--|
| 1 | Damper | Dipalkumar and Upadhyay (2018); Yu, Du, and Sun (2015) |
| 2 | Brake | Patil, Powar, and Sawant (2016); Wang et al. (2013) |
| 3 | Transmission | Chen, Huang, Jian, and Ding (2015); Fei, Zuzhi, Xiangfan, Shuyou, and Hao (2018) |
| 4 | Clutch | Wang, Hou, Tian, Meng, and Taylor (2015); Wang, Zi, et al. (2015) |

One of the applications from Table 2.1 is a prototype of a high-torque MR brake with water cooling system (Wang et al., 2013). The water-cooling system was adopted to assist in heat dissipation from the working gap to the external components to maintain a high braking torque. Later in 2015, a two-way liquid cooling system in MR clutch has been developed and the design is shown in Figure 2.5 (Wang, Zi, et al., 2015). The cooling system was applied to enhance the heat dissipation ability by continuously carrying the friction heat from the clutch operation away from the working gap.

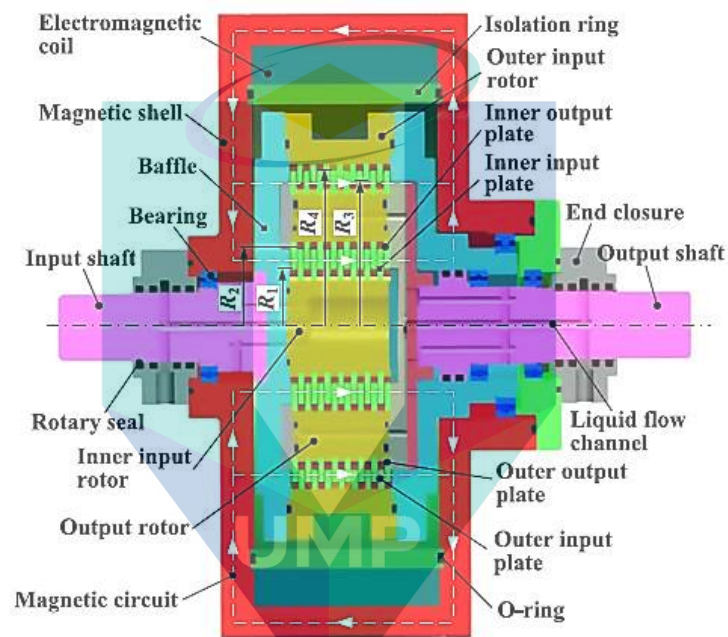


Figure 2.5 Schematic drawing of a two-way liquid cooling MR clutch

Source: Wang, Zi, et al. (2015)

2.3 Challenges in MR Fluid

MR fluid has attracted considerable attention in potential applications, thanks to its alterable and reversible rheological behaviors. Apparently, several applications operate between 30-70 °C in ambient temperature such as in vehicle clutches (Wang, Zi, et al., 2015) and brakes (Wang et al., 2013). An experiment to study the effects of elevated temperature on the performance of MR clutch was conducted (Wang, Zi, et al., 2015). Figure 2.6 shows the relationship of the clutch's total output torque and coil current. From the results, degradation of output torque after long-term service was obvious as coil current increased. The high current created elevated temperature condition for the MR

fluid and later oxidized its magnetic particles. Consequently, the polarisation ability of the particles decreased and affected the performance of the MR clutch.

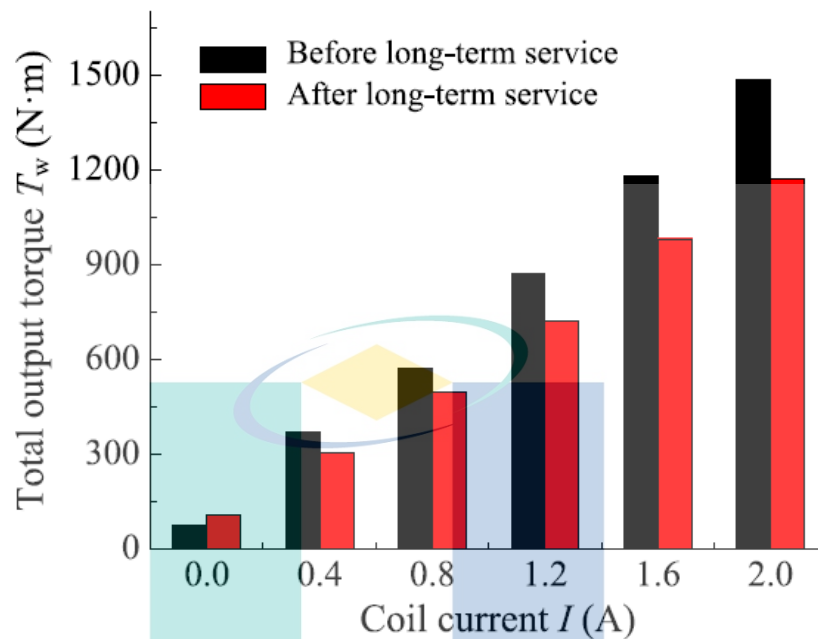


Figure 2.6 Total torque vs coil current before and after long-term service in liquid cooling MR clutch

Source: Wang, Zi, et al. (2015)

Typically, the operating temperature of an MR fluid is in the range of -40 to 150 °C (Patil et al., 2016). An experiment to study the impact of temperature increase on material characteristics of a commercial MR fluid has been conducted (Weiss & Duclos, 1994). It was discovered that as the temperature increased from -40 to 150 °C, the plastic viscosity and dynamic yield stress of the MR fluid decreased by 95% and 10%, respectively.

Another experiment by Wang et al. (2013) was conducted to observe the temperature effect on torque transmission in MR brake and the result is shown in Figure 2.7. The brake torque was in decreasing trend as the temperature was increased within the operating temperature of the MR fluid used. Once the temperature in MR brake went above the operating temperature of the MR fluid, the torque declined sharply. This is because the excessive temperature in the brake has caused evaporation of the MR fluid which led to severe wear of magnetic particles. Subsequently, the polarisation process of the particles was disrupted which in turn has decreased their magnetic shear stress and affected the brake torque.

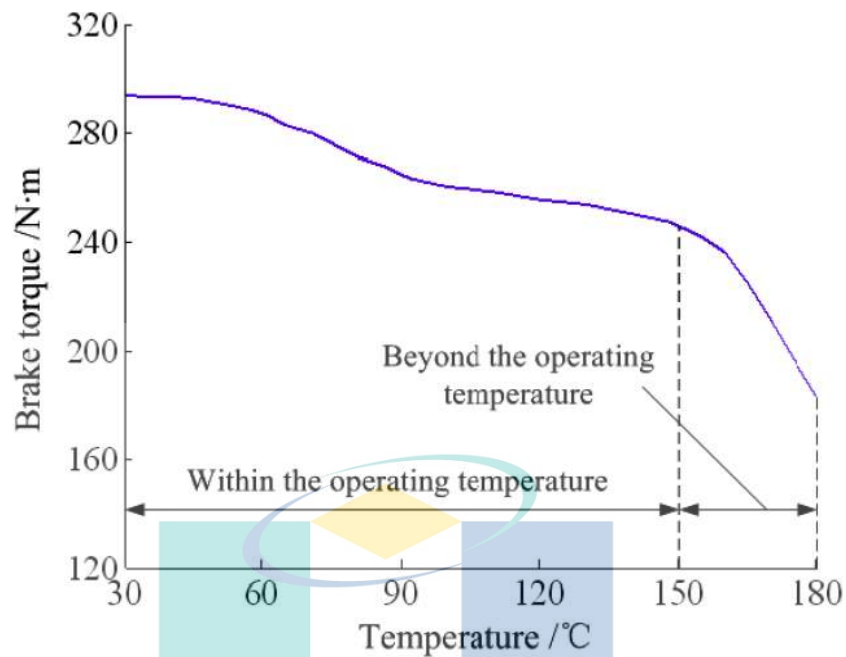


Figure 2.7 Temperature effect on torque transmission in MR brake

Source: Wang et al. (2013)

Regardless of high environmental temperature and excessive operating temperature, MR fluid also experiences internal heat from its own components. When magnetic field is applied, the magnetic particles form into a series of chain-like arrangement in parallel with the magnetic flux as in Figure 2.1(b). As it happened, mutual frictions occur between the magnetic particles in each layer and consequently lead to the increase of MR fluid temperature. This situation caused adverse effects to the performance of MR applications such as on the torque transmission performance in MR brake (Wang et al., 2013).

2.4 Development of MR Fluid

There are three components in MR fluid namely magnetic particles, carrier fluid, and additives (Wang et al., 2020). The magnetic particles are usually made of CIP, iron oxide, or iron/cobalt alloys to achieve high magnetic saturation (Xu, Gong, Xuan, Zhang, & Fan, 2011). The carrier fluid has the main function to carry magnetic particles as well as naturally provides lubrication and damping features. The additives are used to improve bonding stability between carrier fluid and magnetic particles, prevent settling of particles as well as increasing the wear resistance of the fluid. The composition of these three

components determines the MR behavior of the MR fluid since the change of one of the components leads to the change of fluid properties in the absence of magnetic field and MR properties in the presence of magnetic field.

2.4.1 Magnetic Particles

Magnetic particles act as the core component in an MR fluid in which their presence enables a transformation of the MR fluid from a liquid to near-solid state in the presence of magnetic field. Without an external magnetic field, there is no net magnetization exists within the magnetic particles and MR fluid behaves like a Newtonian fluid. When the external magnetic field is applied, the magnetic particles are polarised since each particle acquires an induced dipole.

The magnetic dipole-dipole attraction is occurred between the particles and they form a chain-like formation parallel to the applied field within milliseconds (Fonseca, Gonzalez, Restrepo, Parra, & Ortiz, 2016; Genc & Derin, 2014). This formation of structures is responsible for the development of yield stress and other related rheological properties (Gao, Lu, & Choi, 2018; Paval & Patil, 2015). The induced solid structures are able to produce a respectable yield shear stress, exceeding the requirement of several mechanical applications (40 kPa). Once the magnetic field is removed, the structures of the magnetic particles will break and MR fluid returns back to its original liquid state (Tao, 2001).

There are many types of magnetic particle previously used in MR fluids. Among them are CIP, Fe, and Fe_3O_4 as depicted in Table 2.2. The most common magnetic material used in the preparation of MR fluid is CIP (Phulé, 2001). From the table, CIP has the highest density among other magnetic materials. However, the large density mismatch between CIP and its carrier fluid would encourage rapid settling of the particles and resulted to sedimentation problem in MR fluid (Niu, Hu, Yan, Yang, & Zhang, 2018).

Table 2.2 Different magnetic materials used in MR fluid

| No. | Magnetic material | Density (g/cm ³) | Magnetic saturation (emu/g) | Concentration (vol%) | References |
|-----|--------------------------------|------------------------------|-----------------------------|----------------------|--|
| 1 | CIP | ~7.86 | ~200 | 10-40 | (Cvek, Mrlik, Moucka, & Sedlacik, 2018; Lee & Choi, 2018) |
| 2 | Fe | 7.5 | - | 5-40 | (Rodríguez-Arco, López-López, Kuzhir, & Durán, 2013; Susan-Resiga & Vékás, 2014) |
| 3 | Fe ₃ O ₄ | 5.17 | 82 | 10-40 | (Anupama, Kumaran, & Sahoo, 2018) |

Meanwhile, the maximum concentration of magnetic particles is typically at 40 vol%. Excessive concentration of magnetic particles would lead to high viscosity and affects the lubricity of an MR fluid (Anupama et al., 2018). It also encourages heat generation internally due to the more occurrence of mutual frictions among the magnetic particles (Bossis et al., 2013). This condition is not favourable for MR fluids in elevated temperature applications.

CIP is derived from the decomposition of iron penta-carbonyl [Fe(CO)₅]. The schematic formulation or decomposition of Fe(CO)₅ is shown in Figure 2.8 (Hajalilou, Mazlan, Lavvafi, & Shameli, 2016). CIP is a soft magnetic material which is a significant feature for the reversibility of MR effect. Due to this advantage, CIP can be easily magnetized and demagnetized and hence, the rheological characteristics of MR fluid can be reversibly controlled. CIP is also an excellent MR fluid magnetic particle which possesses essential properties for a strong and reproducible phase transition. These properties include high magnetic saturation close to 200 emu/g, low coercive force, and appropriate particle size for excellent MR behavior (Min, Choi, Kim, Park, & You, 2017; Piao, Chae, & Choi, 2015). Hence, CIP is adopted as the magnetic particles in this study.

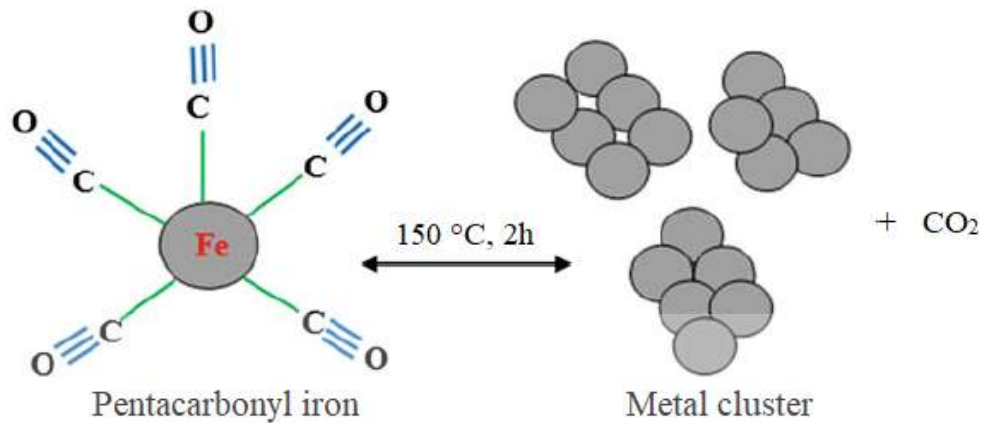


Figure 2.8 Schematic formulation of iron penta-carbonyl [Fe(CO)₅]

Source: Hajalilou et al., (2016)

2.4.2 Suitability of Carrier Fluid

The main component of an MR fluid is the carrier fluid which serves as a continuous insulating medium and has a strong impact on the MR fluid performance. Carrier fluid usually constitutes 50-80 vol% of an MR fluid (Kumbhar et al., 2015). The choice of carrier fluid is important as it determines the speed of response, the chemical, physical and thermal stability, and the lubricity of an MR fluid (Anupama et al., 2018).

As can be seen in Table 2.3, there are several types of carrier fluid with the most frequently used are mineral oil, silicone oil, and HO. These types of fluid have their own functionality and characteristics but they also shared similar qualities such as corrosion resistance, oxidation resistance, high viscosity index, good temperature stability, good heat-transfer characteristics, low vapour pressure, and high flash point (Sarkar & Hirani, 2015; Wereley et al., 2006). However, the mineral oil is neither biodegradable nor environmentally friendly, and hence, does not possess the main characteristics for a carrier fluid (Kumbhar et al., 2015).

Table 2.3 Several types of carrier fluid used in MR fluid

| No. | Carrier fluid | Disadvantages | References |
|-----|---------------|---------------------------------------|---|
| 1 | Mineral oil | Non-biodegradable Non-eco-friendly | Bateer et al. (2014); Shah, Choi, and Choi (2015) |
| 2 | Silicone oil | Expensive Limited resources | Ngatu and Wereley (2007); Prekas et al. (2013) |
| 3 | Hydraulic oil | - | Jiang, Zhang, Xuan, Guo, and Gong (2011); Wereley et al. (2006) |

The main characteristics for a carrier fluid are low freezing point and high boiling point, a suitable viscosity, non-flammable, and environmentally friendly (Wang et al., 2014). The low freezing point and high boiling point are mainly to extend the operating temperature range of MR fluid. Meanwhile, a suitable viscosity is more subjective as it should consider the inclusion of magnetic particles and additives. On one hand, the low viscosity of carrier fluid may improve the fluidity of MR fluid but it might lead to faster sedimentation of magnetic particles. On the other hand, the high viscosity may bring high sedimentation ratio of MR fluid but it can disrupt the movement of magnetic particles during magnetic field effect.

In the context of using MR fluid for elevated temperature applications, a suitable type of carrier fluid to withstand such temperature must be selected. Both silicone oil and HO have wide ranges of operating temperature and are very suitable for elevated temperature applications (Wang et al., 2014). The operating temperature range for a conventional HO is 4-84 °C (Dimitrakis & Profilet, 2008). The only significant differences are silicone oil is more expensive and more difficult to be obtained in the local market as compared to HO. Thus, HO is selected as the suitable carrier fluid in this study for elevated temperature environment.

2.4.3 Additives for Sedimentation Improvement

CIP is currently the most common magnetic particle used in the development of MR fluid preferably due to its soft magnetic property and high magnetic saturation. However, the large density mismatch between CIP and carrier fluid has encouraged a rapid settling of the particles and consequently affects the rheological behaviors and performance of MR fluid (Niu et al., 2018). This phenomenon has become a major drawback for MR fluid to be fully commercialized in technological and industrial applications.

Hence, researchers have opted to resolve this problem by introducing numerous solutions. According to the sedimentation law, it predicts that the sedimentation velocity reduced with the decrease in particle-fluid density mismatch (Wang et al., 2019). To overcome the sedimentation problem in MR fluid, previous studies as shown in Table 2.4 have undertaken several different approaches such as by introducing new candidates of magnetic particles other than the typical CIP and coating magnetic particles.

Table 2.4 Several approaches to overcome the sedimentation problem in MR fluid

| No. | Approach | References |
|-----|----------------------------------|---|
| 1 | Fe ₃ O ₄ | Anupama et al. (2018) |
| 2 | Fe | Rodríguez-Arco et al. (2013) |
| 3 | MgFe ₂ O ₄ | Wang, Ma, et al. (2017) |
| 4 | Particle coating | Cheng, Wang, Liu, and Wereley (2018); Mrlík et al. (2013) |
| 5 | Biopolymer | Bae et al. (2017); Kim et al. (2014) |
| 6 | Surfactant | Yang, Yan, Hu, and Ding (2016) |
| 7 | Filler | Esmailnezhad et al. (2017) Alves, Alcantara, and Neto (2009); Lim, Cho, Jang, and Choi (2004) |
| 8 | Nanoparticles | Hajalilou et al. (2016); Iglesias, López-López, Durán, González-Caballero, and Delgado (2012) |

The alternatives to CIP ($\sim 7.86 \text{ g/cm}^3$) such as Fe₃O₄ and MgFe₂O₄ offered much lower particle density at 5.17 g/cm^3 and 4.57 g/cm^3 , respectively. This approach has indeed reduced the sedimentation ratio of MR fluid due to the low density mismatch between the MgFe₂O₄ particles and the carrier fluid. Taking an example from the usage of MgFe₂O₄ in MR fluid (Wang, Ma, et al., 2017), the sedimentation ratio in 15 days was from 1 to 0.81 while the CIP-based MR fluid was from 1 to only 0.63. Despite this encouraging result, the magnetic saturation of MgFe₂O₄-based MR fluid was as low as 54.3 emu/g when CIP-based MR fluid was about 200 emu/g. This large reduction of approximately 70% of magnetic saturation would inhibit the optimum performance of MR fluid devices.

In the event of coating magnetic particles, a method of coating CIP with cholesteryl chloroformate was attempted to also reduce the large density mismatch between CIP and carrier fluid (Mrlík et al., 2013). The coated CIP improved the sedimentation ratio of MR fluids from 1 to 0.55 after 30 hours compared to bare CIP from 1 to 0.35. This result gave the indication that the modified CIP were more compatible with the carrier fluid used which led to a higher sedimentation ratio in the long term.

Additionally, Figure 2.9 shows the magnetization curves of bare CIP and the coated CIP. It was clear that the magnetic saturation of the coated CIP was only slightly lower when compared to bare CIP due to a compact layer of cholesteryl groups on the surface of the CIP. Yet, the magnetic properties, lubricity, and MR performance of MR fluid with coated magnetic particles are still compromised. The coating method is also a complicated process which involves surface treatment and addition of monomer or

stabilizer (Fang, Choi, & Seo, 2010; Fang, Liu, & Choi, 2009; Liu, Fang, & Choi, 2011; Park et al., 2010).

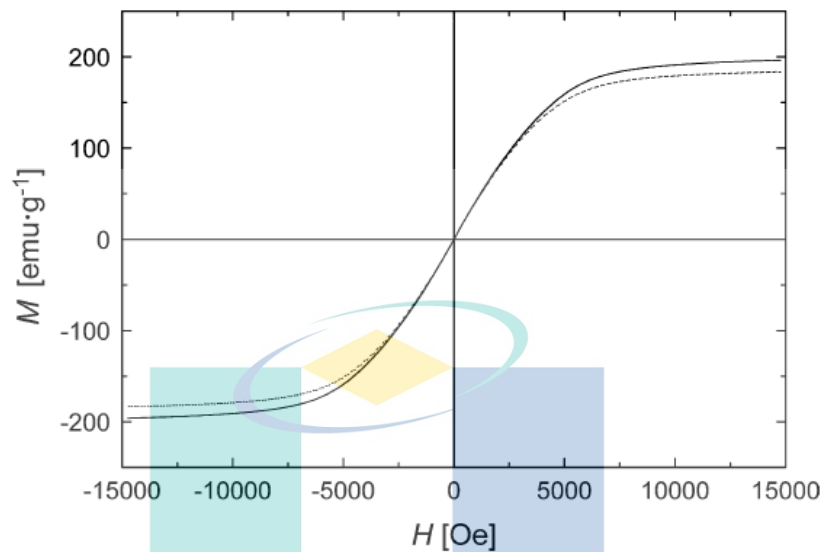


Figure 2.9 Magnetisation curves of bare CIP (solid line) and coated CIP (dashed line) particles

Source: Mrlík et al. (2013)

Nevertheless, the need for improvement in the sedimentation issue of MR fluid remains. Hence, another solution to mitigate the sedimentation problem is introduced by including a specific additive. As in Table 2.4, several other known additives used were biopolymers, surfactants, and fillers, but one of the most widely used and highly effective additive in MR fluid is SiO_2 . SiO_2 is a type of filler additive that can occupy the interspaces between CIP (Park & Choi, 2018). The relatively lower density than CIP and high specific surface area of SiO_2 provide buoyancy to the CIP.

An experiment was conducted to observe the effects of SiO_2 in MR fluid (Lim et al., 2004). With the addition of 3 wt% (particle weight fraction) of SiO_2 in mineral oil-based MR fluid, the sedimentation ratio has massively increased. As shown in Figure 2.10, the sedimentation ratio of MR fluid without SiO_2 was reduced from 1 to approximately 0.96 after 800 hours compared to MR fluid without SiO_2 from 1 to 0.75.

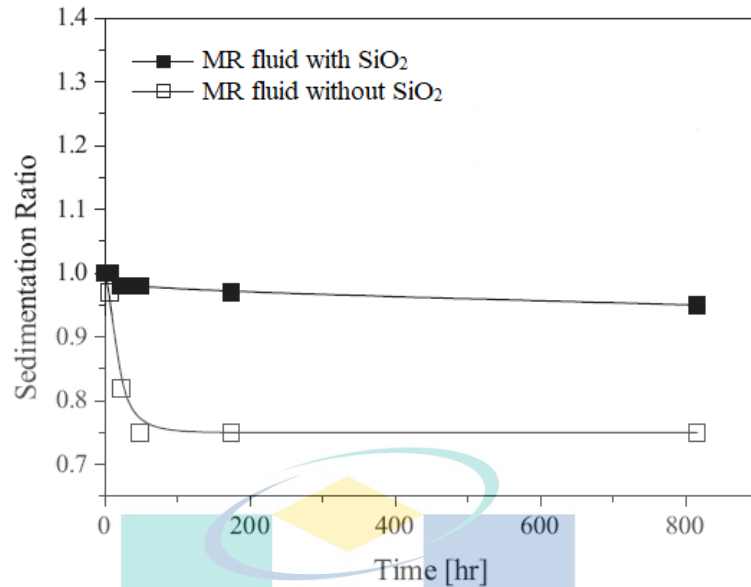


Figure 2.10 Sedimentation ratio for MR fluid without SiO₂ and MR fluid with SiO₂
 Source: Lim et al. (2004)

There are two different surface properties of SiO₂ namely hydrophobic and hydrophilic. As the names imply, nonpolar molecules that repel the water molecule are said to be hydrophobic while molecules forming ionic or hydrogen bond with the water molecule are said to be hydrophilic. From the fundamental point of view, it should be interesting to investigate the behavior of MR fluid stabilized by these two properties of SiO₂ particles.

An experiment to study the effects of hydrophobic SiO₂ and hydrophilic SiO₂ in MR fluid was conducted and there were a few interesting highlights (Alves et al., 2009). It was found that the MR fluids prepared with hydrophilic SiO₂ presented larger shear stress values than the MR fluids with hydrophobic SiO₂, as indicated in Figure 2.11. These results could be explained by the hydrophilic-hydrophilic interaction between the SiO₂ particles and the nonpolar carrier fluid which favours a more homogeneous distribution of them in the suspension. Therefore, hydrophilic SiO₂ is chosen for this study as the suitable additive in MR fluid for sedimentation improvement.

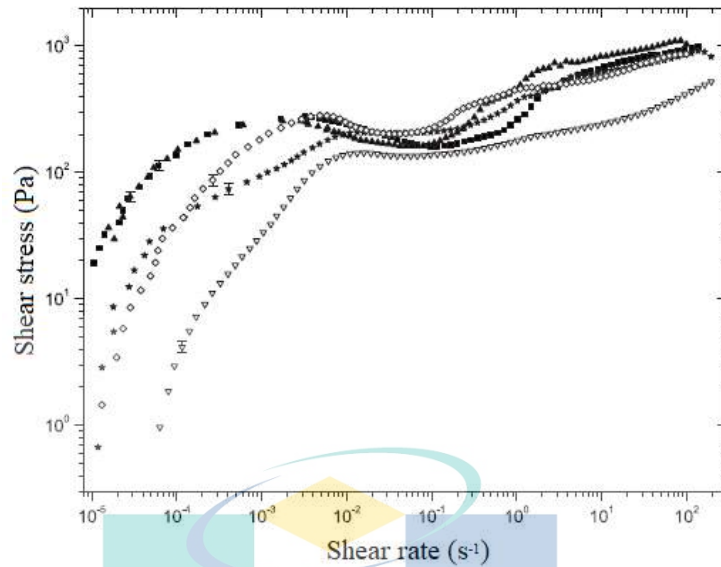


Figure 2.11 Shear stress as a function of shear rate of MR fluids with hydrophilic SiO₂ (closed symbol) and MR fluids with hydrophobic SiO₂ (open symbol)

Source: Alves et al. (2009)

Additionally, nanoparticles are also used to efficiently prevent sedimentation due to their low density property and large specific surface area. Figure 2.12 shows the schematic image of MR effect containing magnetic particles and nanoparticles (Hajalilou et al., 2016). It is clearly seen that the added nanoparticles dispersed in the cavities between the microparticles in the applied magnetic field.



Figure 2.12 Schematic of MR effect comprising magnetic particles and nanoparticles
Source: Hajalilou et al., (2016)

2.4.4 Synthesis of MR Fluid

MR fluid can be synthesized in a very simple procedure which is by mixing all the components altogether in one step. However, several factors need to be considered in the synthesis process such as the mixing order and the material and concentration of MR fluid components (Ashtiani, Hashemabadi, & Ghaffari, 2015). In an experimental study

concerning with the usage of SiO₂, MR fluid sample was initially prepared with CIP (79.36 wt%), mineral oil (19.84 wt%), and SiO₂ (0.80 wt%). The mixing order started with SiO₂ suspension by mixing 98 wt% of mineral oil with 2 wt% of SiO₂ until a homogenous gel was attained. The suspension was manually mixed with a round end stirring rod for about 30 minutes. Then, CIP was added into the SiO₂ suspension and mixed again for about 15 minutes. The MR fluid sample was kept at rest for 24 hours after homogenization to release the trapped air bubbles in the sample (Alves et al., 2009).

2.4.4.1 Two-step Method

Meanwhile, an alternative method of synthesis called the two-step method was also adopted in the making of MR fluid. Rather than mixing the components altogether in one step, this method involves two steps to prepare the MR fluid. The first step includes preparation of particles and the second step is comprising the dispersion of particles into carrier fluid by ultrasonication (Kumar & Subudhi, 2018). In another experiment which is also related to the usage of SiO₂, the researchers highlighted on the mixing order of the MR fluid components by using the two-step method. CIP (10 vol%) were firstly mixed with SiO₂ and the combined particles were later added into silicone oil (50-99 vol%). The mixture was manually stirred and put into an ultrasonic bath. The ultrasonic bath is very useful in cleaning and degassing of liquids. Then, the mixture was again stirred by hand and immersed in an ultrasonic homogenizer. The instrument was used to ensure the homogeneity of the mixture sample (López-López, de Vicente, González-Caballero, & Durán, 2005).

Besides MR fluid, the two-step method was also broadly used by researchers in the making of nanofluids (Bagheli, Fadafan, Orimi, & Ghaemi, 2015; Goharkhah, Salarian, Ashjaee, & Shahabadi, 2015; Lee et al., 2020). In an experiment of a nanofluid utilized with metal nanoparticles, Cu nanoparticles (1.0-3.8 wt%) were mixed with ethylene glycol by using the two-step method. The Cu nanofluid was stirred by a magnetic stirrer for 20 minutes in order to disperse the particles and stabilize the fluid. An ultrasonic vibrator was then used to break down any agglomerates of the Cu particles and the ultrasonic times were varied from 15 to 75 minutes. It is worth mentioning that the Brownian motion of the 50 nm Cu particles intensified and the aggregates were broken down when subjected to longer ultrasonic time. This result led to low flow

resistance and thereby contributed to low viscosity in the nanofluid (Li, Li, Zhong, Zhai, & Li, 2019). Hence, the two-step method is adopted in the current study for the making of MR fluids.

2.5 Thermal Conductivity of MR Fluid

There are challenges for MR fluid to be applied in elevated temperature applications. The challenges are because of high environmental temperature, excessive operating temperature, and high internal heat produced from MR fluid components. One of the ways to overcome these challenges is by increasing the heat transfer rate of MR fluid. Heat transfer in a medium can occur by conduction, convection, and radiation (Varley, 2003). The highest heat transfer rate is occurred through conduction. The rate of heat transfer by conduction is given by Fourier's law of heat conduction as shown in Eq. (2.1) (Zhao, Qian, Gu, Jajja, & Yang, 2016):

$$k = \frac{Ql}{A\Delta T} \quad 2.1$$

where k is thermal conductivity, Q is heat flow rate, l is distance of the medium, A is surface area of the medium, and ΔT is temperature difference. From Eq. (2.1), it is clear that there is a direct relationship of heat transfer rate and thermal conductivity. Hence, the heat transfer rate of MR fluid can be increased by increasing the thermal conductivity of the MR fluid.

2.5.1 Factors Affecting Thermal Conductivity

To improve the thermal conductivity of MR fluid, there are several factors worth to be looked at and part of them have been discussed by previous researchers. As shown in Figure 2.13, the thermal conductivity of an MR fluid with 20 vol% CIP is increased from approximately 0.76-1.05 W/m·K with the magnetic flux density of 50 Gauss (0.005 Tesla) and 150 Gauss (0.015 Tesla), respectively (Forero-Sandoval et al., 2017).

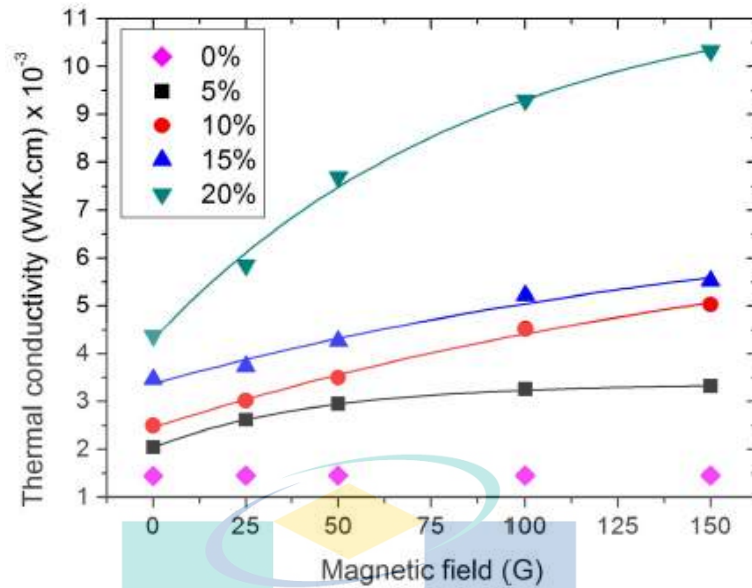


Figure 2.13 Thermal conductivity vs magnetic field for different concentrations of CIP
Source: Forero-Sandoval et al. (2017)

The finding was also in parallel with other experimental work in which the thermal conductivity of MR fluid increased along with increasing magnetic field (Yildirim & Genc, 2013). The thermal conductivity enhancement ratio of MR fluid was increased from 10% at 0.0024 Tesla to 18% at 0.015 Tesla. Hence, thermal conductivity can be enhanced when MR fluid is subjected to a higher magnetic field. This behavior is attributed to the formation of magnetic particles into chain-like structures when subjected to magnetic field, which provides high conductivity heat transfer paths (Mistik, Shah, Hadimani, & Siores, 2012).

In the meantime, the thermal conductivity of MR fluid is increased when the direction of magnetic flux is in parallel with the thermal gradient. An experiment was conducted to investigate the effects of magnetic flux direction with thermal gradient (Reinecke et al., 2008). When subjected to magnetic field, it was found that the thermal conductivity enhancement of the MR fluid were approximately 100% when the magnetic flux direction was parallel with thermal gradient due to the better heat conduction from the formation of chains of the magnetic particles.

Meanwhile, the concentration of magnetic particles also affects the thermal conductivity of MR fluid. Yildirim and Genc (2013) conducted an experiment to study the concentration effect of iron particles to thermal conductivity in MR fluid. As shown in Figure 2.14, they achieved an increment from approximately 0.49-0.61 W/m·K by

increasing the concentration of iron particles from 5-40 vol% under constant magnetic field. The number and size of the chain structures of iron induced by the field were numerous and larger as the concentration of iron particles increased, hence provided multiple heat conduction paths which resulted to higher thermal conductivity (Forero-Sandoval et al., 2017).

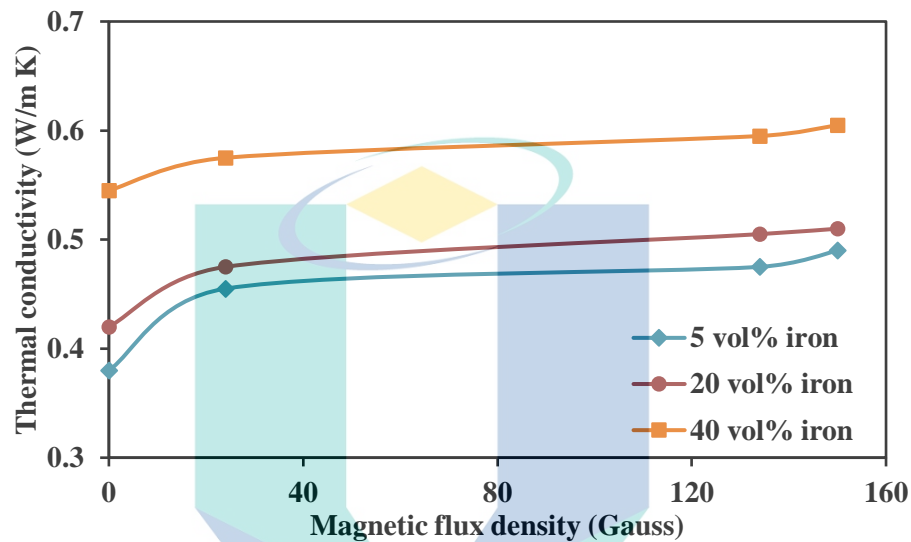


Figure 2.14 Thermal conductivity of MR fluids with different concentration of magnetic particles

Source: Yildirim and Genc (2013)

Furthermore, an investigation to study the effect of particle size in Al_2O_3 nanofluid was conducted (Chon, Kihm, Lee, & Choi, 2005). It was found that the thermal conductivity of the nanofluid was increased by up to 5% and 10% with 150 nm and 47 nm of Al_2O_3 nanoparticles, respectively. The findings were in agreement with another study that used 20 nm, 50 nm, and 100 nm of Al_2O_3 nanoparticles (Teng, Hung, Teng, Mo, & Hsu, 2010).

The result of the particle size effect to thermal conductivity at 30 °C can be observed in Figure 2.15. It can be seen that the thermal conductivity ratio (the ratio of nanofluid thermal conductivity to carrier fluid thermal conductivity) across all weight fractions became higher as the particle size were smaller and the reason of this enhancement was due to the smaller particle size has association with larger surface area of solid-liquid interface.

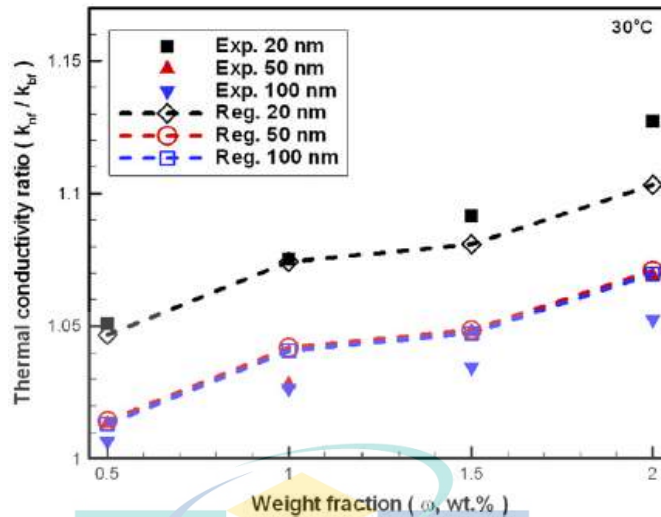


Figure 2.15 Effect of different particle sizes in $\text{Al}_2\text{O}_3/\text{water}$ nanofluid to thermal conductivity ratio at $30\text{ }^\circ\text{C}$

Source: Teng et al. (2010)

An experiment was conducted to observe the effects of using nanoparticles at elevated temperature (Patel, Sundararajan, & Das, 2010). From Figure 2.16, the thermal conductivity enhancement for 3 vol% Cu nanofluid was 21% at $20\text{ }^\circ\text{C}$ but reached up to 33% at $50\text{ }^\circ\text{C}$. Due to their nano-sized form, the 80 nm Cu particles were always in Brownian motion. As the temperature increased, the Brownian motion velocity of the Cu particles intensified. The particles' increased velocity created additional paths for heat flow in the carrier fluid and thus, enhancing the thermal conductivity of the nanofluid.

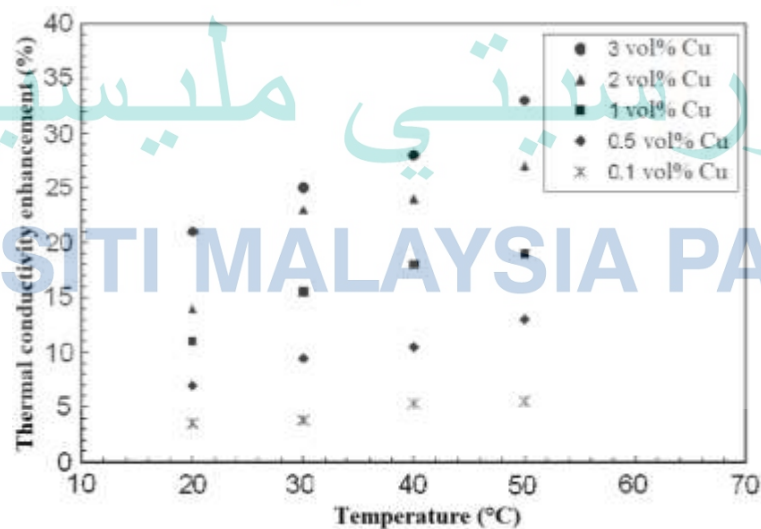


Figure 2.16 Temperature effect for 80 nm Cu nanofluid

Source: Patel et al. (2010)

Another vital factor that affect the thermal conductivity of MR fluid is the sedimentation of magnetic particles. Due to the large mismatch of density between magnetic particles and carrier fluid, the micron-sized particles tend to be quickly settled in the medium as a result of gravitational force (Niu et al., 2018). The thermal conductivity of Cu nanofluid and carbon nanotubes (CNT) nanofluid were experimentally measured in every 5-min interval for 25 minutes without any disturbance to the samples. As shown in Figure 2.17, the thermal conductivity ratio of Cu and CNT nanofluids were dramatically reduced from approximately 1.75 to 1.05 and from 1.3 to 1.025, respectively. It is believed that sedimentation of the particles was the main cause of the reduction of thermal conductivity with respect to time because the particles were not in motion (Jana et al., 2007).

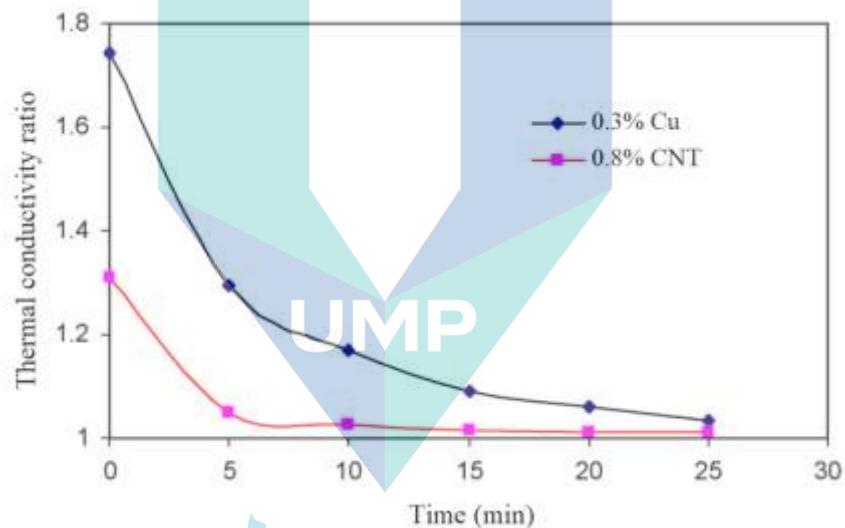


Figure 2.17 Thermal conductivity ratio of Cu and CNT nanofluids as a function of sedimentation time

Source: Jana et al. (2007)

2.5.1.1 Metal Additives

High thermal conductivity is known to be one of the outstanding characteristics of metals and by including metal particles as an additive, it could have a massive effect to the thermal conductivity of MR fluid (Lin, Jia, Alva, & Fang, 2018). The typical thermophysical properties of several metal particles are tabulated in Table 2.5. It can be observed that Cu particle has the highest thermal conductivity among other particles. Meanwhile, Al particle has the lowest density and the highest specific heat.

Table 2.5 Thermophysical properties of metal particles at 300 K

| Particles | Thermal conductivity, k (W/m·K) | Density, ρ (g/cm ³) | Specific heat, c_p (kJ/kg K) |
|--------------------------------|--------------------------------------|---|-----------------------------------|
| CuO | 17 | 6.50 | 0.525 |
| Al ₂ O ₃ | 39 | 3.97 | 0.775 |
| Al | 237 | 2.70 | 0.877 |
| Cu | 401 | 8.93 | 0.385 |

Source: Sattler (2010)

The enhancement of thermal conductivity has been reported in the area of nanofluids with metal and metal oxide particles. At 50 °C and 3 vol% of concentration, Al and Al₂O₃ nanoparticles enhanced thermal conductivity by 27% and 17%, respectively (Patel et al., 2010). The difference of thermal conductivity enhancement between these nanoparticles was due to the fact that metal particle is a material with higher thermal conductivity value compared to a metal oxide particle.

Another encouraging result was obtained from the usage of Cu nanoparticles (Eastman, Choi, Li, Yu, & Thompson, 2001). It was shown that Cu nanoparticles increased the thermal conductivity ratio up to 40% with only about 0.3 vol% of concentration. Such a small amount of concentration from the particles can massively enhance the thermal conductivity as Cu material is known to be among the highest thermal conductivity material and is widely used in heat transfer applications. Besides, Cu material is non-toxic, chemically stable and easily available (Li et al., 2019).

2.5.2 Thermal Conductivity Models

Thermal conductivity property of MR fluid can either be calculated theoretically or experimentally. This section presented the most significant theoretical models from the practical point of view to predicting the thermal conductivity of MR fluid. It is mutually agreed among the field of study that the earliest model and commonly used to calculate the thermal conductivity of a solid suspension is the Maxwell model (Maxwell, 1904).

Maxwell was the first to propose a model to determine the apparent thermal conductivity of suspensions containing solid particles. Reinecke et al. (2008) and Heine, de Vicente, and Klingenberg (2006) adopted the Maxwell model which describes as

statistically homogeneous liquid-solid suspensions with randomly dispersed, uniformly sized and non-interacting spherical particles. This model is given as in Eq. (2.2) (Reinecke et al., 2008):

$$k = k_c \frac{k_p + 2k_c + 2\varphi(k_p - k_c)}{k_p + 2k_c - \varphi(k_p - k_c)} \quad 2.2$$

where k is apparent thermal conductivity of solid suspension, k_c is thermal conductivity of carrier fluid, k_p is thermal conductivity of solid particles, and φ is particle volume fraction.

The Maxwell model satisfactorily predicts for spherical-shaped particles at low particle volume fractions and in ambient conditions (Das, 2017). For larger volume fractions, the thermal conductivity is more preferred to be modelled by using Bruggeman (1935), also adopted by Reinecke et al. (2008). This model accounts for the thermal interaction between neighboring spheres as in Eq. (2.3):

$$\left(\frac{k - k_p}{k_c - k_p}\right) \left(\frac{k_c}{k}\right)^{\frac{1}{3}} = 1 - \varphi \quad 2.3$$

2.5.3 Characterization of Thermal Conductivity

There are several ways to measure the thermal conductivity property of a suspension including the MR fluid. The most widely used is the THW method and the schematic of the THW setup is shown in Figure 2.18. THW method has the capacity to eliminate error due to natural convection besides getting faster results compared to other methods. Typically, the THW instrument has a metallic hot-wire probe to be inserted into the MR fluid. The hot-wire probe is functioned both as a heater and a thermometer. A constant current is supplied to the wire to raise its temperature. The heat dissipated in the wire increases the temperature of the probe and the MR fluid sample. This temperature rise depends on the thermal conductivity of the sample (Paul, Chopkar, Manna, & Das, 2010).

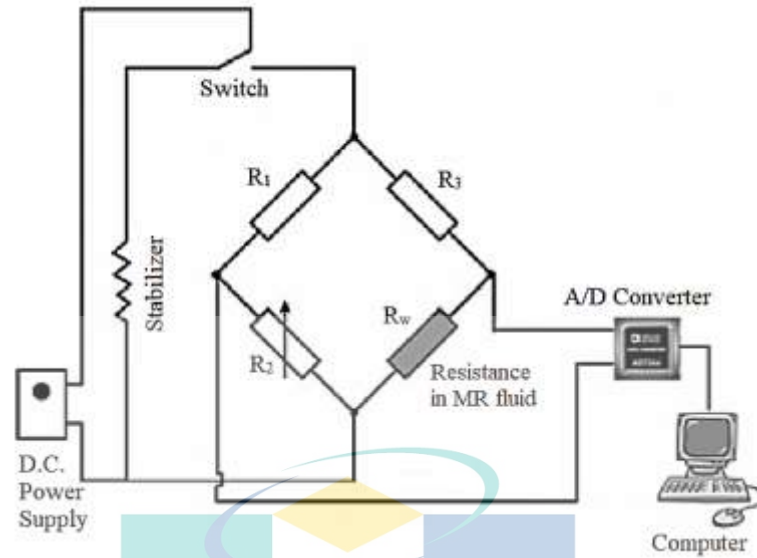


Figure 2.18 Schematic of a transient hot-wire (THW) experimental setup R_w
 Source: Paul et al. (2010)

Thermal conductivity is computed from the slope of variation of ΔT as a function of $\ln(t)$ and the equation of thermal conductivity is given in Eq. (2.4) (Mishra, Lahiri, & Philip, 2018):

$$k = \frac{q}{4\pi(\Delta T_2 - \Delta T_1)} \ln\left(\frac{t_2}{t_1}\right) \quad 2.4$$

where k is thermal conductivity of medium, q is heat flux per unit length, ΔT_1 is temperature difference for time t_1 , and ΔT_2 is temperature difference for time t_2 .

The THW method is proven to be an effective way to measure the thermal conductivity of a suspension and is widely used by researchers in recent years particularly in the area of nanofluids. The related literature was summarized in Table 2.6. However, in the case of MR fluid, the measurement can only be properly conducted in the absence of magnetic field. A magnetic field environment for MR fluid would comprise the usage of an electromagnet or permanent magnets to produce magnetic fields and thus, a complex arrangement or major setup modifications would be needed if the THW method is to be used for measuring the thermal conductivity. The metallic probe used in the THW instrument would also react to the magnetic fields and compromise the measured thermal conductivity values.

Table 2.6 Previous literature of using the THW method to measure thermal conductivity

| No. | Research area | References |
|-----|---------------|---|
| 1 | Nanofluid | Agromayor et al. (2016), Esfe, Firouzi, and Afrand (2018), Esfe, Rostamian, and Shabani-samghabadi (2017), Esfe, Saedodin, Biglari, and Rostamian (2015), Katiyar, Dhar, Nandi, and Das (2016), Khedher, Sidik, Hamzah, and Mamat (2016), Sharif, Hamzah, Redhwan, and Mamat (2016), Shahsavar, Saghafian, Salimpour, and Shafii (2015); Shahsavar, Salimpour, Saghafian, and Shafii (2016), (Gavili, Zabihi, Isfahani, & Sabbaghzadeh, 2012) |
| 2 | MR fluid | (Cheng, Hong, & Liu, 2014), (Reinecke et al., 2008) |

Hence, researchers adopted a more suitable approach to measure the thermal conductivity of MR fluid in the presence of magnetic field. Cha et al. (Cha, Ju, Ahur , & Wereley, 2010) have developed a transient hot-square instrument that enabled direct measurements of thermal conductivity in the direction parallel to an external magnetic field. Figure 2.19 schematically shows the experimental setup of the transient hot-square instrument. The source of heat is from a thin-film serpentine heater which is located on a glass plate to electrically isolate the heater from the MR fluid sample.

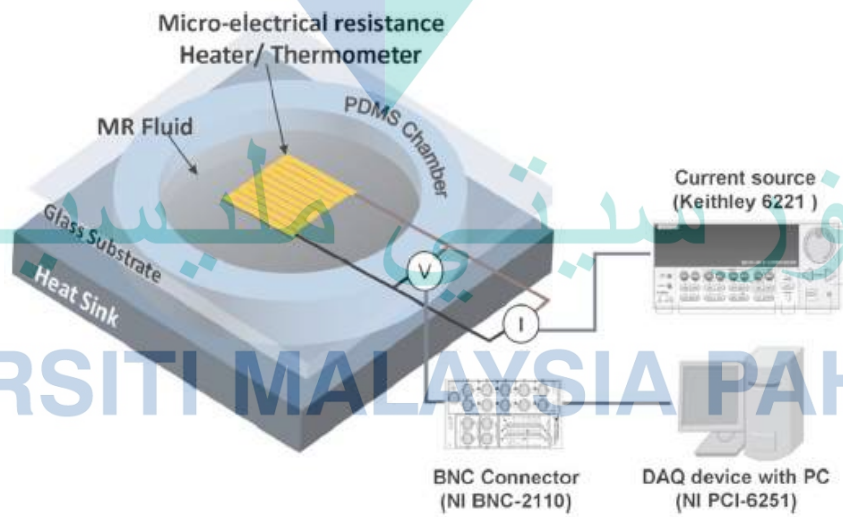


Figure 2.19 Schematic of the transient hot-square measurement setup
Source: Cha et al. (2010)

The sample is contained below the heater in a polydimethylsiloxane (PDMS) chamber which is positioned on top of a heat sink. The instrument is placed between the two poles of a C-shaped permanent magnet as the source of an external magnetic field.

When the heater is subjected to a current pulse, the resulting change in its electrical resistance and temperature is monitored as a function of time. Then, the temporal temperature profile is analyzed to determine the thermal conductivity of the MR fluid sample.

Another alternative to measuring the thermal conductivity of MR fluid in the presence of magnetic field is the guarded hot-plate method or also termed as GHP method. GHP method is a steady-state measurement technique which measures the thermal conductivity of a sample when the thermal state of a sample reaches complete equilibrium. A steady-state condition is attained when the temperature at each point of the sample is constant and the temperature does not change with time. Compared to the THW method, GHP method consumes much longer time to reach the required equilibrium. Nevertheless, it is the primary and most accurate measurement method provided with a well-designed experimental setup (Yüksel, 2016).

The thermal conductivity of a material is determined by measuring temperature difference at a certain distance under a steady-state heat flow through the sample. Figure 2.20 shows the schematic of a steady-state GHP method by absolute technique. By this absolute technique, the sample is placed between a heat source and a heat sink.

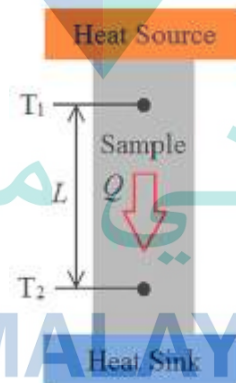


Figure 2.20 Schematic of the absolute technique for measuring thermal conductivity
Source: Zhao et al. (2016)

With known power output from the heat source, the temperature drop across a given length of the sample occurs and thermal conductivity of the sample can be calculated by using Fourier's law of heat conduction, as shown in Eq. (2.1) where k is thermal conductivity of the sample, Q is rate of heat flow through the sample, L is

thickness of the sample between thermocouples T_1 and T_2 , A is surface area of the sample, and ΔT is temperature difference between the thermocouples.

2.6 Magnetorheological Response of MR Fluid

The MR response of MR fluid is initiated from the polarization induced in the suspended particles by an applied magnetic field (Anupama et al., 2018). The interaction between the induced dipoles causes the particles to form columnar structures, parallel to the applied field. These chain-like structures restrict the motion of the fluid, thereby increasing the viscous characteristics of the suspension. The mechanical energy needed to yield these structures increases as the applied field increases, resulting in field-dependent yield stress (Jolly, Bender, & Carlson, 1999).

In the absence of an applied magnetic field, MR fluid exhibits a typical Newtonian behavior. Newtonian behavior of a fluid is when the relationship between shear stress and shear rate of the fluid is in a straight line (Wang, Zhao, et al., 2017). In other words, shear stress of a Newtonian fluid is directly proportional to shear rate. The fluid's viscosity remains constant regardless of the amount of shear rate applied. However, at increasing shear rates, several studies were found on the decreasing viscosity of MR fluid due to the shear-thinning behavior (Dorosti et al., 2020; Piao et al., 2015; Zhang, Li, Cui, & Yang, 2020).

Shear-thinning is defined as a reduction of viscosity at increased shear rates. It is commonly related to the formation of adjacent particle layers by which the layers were formed due to the action of the shear force applied on the MR fluid (Cheng, McCoy, Israelachvili, & Cohen, 2011). Figure 2.21 shows the effect of shear thinning in the viscosity of MR fluids at increased shear rate. It can be seen that the shear viscosity of the MR fluids decreased as the shear rate increased. The particle layers from the magnetic particles in the MR fluids made the samples to flow more easily which justified the result of the decrease in shear viscosity.

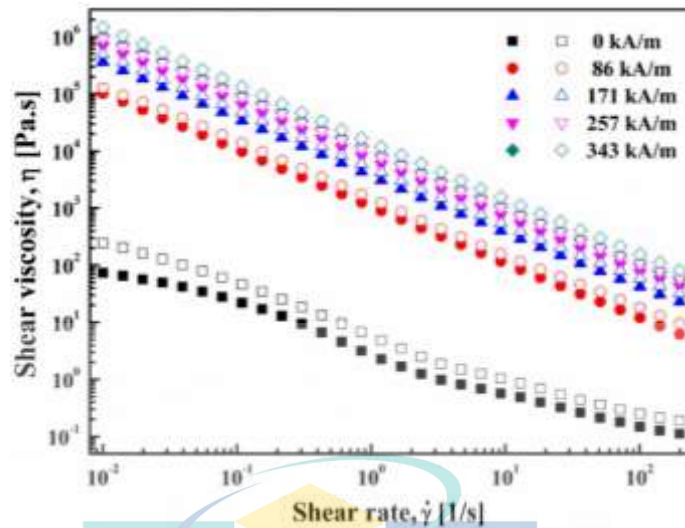


Figure 2.21 Shear viscosity versus shear rate of MR fluids
Source: Piao et al. (2015)

Meanwhile, in the presence of an external magnetic field, MR fluid shows a non-Newtonian behavior. A non-Newtonian fluid is basically the opposite of a Newtonian fluid. There is a non-linear relationship between shear stress and shear rate which means that the shear stress does not vary in the same proportion as the shear rate. When shear is applied to a non-Newtonian fluid, the viscosity of the fluid changes (Simpson & Janna, 2008).

Bingham plastic is a typical model used for a non-Newtonian fluid which fluid will begin to flow when its yield stress is exceeded (Siginer, De Kee, & Chhabra, 1999). The fluid would require minimum yield stress to be exceeded to initiate a movement of the fluid. This characteristic is very similar to the behavior of MR fluid when being subjected to magnetic field. A magnetized MR fluid behaves like a solid when insufficient stress is applied to it but turns to liquid when enough stress to break the chains of magnetic particles in the fluid is applied. Hence, the model is effective at describing the characteristics of MR fluid. In the Bingham plastic model, the total yield stress, τ is given by Eq. (2.5) (Sherman, Becnel, & Wereley, 2015):

$$\tau = \tau_o(H) + \eta\dot{\gamma} \quad 2.5$$

where τ_o is yield stress caused by an applied magnetic field (Pa), H is magnetic field strength (A/m), η is plastic viscosity (Pa·s), and $\dot{\gamma}$ is shear rate (s^{-1}).

The yield stress capability of MR fluid depends on the magnetization characteristics of its particles and can be expressed as the magnetization, M with the magnetic field strength, H (Olabi & Grunwald, 2007). A typical MR fluid can achieve 10-100 kPa of yield stress within a possible magnetic field strength range (Cho, Lim, Jang, Choi, & Jhon, 2004). For low strains prior to yield, the shear modulus of an MR fluid also shows a very large increase in an applied magnetic field.

MR fluid eventually reaches a saturation point where increases of H do not increase the yield strength of the MR fluid. This phenomenon is also termed as magnetic saturation and it typically occurs around 300 kA/m (Kciuk & Turczyn, 2006). An example of the association between yield stress and magnetization property of a commercial MR fluid (MRF-J01) can be seen in Figure 2.22. The magnetic yield stress, τ_m is proportionally increased with increasing magnetic induction, B but began to reach saturation at around 60 kPa when B is at 0.55 T.

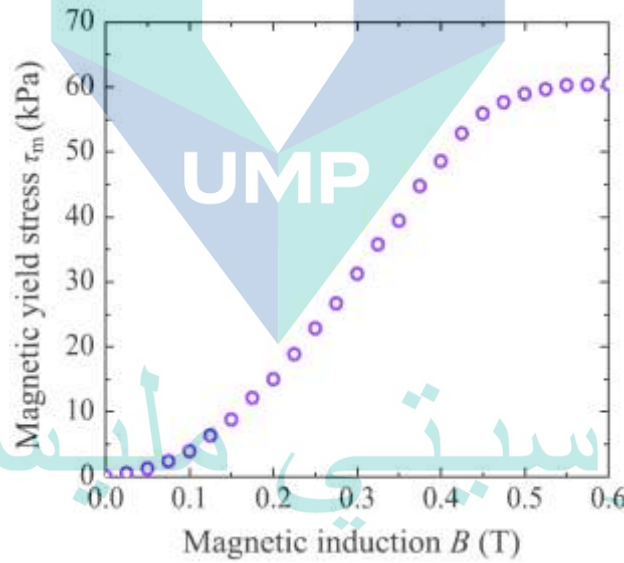


Figure 2.22 Magnetic yield stress versus magnetic induction of MRF-J01
Source: Wang, Zi, et al. (2015)

To gain more understanding on the relationship of yield strength and H of MR fluid, it is worth to observe the hysteresis curve for a ferromagnetic material in the form of M - H curve. As depicted in Figure 2.23, magnetic particles in MR fluid begin to be magnetized along the dashed line when subjected to increased H . The M value soon becomes stagnant at a certain magnetic field strength which indicates the capability of the magnetic particles. At this point, magnetic saturation occurs and a further increase of

H does not induce the M value. The high value of magnetic saturation points to the high yield strength of the MR fluid as the chain of particles become very stiff and hard to be fragmented (Anupama et al., 2018). A similar phenomenon can also be observed in Figure 2.9 that shows the M - H curve of a CIP as the ferromagnetic material (Sung & Rudowicz, 2003). The M of the CIP became stagnant at approximately 200 emu/g when H was around 15 kOe.

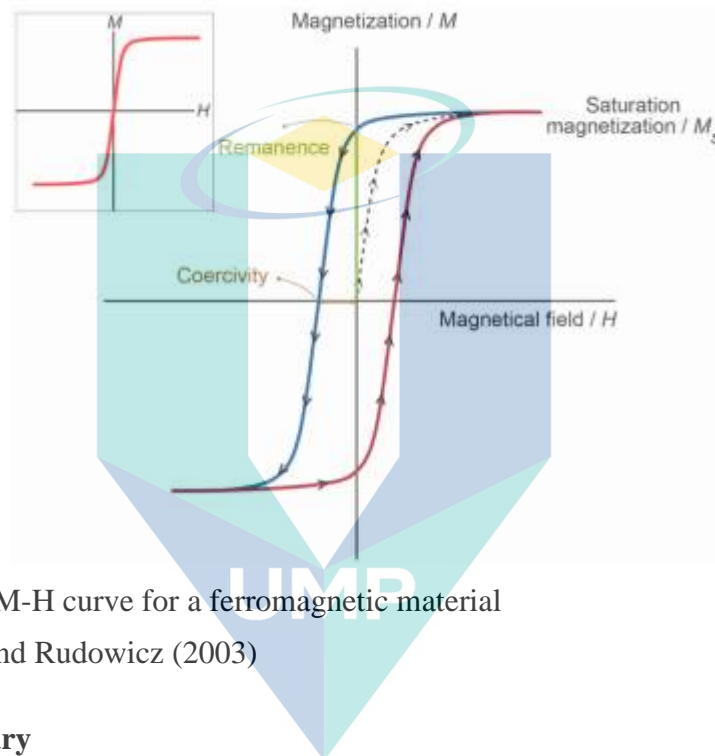


Figure 2.23 M-H curve for a ferromagnetic material
Source: Sung and Rudowicz (2003)

2.7 Summary

This chapter started with the literature of MR fluid and the challenges faced when used in elevated temperature applications. Researchers have opted to enhance the thermal conductivity by increasing the magnetic field strength and the concentration of magnetic particles. Although these methods were proven to enhance thermal conductivity, they have led to other problems which were the increased operating temperature from the amplified current to increase magnetic field strength and the decreased sedimentation ratio due to the highly concentrated magnetic particles.

In this research, the principal idea of enhancing the thermal conductivity of MR fluid is on the addition of Cu and Al as the nano metal additive. The particle size factor, especially at elevated temperature, has also played a crucial role in enhancing the thermal conductivity. This factor has long been studied in the area of nanofluid. The encouraging

results of using nano-sized particles to enhance thermal conductivity have led this study to apply Cu and Al particles in nano-sized scale.

Sedimentation behavior in MR fluid is also a major challenge that negatively affects the rheological behaviors of MR fluid. These problems have consequently caused the degraded performance of MR fluid and its applications. Sedimentation is also a factor that can affect the thermal conductivity of MR fluid. From the literature given, hydrophilic SiO₂ is proven to effectively prevent sedimentation in MR fluid. Therefore, both Cu and Al nanoparticles along with the inclusion of hydrophilic SiO₂ are to be considered as the additive components.

The experimental works will be using two different instruments based on the THW and GHP methods to measure the thermal conductivity of MR fluids in the absence and the presence of magnetic field, respectively. Two typical thermal conductivity models of Maxwell and Bruggeman have been discussed and were included as the basis or comparisons for the experimental results.

This chapter also highlighted the development of MR fluid. Due to having superior properties than other materials, CIP and HO are to be selected as the magnetic particles and carrier fluid, respectively. The selected components and additives will be synthesized by the two-step method that is broadly used in the making of nanofluids. The specified concentration of each component is defined in the next chapter. Finally, this chapter discussed the literature on MR response whereby rheological and magnetic properties of MR fluid are involved. These two properties are considered in this study to determine the performance of the synthesized MR fluids in the presence of magnetic field.

There are a few knowledge of gaps can be found in this study. Firstly, the addition of metal nanoparticles and SiO₂ as additives of MR fluid to enhance both the thermal conductivity and sedimentation ratio properties have not been explored yet. Secondly, the method of using DOE to determine the optimal composition of MR fluid components is practically very new in the area of MR fluid. This method is explained further in the next chapter. Finally, the third gap is on the development of a new module based on the GHP method to measure the thermal conductivity property of MR fluid in the presence of magnetic field.

CHAPTER 3

METHODOLOGY

3.1 Introduction

This chapter presents the methodology on the study of nano metal additive enhanced MR fluid. The research-type for this study is experimental research that involves the experimental design process at the beginning of the study. It has six stages that started with the synthesis of nano metal added MR fluid samples for each experiment as shown in Figure 3.1. The components involved in MR fluid synthesis are carbonyl iron particles (CIP), hydraulic oil (HO), metal additives (Cu and Al), and fumed silica (SiO₂). The materials are then characterized for physical properties such as morphology and size. The second stage is the investigation of MR fluid formulation for high sedimentation ratio through visual observation. The variable parameters involved in the investigation are the concentration range of each MR fluid component. Meanwhile, the constant parameters are range of particle size, viscosity of carrier fluid, ambient temperature, sonication settings, and agitation regime. The third stage is the investigation of MR fluid formulation for enhanced apparent thermal conductivity in the absence of magnetic field. The variable and constant parameters used at this stage are similar with the second stage.

The fourth stage is the optimal composition of nano metal added MR fluid for high sedimentation ratio and apparent thermal conductivity. The optimization method used is the combined D-optimal design of experiment (D-optimal DOE) model. Only optimal composition with desirability above 90% from the model will be used for the next stage. The fifth stage is the analysis of the thermal conductivity of the selected category of MR fluid samples in the presence of magnetic field. The investigation involves the development of a guarded hot-plate module. The final stage is the determination of the MR response in the presence of magnetic field. The MR response is divided into two responses, rheological response and magnetization response. The specified parameters under rheological response are viscosity and shear stress properties

while the parameters under magnetization response are magnetization and magnetic saturation properties.

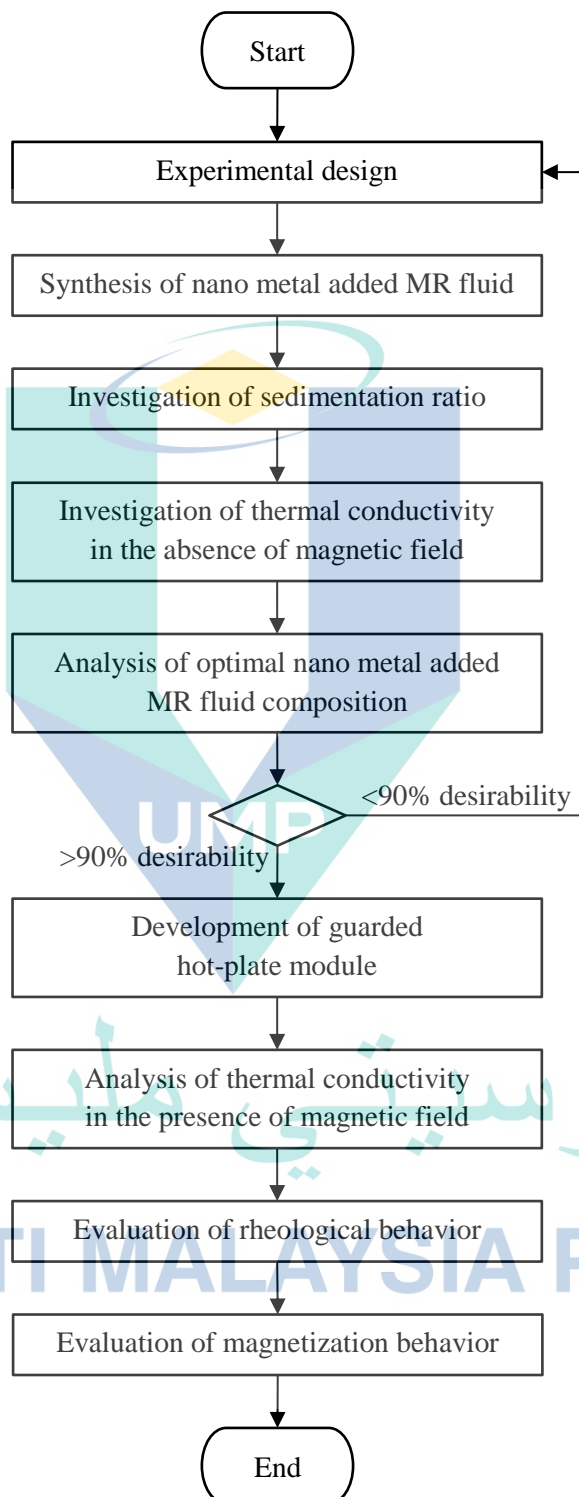


Figure 3.1 Methodology flow chart

This chapter is written according to the research flow as depicted in Figure 3.1. Firstly, the description of the materials used in the process of nano metal added MR fluid is explained with the aid of photographs and micrographs. This visual analysis technique measures the morphology and particle size of each material.

Next, the chapter explains the experimental design of MR fluid. The combined D-optimal model used in this study is explained with parameters composition range. According to the model requirement, three categories of MR fluid samples were synthesized which are MR fluids without metal additive (MRF), MR fluids with Cu (MRF-Cu), and MR fluids with Al (MRF-Al).

The chapter continues with the method used to measure the sedimentation ratio of MR fluid samples. After obtaining the sedimentation ratio, the section presents the method of measuring the apparent thermal conductivity of MR fluid samples in the absence of magnetic field.

After that, the chapter presents the method used to measure the thermal conductivity of the selected category of MR fluid samples in the presence of magnetic field. The development of the guarded hot-plate module for the measurement then comprehensively explains. Next, the method used to determine the MR response of the selected category of MR fluid samples in the presence of magnetic field is presented. The chapter ends with the summary that highlights the conducted works in this chapter.

3.2 Development of MR Fluid

The physical appearance of MR fluid components are shown in Figure 3.2. The first component is the CIP as the magnetic particles. The CIP are in powder form and appear to be grey in color. The second component is HO as the carrier fluid and the liquid is yellow in color. The third component is the additives comprised of Cu, Al, and hydrophilic SiO₂. Cu and Al are the metal additives while hydrophilic SiO₂ is the filler additive. These additives are all in powder form and their appearance are in brown, light grey, and white, respectively.

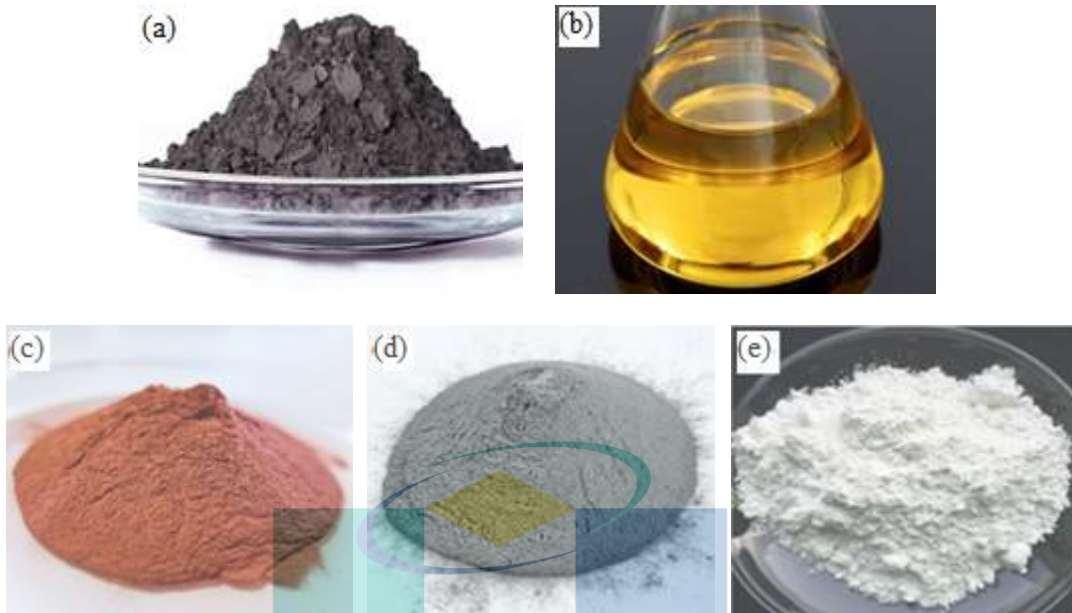


Figure 3.2 MR fluid components comprised of (a) CIP, (b), HO, (c) Cu, (d), Al, and (e) SiO₂

3.2.1 Morphology of Particles

CIP, Cu, Al, and SiO₂ were the particles involved in the making of MR fluid in this study. The type of information of these particles such as size and shape is known through particle morphology analysis. The morphology of these particles was individually characterized by scanning electron microscopy (SEM) and field emission scanning electron microscopy (FESEM). SEM (Carl Zeiss EVO 50, Germany) was used to characterize the morphology of the micron-sized CIP while FESEM (Jeol JSM7800F, Japan) was used to characterize the morphology of the nano-sized Cu, Al and SiO₂. FESEM provides higher resolution of sample surface compared to SEM which makes it suitable to scan the particles in nanometer scale.

Before using SEM, CIP sample in powder form was sprinkled over an aluminum stub by using double-sided adhesive carbon tape for powder mounting. A tweezer was then used to insert the stub into a specimen holder located in the vacuum chamber. After closing the vacuum chamber, the surface morphology of the CIP was scanned by SEM. A similar procedure was repeated for the samples of Cu, Al, and SiO₂ before using FESEM.

Figure 3.3 depicts the morphology of each MR fluid component involved in the MR fluid samples. The particles for each component were seen to be spherical in shape. In Figure 3.3(a), CIP sample is polydisperse and has larger size than Cu, Al, and SiO₂. The average particle size for the CIP is 2-5 μm . Meanwhile, the additives of Cu, Al, and SiO₂ in Figure 3.3(b), Figure 3.3(c), and Figure 3.3(d), respectively, were barely looked different since they entirely shared the same spherical shape and average particle size of 45-70 nm.

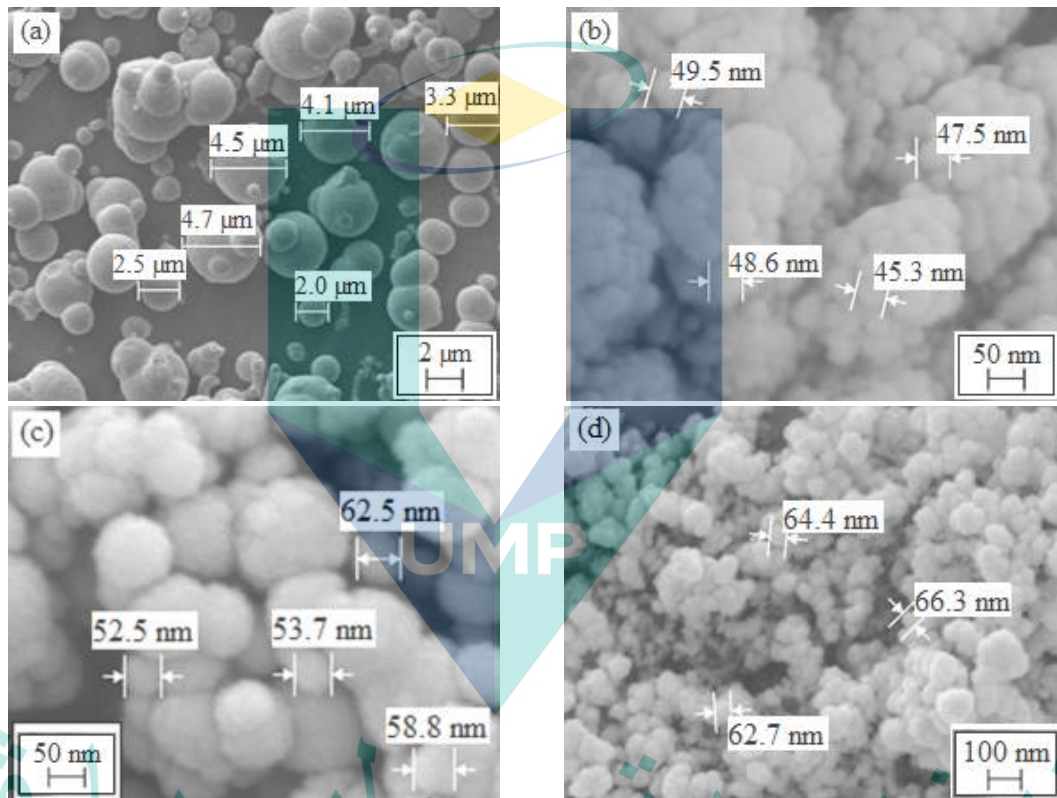


Figure 3.3 SEM image of (a) CIP and FESEM images of (b) Cu, (c) Al, and (d) SiO₂

3.2.2 Experimental Design

MR fluid samples in this study was a mixture of different MR fluid composition. As a mixture, the total concentration of MR fluid components must be equal to 100%. Hence, the components are dependent with each other. For an example, if the concentration of HO is set at 60% of the mixture, the remaining 40% would consist the concentration of CIP at 35% and additives at 5%. For ease of specifying the concentration range of MR fluid components, volume concentration percentage (vol%) was used as the concentration parameter instead of weight concentration percentage (wt%).

Table 3.1 shows the concentration range of the related MR fluid components. Among all the components, HO constituted the largest concentration at 50-75 vol% since carrier fluid typically contains 50-80 vol% of a good MR fluid (Kumbhar et al., 2015). The remaining concentrations were shared between CIP (20-40 vol%) (Yildirim & Genc, 2013) and additives (0-5 vol% each for metal additive and SiO₂ additive) (Li, Xuan, & Wang, 2005). The upper limit of the total concentration of particles (CIP and additives) should not be above 50 vol% to avoid compromisation in the performance of MR fluid (Kumbhar et al., 2015). Excessive concentration of particles would lead to high viscosity and affects the lubricity of an MR fluid (Anupama et al., 2018).

Table 3.1 Concentration range of MR fluid components

| MR fluid components | Density (g/cm ³) | Concentration range (vol%) |
|---------------------|------------------------------|----------------------------|
| HO | 0.874 | 50-75 |
| CIP | 7.860 | 20-40 |
| Cu | 8.940 | 0-5 |
| Al | 2.700 | 0-5 |
| SiO ₂ | 0.037 | 0-5 |

The first stage of the experimental design process was the synthesis of nano metal added MR fluid. Meanwhile, the second and third stage of the design process were the investigation of MR fluid formulation for high sedimentation ratio and enhanced apparent thermal conductivity in the absence of magnetic field, respectively. These three stages were related to each other as the MR fluid formulation for high sedimentation ratio and enhanced apparent thermal conductivity properties were achieved through the synthesis of nano metal added MR fluid samples. Based on the selected concentration range of MR fluid components, a set of MR fluid samples can be synthesized.

The synthesis of nano metal added MR fluid samples was aided by design of experiment (DOE). DOE is an effective tool that provides an economical solution by minimizing the amount of performed experiments and only the most informative combination of parameters is chosen (Eriksson, 2001). Through DOE, a set of experiments can be designed to investigate the independent and dependent variables (Triefenbach, 2008). In this experiment, there were two types of independent variable

namely the mixture parameter and categorical parameter. The mixture parameter was the concentration of each MR fluid component. The categorical parameter was the nano metal particles of Cu and Al as the additives. The effects of each metal additive in the mixture of MR fluid can be analyzed. The dependent variables for this experiment were the sedimentation ratio and apparent thermal conductivity properties.

Since the experimental needs in this study was to investigate the MR fluid mixture together with two categorical parameters, the combined D-optimal model was the most suitable method that can be employed. Factorial and response surface designs did not comply with the requirement of this study. The combined D-optimal model has four unique features namely (1) flexible number of experiment, (2) multiple levels of experiment factors, (3) constraint condition in optimization process, and (4) evaluation of mixture and categorical parameters (You, Chen, Liu, & Jia, 2014).

The combined D-optimal model for this experiment was analyzed by using Design-Expert software. The categories of MR fluid samples were MR fluids without metal additive (MRF), MR fluids with Cu (MRF-Cu), and MR fluids with Al (MRF-Al). This experiment had 10 MR fluid samples with different combination of components and concentrations as shown in Table 3.2. From the table, MR fluid samples can then be synthesized accordingly. The MR fluid sample description was coded as MRF-(metal additive)(vol%). For example, MR fluid sample that contained with 2.5 vol% Cu was described as MRF-Cu2.5. Samples without metal additive were only described as MRF.

Table 3.2 Composition of MR fluid samples

| No. | Description | HO (vol%) | Particle concentration (vol%) | | | |
|-----|-------------|--------------|-------------------------------|------|------|------------------|
| | | | CIP | Cu | Al | SiO ₂ |
| 1 | MRF | 75.0 | 20 | 0 | 0 | 5.00 |
| 2 | MRF | 60.0 | 40 | 0 | 0 | 0 |
| 3 | MRF-Cu2.5 | 65.0 | 30 | 2.50 | 0 | 2.50 |
| 4 | MRF-Cu3.75 | 57.5 | 35 | 3.75 | 0 | 3.75 |
| 5 | MRF-Cu5 | 75.0 | 20 | 5.00 | 0 | 0 |
| 6 | MRF-Cu5 | 50.0 | 40 | 5.00 | 0 | 5.00 |
| 7 | MRF-Al2.5 | 65.0 | 30 | 0 | 2.50 | 2.50 |
| 8 | MRF-Al3.75 | 57.5 | 35 | 0 | 3.75 | 3.75 |
| 9 | MRF-Al5 | 75.0 | 20 | 0 | 5.00 | 0 |
| 10 | MRF-Al5 | 75.0 | 40 | 0 | 5.00 | 5.00 |

The synthesized samples were then experimentally measured for the two dependent variables specified in the combined D-optimal model which were the sedimentation ratio property and the apparent thermal conductivity property. Note that the apparent thermal conductivity property for the samples at this stage was being measured in the absence of magnetic field. The effects of a different combination of components and concentrations in the MR fluid samples can be analyzed after completing the measurements.

As the fourth stage of the experimental design process, the combined D-optimal model was used to determine the optimal composition of MR fluid for high sedimentation ratio and apparent thermal conductivity properties. The optimization from the model provided indicators for the suitable category of the synthesized nano metal added MR fluid samples to be used as the optimal MR fluid. The indicators were measured by desirability percentage. Either MRF-Cu or MRF-Al category with minimum desirability of 90% will be selected. If none of the determined optimal composition is above 90%, the experimental design will be repeated as shown in Figure 3.1.

Table 3.3 shows the numerical optimization in the model where the limits of each component concentration and the goals for the properties were specified. The concentration goal were labeled as ‘in range’ to define the concentration boundary of the optimal MR fluid components. The properties’ goal were defined as ‘maximize’ to achieve the maximum value of sedimentation ratio and thermal conductivity for the optimal MR fluid. All components and properties were treated to be equally important to avoid any preference to a particular component or property.

Table 3.3 Optimization of MR fluid mixture with high sedimentation ratio and thermal conductivity properties

| MR fluid components and properties | Concentration (vol%) | | Criteria | |
|---------------------------------------|----------------------|------|----------|------------|
| | Low | High | Goal | Importance |
| HO | 50 | 75 | in range | 3 |
| CIP | 20 | 40 | in range | 3 |
| SiO ₂ | 0 | 5 | in range | 3 |
| Metal additive | 0 | 5 | in range | 3 |
| Sedimentation ratio | - | - | maximize | 3 |
| Thermal conductivity | - | - | maximize | 3 |

Meanwhile, the fifth stage of the experimental design process was the analysis of thermal conductivity in the presence of magnetic field. The investigation involved the development of a guarded hot-plate module. The module is capable to measure the thermal conductivity of MR fluid in a parallel direction with the magnetic field. Only one category of the nano metal added MR fluid samples was selected for the analysis. Various concentrations (1, 3, and 5 vol%) of nano metal additive under the selected category were used for the investigation as shown in Table 3.4. The MR fluid sample description was coded as MRF-(metal additive)(vol%). Thus, the independent variable at this stage was the concentration of nano metal additive. By this way, the effects of nano metal additive concentration on the thermal conductivity of MR fluid in the presence of magnetic field can be analyzed.

Table 3.4 Composition of nano metal added MR fluid samples

| No. | Description | HO (vol%) | Particle concentration (vol%) | | |
|-----|-----------------------|--------------|-------------------------------|------------|------------------|
| | | | CIP | Nano metal | SiO ₂ |
| 1 | MRF-(metal additive)1 | 54 | 40 | 1 | 5 |
| 2 | MRF-(metal additive)3 | 52 | 40 | 3 | 5 |
| 3 | MRF-(metal additive)5 | 50 | 40 | 5 | 5 |

Finally, the last stage of the experimental design process was the determination of the MR response in the presence of magnetic field. The MR response was divided into two responses, rheological response and magnetization response. The dependent variables under rheological response were viscosity and shear stress properties while the dependent variables under magnetization response were magnetization and magnetic saturation properties. The investigated samples at this stage were given in Table 3.4. They were the same samples used for the analysis of thermal conductivity in the presence of magnetic field. Hence, the effects of nano metal additive concentration on the rheological and magnetization behaviors of MR fluid in the presence of magnetic field can be analyzed.

3.2.3 Synthesis of MR Fluid

In this study, synthesis of MR fluid samples was carried out by using two-step method via mixing and ultrasonication steps. The two-step method was adopted from previous studies (Alves et al., 2009; Li et al., 2019; López-López et al., 2005). The synthesized MR fluid samples were based on the composition of MR fluid components

as in Table 3.2. Figure 3.4 shows the representation of the two-step method. Firstly, nano metal powders were mixed with SiO₂ powders and HO in a beaker. The mixture was then stirred by a glass rod until it is fully dissolved. Next, the dissolved mixture was homogenized in an ultrasonic bath (Branson 3800 CPXH, USA) at 60 °C for 90 minutes and degassed for 15 minutes. The purpose of the high temperature (60 °C) and long duration (90 minutes) settings was to reduce the viscosity of the mixture in order to easily break the big nanoparticle clusters of nano metal and SiO₂ powders into smaller clusters (Wang, Wang, Yan, Wang, & Feng, 2016). The applied temperature and duration were the maximum limit of the ultrasonic bath. Meanwhile, the degassing step was done to remove air in the solution.

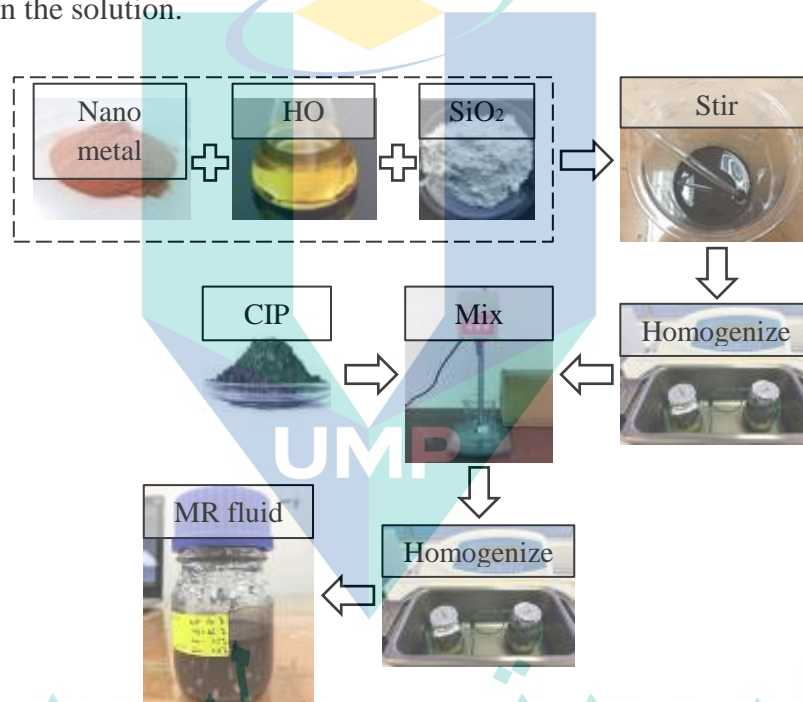


Figure 3.4 Two-step method of synthesizing MR fluid

After that, the solution was mixed with CIP by an overhead stirrer (Smith DJ-2, China) at 800 rpm for about 30 minutes. The overhead stirrer was utilized referring to the standard pivoting blade impeller which is suitable for agitating solution at high speed. Finally, the sample went through secondary homogenization and again degassed. The secondary homogenization was considered to break the remaining aggregated CIP while the degassing process was to remove air bubbles created from the agitation by the overhead stirrer.

3.3 Investigation of Sedimentation Ratio

The investigation of MR fluid formulation for high sedimentation ratio was conducted through the visual observation method. From this method, sedimentation of the synthesized MR fluid samples was observed by inspecting the sediment-supernatant interface at room temperature. All samples were contained in glass tubes on a flat surface and monitored for 28 days without any excitation. Figure 3.5 shows the schematic of the sedimentation measurement. Two regions were developed during the sedimentation period namely the supernatant region and the sediment region. The height of sediment (H_S) and the total height of the MR fluid sample (H_T) were recorded.

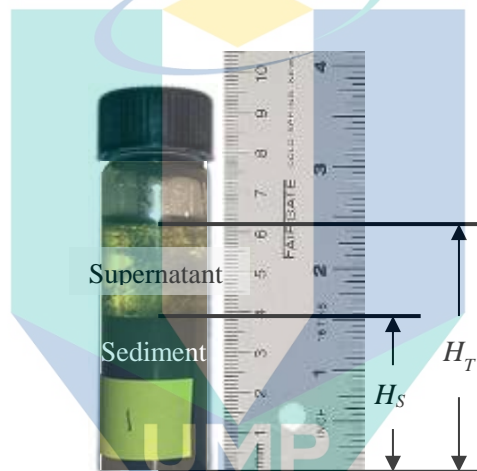


Figure 3.5 Sedimentation measurement of MR fluid sample

Then, the sedimentation ratio, SR is calculated by using Eq. (3.1) (Wang et al., 2019):

$$SR = \frac{H_S}{H_T} \times 100\% \quad 3.1$$

Table 3.5 shows the composition of the synthesized MR fluid samples for sedimentation ratio analysis. The sedimentation ratio was being recorded at the time of one, four, eight, 16, 24, and 48 hours, immediately after MR fluid samples were completely mixed. The record continued with seven, 14, and 28 days later. Sedimentation ratio of the commercial MRF-132DG sample was used as the reference sample.

Table 3.5 Composition of MR fluid samples for sedimentation ratio analysis

| No. | Description | HO (vol%) | Particles (vol%) | | | |
|-----|-------------|-----------|------------------|------|------|------------------|
| | | | CIP | Cu | Al | SiO ₂ |
| 1 | MRF | 75.0 | 20 | 0 | 0 | 5.00 |
| 2 | MRF | 60.0 | 40 | 0 | 0 | 0 |
| 3 | MRF-Cu2.5 | 65.0 | 30 | 2.50 | 0 | 2.50 |
| 4 | MRF-Cu3.75 | 57.5 | 35 | 3.75 | 0 | 3.75 |
| 5 | MRF-Cu5 | 75.0 | 20 | 5.00 | 0 | 0 |
| 6 | MRF-Cu5 | 50.0 | 40 | 5.00 | 0 | 5.00 |
| 7 | MRF-Al2.5 | 65.0 | 30 | 0 | 2.50 | 2.50 |
| 8 | MRF-Al3.75 | 57.5 | 35 | 0 | 3.75 | 3.75 |
| 9 | MRF-Al5 | 75.0 | 20 | 0 | 5.00 | 0 |
| 10 | MRF-Al5 | 50.0 | 40 | 0 | 5.00 | 5.00 |

Finally, the sedimentation ratio performance of MR fluid samples was compared against the commercial MRF-132DG sample. The comparison was conducted by the calculation of sedimentation ratio enhancement, SR_{en} as given in Eq. (3.2):

$$SR_{en} = \frac{SR_{MRF} - SR_{MRF132DG}}{SR_{MRF132DG}} \times 100\% \quad 3.2$$

where SR_{MRF} is the sedimentation ratio of MR fluid samples and $SR_{MRF132DG}$ is the sedimentation ratio of MRF-132DG.

3.4 Investigation of Thermal Conductivity in the Absence of Magnetic Field

The investigation of MR fluid formulation for enhanced thermal conductivity in the absence of magnetic field was conducted by using the thermal properties analyzer instrument (Decagon KD2 Pro, USA). The commercial instrument met the standards of both ASTM D5334 (ASTM, 2014) and IEEE 442-1981 (IEEE, 1981). The thermal properties analyzer instrument is based on the transient hot-wire (THW) method which has a metallic hot-wire probe (KS-1 sensor) to be inserted into the MR fluid. A constant current was supplied to the sensor to raise its temperature. The heat dissipated in the sensor increased the temperature of the sensor and the MR fluid sample. This temperature

rise depends on the thermal conductivity of the sample. Then, the thermal conductivity of MR fluid samples was computed by using Eq. (2.4).

The KS-1 sensor has an accuracy of $\pm 5\%$ and was first calibrated by measuring the thermal conductivity of glycerine before measuring the thermal conductivity of MR fluid samples. Glycerine was provided by the instrument's supplier and is commonly used as a standard sample for measuring thermal conductivity (Nollet & Toldrá, 2015). The obtained measurement value of glycerine was ensured to be the same with the standard value before measuring the MR fluid samples.

Table 3.6 shows the composition of MR fluid samples for thermal conductivity analysis in the absence of magnetic field. The thermal conductivity of the MR fluid samples was experimentally measured at a temperature of 30 °C. The temperature was chosen for comparison with the method used for measuring thermal conductivity in the presence of magnetic field. For each sample, the measurement was recorded for three times as shown in Appendix A. Each measurement was taken with 15-minute interval to get the average thermal conductivity. Thermal conductivity of the commercial MRF-132DG sample was used as the reference sample.

Table 3.6 Composition of MR fluid samples for thermal conductivity analysis in the absence of magnetic field

| No. | Description | HO (vol%) | Particles (vol%) | | | |
|-----|-------------|-----------|------------------|------|------|------------------|
| | | | CIP | Cu | Al | SiO ₂ |
| 1 | MRF | 75.0 | 20 | 0 | 0 | 5.00 |
| 2 | MRF | 60.0 | 40 | 0 | 0 | 0 |
| 3 | MRF-Cu2.5 | 65.0 | 30 | 2.50 | 0 | 2.50 |
| 4 | MRF-Cu3.75 | 57.5 | 35 | 3.75 | 0 | 3.75 |
| 5 | MRF-Cu5 | 75.0 | 20 | 5.00 | 0 | 0 |
| 6 | MRF-Cu5 | 50.0 | 40 | 5.00 | 0 | 5.00 |
| 7 | MRF-Al2.5 | 65.0 | 30 | 0 | 2.50 | 2.50 |
| 8 | MRF-Al3.75 | 57.5 | 35 | 0 | 3.75 | 3.75 |
| 9 | MRF-Al5 | 75.0 | 20 | 0 | 5.00 | 0 |
| 10 | MRF-Al5 | 50.0 | 40 | 0 | 5.00 | 5.00 |

The 15-minute interval was to allow a cooldown period for the sample to avoid any compromise in the subsequent measurement (Nabil, Hamzah, Hamid, Mamat, & Hagos, 2017). Simultaneously, a water bath (Mettler WNB 7, Germany) was used to control the environment temperature of the MR fluid samples within the accuracy of 0.1 °C. Figure 3.6 shows the experimental setup of the thermal conductivity measurement. The general setup of the measurement consists of Mettler water bath and thermal properties analyzer instrument can be seen in Figure 3.6(a). Meanwhile, an MR fluid sample contained in a glass tube positioned inside the water bath is shown in Figure 3.6(b). After the measurement, the thermal conductivity value as indicated in Figure 3.6(c) is recorded.

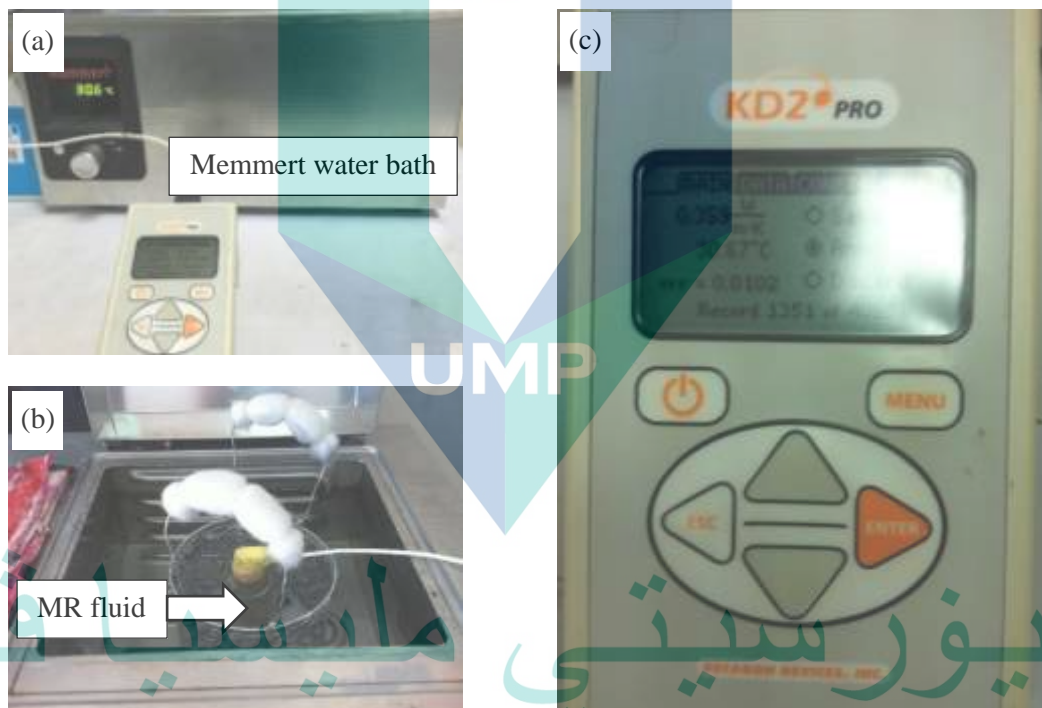


Figure 3.6 Thermal conductivity measurement of MR fluid with its (a) general setup, (b) close-up view in thermal bath, and (c) recorded thermal conductivity value by thermal properties analyzer instrument

The recorded thermal conductivity values were then compared to the values estimated by the Maxwell (1904) and Bruggeman (1935) models in the next chapter. The Maxwell model is suitable to predict the thermal conductivity of samples with low particle volume fractions and in ambient conditions (Das, 2017) while the Bruggeman model predicts better for larger volume fractions (Reinecke et al., 2008). The comparison

was to ensure that the experimental thermal conductivity values complied with the values projected by both models.

The thermal conductivity performance of MR fluid samples was finally compared against the commercial MRF-132DG sample. The comparison was conducted by the calculation of thermal conductivity enhancement, k_{en} as given in Eq. (3.3):

$$k_{en} = \frac{k_{MRF} - k_{MRF132DG}}{k_{MRF132DG}} \times 100\% \quad 3.3$$

where k_{MRF} is the thermal conductivity of MR fluid sample and $k_{MRF132DG}$ is the thermal conductivity of MRF-132DG.

3.5 Investigation of Thermal Conductivity in the Presence of Magnetic Field

The investigation of thermal conductivity in the presence of magnetic field involved with the selected category of nano metal added MR fluid sample. The selected category of MR fluid sample was based from the results in the combined D-optimal model. Various concentrations of nano metal additive under the selected category as in Table 3.4 were used to analyze the effects of the additive concentration on the thermal conductivity behavior. The thermal conductivity of the commercial MRF-132DG sample in the presence of magnetic field was used as the reference sample.

To analyze the thermal conductivity of MR fluid in the presence of magnetic field, a thermal conductivity module was used. The thermal conductivity module is called as the guarded hot-plate (GHP) module due to its adoption of the GHP method. According to the GHP method by absolute technique, the thermal conductivity of MR fluid sample is determined by measuring the temperature difference (thermal gradient) at a certain distance under a steady-state heat flow through the MR fluid sample. From this technique, the sample is to be placed between a heat source and a heat sink. The GHP module complies with the previous studies' method (Mistik et al., 2012; Yildirim & Genc, 2013) and "ISO 8301:1991 Thermal insulation – Determination of steady-state thermal resistance and related properties – Heat flow meter apparatus" measurement standard (ISO, 1991). It is capable to measure the thermal conductivity of MR fluid in the presence of magnetic field and when the magnetic flux direction is parallel with thermal gradient (Yildirim & Genc, 2013).

The actual and dimension diagrams of the GHP module are shown in Figure 3.7. As in Figure 3.7(a), the main parts of the module are polytetrafluoroethylene (PTFE) cap, polymethyl methacrylate (PMMA) vessel, and Al heat sink, with all of them in cylindrical shape. The PTFE cap is made of PTFE material that offers excellent thermal and electrical insulation properties. These properties are important as the cap contains a plate heater inside it. The PTFE material has a high melting point at 342 °C (Price & Jarratt, 2002). The PMMA vessel was designed to contain the MR fluid sample. PMMA is an optically transparent material which helps in the visibility of MR fluid sample inside the vessel. The maximum operating temperature of PMMA is 71 °C (Steinhaus, 1999). The PMMA vessel was enclosed with the PTFE cap and the Al heat sink.

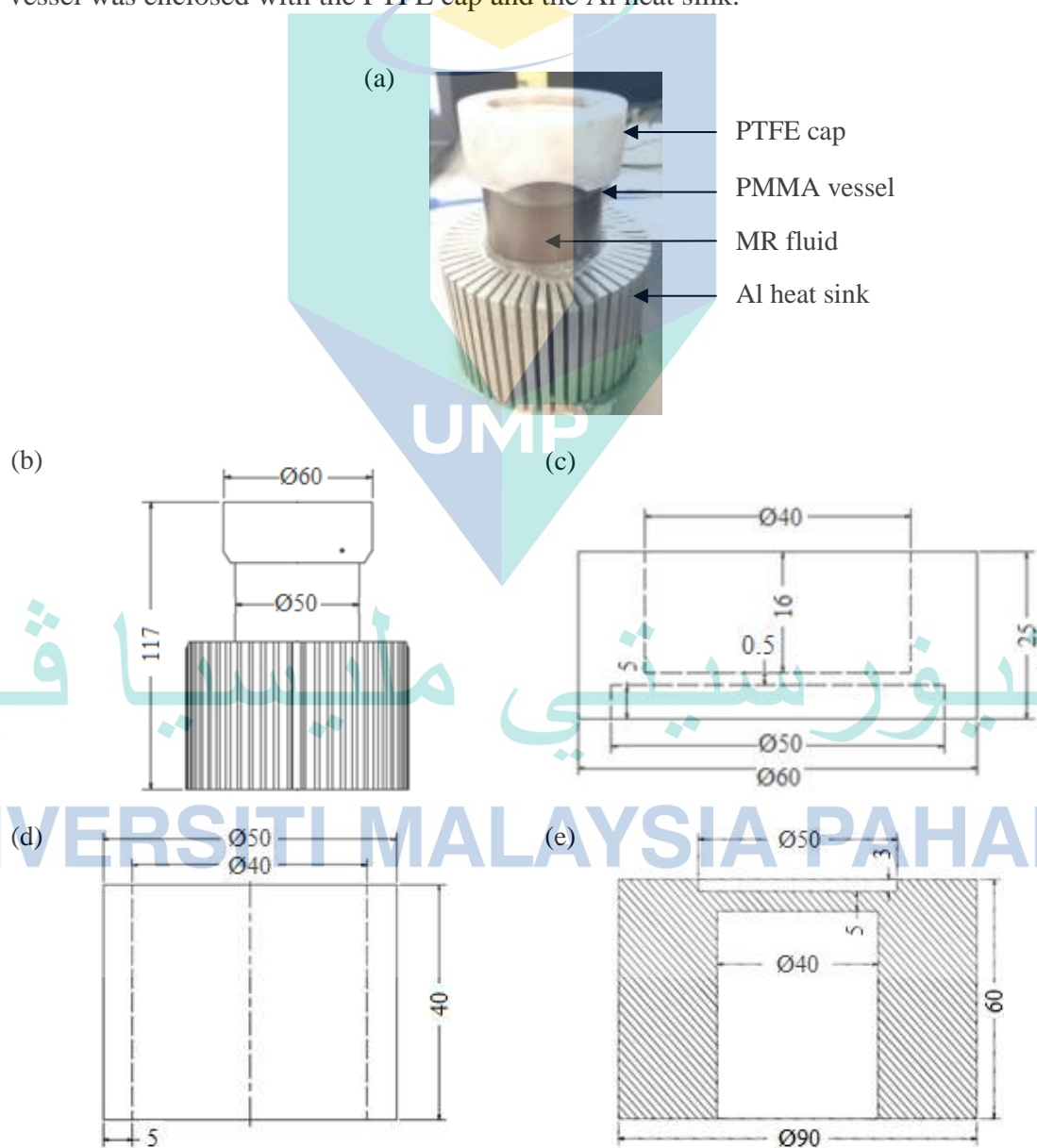


Figure 3.7 Actual and schematic diagrams of GHP module

Figure 3.7(b) shows the dimensions of the GHP module that has an overall height of 117 mm. Figure 3.7(c) represents the dimensions of the PTFE cap with 60 mm in diameter and 25 mm in height. The cap's 50 mm inner diameter and 5 mm depth are to fit with the PMMA vessel in Figure 3.7(d). The PMMA vessel can contain 50.3 mL of MR fluid volume. The vessel's 50 mm outer diameter is to fit into the heat sink in Figure 3.7(e). The heat sink has an overall height of 60 mm and an overall diameter of 90 mm.

Meanwhile, to supply magnetic field in the GHP module, two disk-shaped permanent magnets for the size of 40 mm diameter and 10 mm width were used. The material of the magnets was Neodymium-Iron-Boron (NdFeB) with N52 grade. N52 is the highest material grade with a magnetic flux density of about 0.2 Tesla for the magnets' size. The maximum energy product for N52 is 52 kJ/m³.

The two magnets were located and arranged vertically. Each magnet was located inside the PTFE cap and the heat sink. As in Figure 3.7(c), the PTFE cap was partly hollow from the top for the magnet slot. The Al heat sink as in Figure 3.7(e) was partly hollow from the bottom to give access to the other magnet. By this arrangement, magnetic fields were formed and magnetize the MR fluid sample in the PMMA vessel. The magnetic flux direction will be parallel with the thermal gradient that is produced from the plate heater in the PTFE cap.

The magnetic flux density developed by the magnets was measured by a gaussmeter as shown in Figure 3.8. As in the figure, the 50 mm gap between the magnets were to imitate the distance between the magnets in the GHP module. The gaussmeter probe was placed in the middle of the magnets to assume that the probe location is at the center point of the PMMA vessel. The measured value of 0.075 Tesla by the gaussmeter was higher than the value (0.015 Tesla) applied by Yildirim and Genc (2013) to magnetize MR fluid. Hence, it was confirmed that the magnetic flux were developed inside the module vessel with a gap of 50 mm between the magnets to magnetize MR fluid. The magnets were installed in the GHP module and the thermal conductivity of the sample in the presence of magnetic field can be measured.

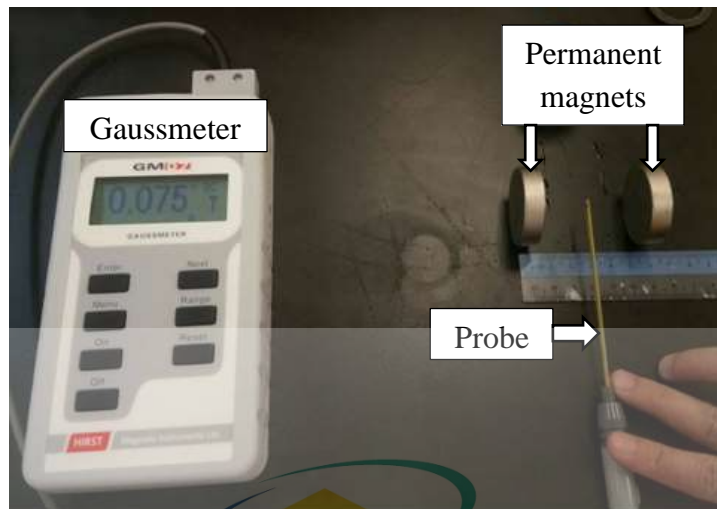


Figure 3.8 Measurement of magnetic flux density on magnet gap

3.5.1 Operation of Guarded Hot-Plate Module

Figure 3.9 shows the arrangement of the GHP module operation. The module mainly consisted of a power supply, a plate heater, a single-board microcontroller, three thermocouples (T_1 , T_2 , and T_3), a pair of permanent magnets, and a computer. A single output DC power supply (B&K Precision, USA) was directly connected to a plate heater. The plate heater (Misumi, Japan) is a ceramic type with a dimension of 15 x 15 x 1.5 mm. It has an operating voltage of up to 40 V and operating electric power of up to 19 W. The heater's maximum operating temperature is almost 300 °C. The temperature of the plate heater was dependent on the voltage and current set by the power supply.

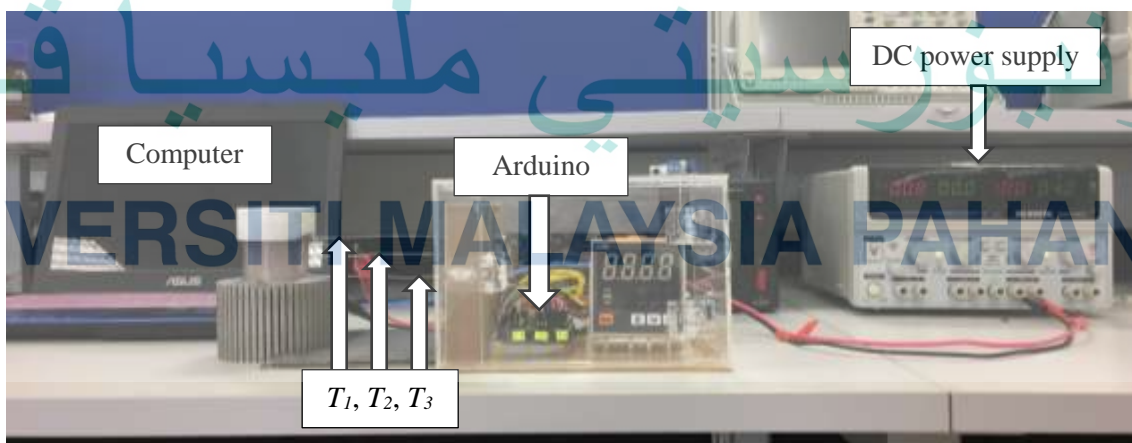


Figure 3.9 Arrangement of the GHP module operation

As the heat source of the module, the plate heater was located inside the PTFE cap to be as close and direct as possible to the MR fluid sample. However, due to the

heater's incapability of direct contact with a liquid sample, a Cu metal plate was added as a layer between the heater and the sample. Fiberglass wool and a PTFE plate were also put up on top of the heater as a heat insulator and a flat base for the top magnet, respectively. Figure 3.10 shows the layers of material in the PTFE cap. The thickness of Cu plate, fiberglass wool, and PTFE plate was measured at 1 mm each.

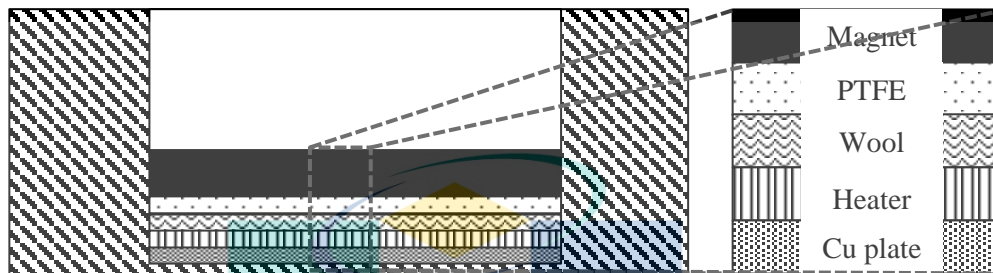


Figure 3.10 Layers of material in PTFE cap

Meanwhile, the single-board microcontroller used for the module was Arduino Mega2560. As the brain of the module, the microcontroller was used to convert analog output from the thermocouples to a digital value. It was powered by a computer through a USB connection and programmed through Arduino software. The software is the platform for developing programming codes before being uploaded to the microcontroller.

The GHP module used three K-type thermocouple probes (RS Components, Malaysia) penetrated from one side of the vessel to measure the temperature of the MR fluid sample. The thermocouples were all identical in size with their probe dimension at 1 mm of diameter and 25 mm of length. They were inserted halfway through the vessel's grinded holes and separated by 15 mm from each other. The top thermocouple was named as T_1 , the middle thermocouple as T_2 , and the bottom thermocouple as T_3 . The thermocouple's accuracy is $\pm 1^\circ\text{C}$ with temperature stability of 0.05°C and is able to read the temperature from -150 to 1000°C . The thermocouple probes are made of nickel which is a magnetic material. The probes have been tested by tapping them onto the permanent magnet to observe any effect to magnetic flux. It was found that the probes were irresponsive to the magnet which indicate that there was no interaction to magnetic flux.

Each thermocouple was calibrated by comparing standard value and measurement value. The calibration process was done by heating tap water at boiling point and the thermocouple was dipped into the boiled water. The boiled water was measured by using

a digital multimeter to ensure the temperature of the water. The reading was captured in CoolTerm1.4.7 software installed on the computer. The dipped thermocouple was static until it read 100 °C and soon it was taken out when the reading was stable. Then, the boiled water was let to be cooled down at room temperature until it reached 50 °C. The same process was repeated until the thermocouple gave a stable value of 50 °C. Next, the thermocouple was dipped into a jar of cold water at 10 °C and a bowl of ice at 0 °C. The process was again repeated until the thermocouple read the same and stable temperature.

After the module setup, the vessel was entirely filled with MR fluid sample to avoid any air gap. With this approach, the Cu plate located at the bottom of the cap is in direct contact with the sample to eliminate the possibility of radiation heat loss due to the air gap. The related MR fluid sample was the selected category of nano metal added MR fluid sample. Then, the two permanent magnets were simultaneously placed in the GHP module to magnetize the MR fluid sample. One magnet was slotted in the cap while the other was slotted in the heat sink.

The experiment was always kept in an enclosed space at room temperature. The power supply was initialized to a certain voltage to increase the temperature of the plate heater. At this point, all thermocouples in the vessel will also show an increase in temperature. The first temperature of the sample was then recorded when thermocouple T_1 shows at 30 °C after at least 15 minutes of heating or when the temperature shown by all thermocouples has finally become stable. The temperature of the sample was again recorded for a higher voltage when T_1 reaches 50 °C and 70 °C. The temperature variation was to investigate the thermal conductivity behavior of nano metal added MR fluid at elevated temperature. The sample was then let to be cooled down to room temperature.

To calculate the thermal conductivity of MR fluid sample, the flow of heat was assumed to be unidirectional and along the direction of the symmetrical axis of the vessel. Following the Fourier's law of heat conduction equation, the measurements required for the calculation of thermal conductivity, k are governed by Eq. (3.4) (Zhao et al., 2016):

$$k = \frac{Ql}{A\Delta T} \quad 3.4$$

where Q (W) is the rate of heat flow through the MR fluid sample, l is the thickness of the sample between T_1 and T_3 (0.03 m), A is the surface area of the MR fluid sample which is the squared of the inner radius of PMMA vessel (0.00126 m²), and ΔT (K) is the temperature difference between T_1 and T_3 . In an ideal case, Q can be taken directly from the power, P produced from the plate heater which is shown in Eq. (3.5) (Tritt, 2005):

$$Q = P = VI \quad 3.5$$

with V (V) as the voltage and I (A) as the current. Table 3.7 shows the power (P) for the GHP module to achieve T_1 at 30-70 °C by using Eq. (3.5). The voltage and current were regulated by the power supply to increase the temperature of the plate heater. It can be seen that to increase the temperature at T_1 , P needed to be increased as well.

Table 3.7 Determination of the required power for the GHP module

| Temperature of heater (°C) | Temperature at T_1 (°C) | Voltage, V (V) | Current, I (A) | Power, P (W) |
|----------------------------|---------------------------|------------------|------------------|----------------|
| 53.0 | 30 | 1.6 | 0.07 | 0.12 |
| 136.0 | 50 | 9.6 | 0.31 | 2.98 |
| 269.0 | 70 | 15.0 | 0.40 | 6.00 |

As can be seen in Table 3.7, the temperatures of the plate heater were high to achieve the desired temperatures at T_1 . The temperature difference was because of the inefficiency of the plate heater, the presence of Cu plate between the heater and sample, and the flow of heat was not parallel with the symmetrical axis of the vessel (Bomberg & Solvason, 1981; Tritt, 2005). The temperature difference directly contributed to the different value of Q and will subsequently affect the calculation of thermal conductivity.

Hence, the different value of Q is termed as the GHP constant (ζ) to compensate the difference and determine the actual value of thermal conductivity as shown in Eq. (3.6).

$$k = \frac{\zeta Q l}{A \Delta T} \quad 3.6$$

3.5.2 Validity and Reliability of Guarded Hot-Plate Module

Before measuring the thermal conductivity of MR fluid samples in the presence of magnetic field, the GHP module was firstly tested for the validity of measurement in

the absence of magnetic field. This step was to compare the calculated values in Eq. (3.4) with the thermal properties analyzer instrument that was only able to measure the thermal conductivity in the absence of magnetic field. MRF-132DG was chosen as the standard sample for the measurement of thermal conductivity at different temperatures (30-70 °C).

The thermal conductivity data across different temperatures is presented in Table 3.8. From the results, thermal conductivity of MRF-132DG were slightly increased as the temperature increased for both instruments. Hence, there were similar trends shown in both samples between the thermal properties analyzer and the GHP module instruments. The thermal conductivity values by the thermal properties analyzer were from 0.357-0.395 W/m·K while the thermal conductivity values by the GHP module were from 3.718-4.064 W/m·K.

Table 3.8 Thermal conductivity of MRF-132DG across different temperatures by thermal properties analyzer and GHP module

| No. | Instrument | Thermal conductivity (W/m·K) | | |
|-----|-----------------------------|------------------------------|-------|-------|
| | | 30 °C | 50 °C | 70 °C |
| 1 | Thermal properties analyzer | 0.357 | 0.383 | 0.395 |
| 2 | GHP module | 3.718 | 3.789 | 4.064 |

The difference in thermal conductivity values between the instruments was due to the exclusion of ζ as the GHP constant. To compensate the difference and determine the actual value of thermal conductivity by the GHP module, the value of ζ is found to be 0.097. Eq. (3.6) was used and the actual thermal conductivity values of MRF-132DG by the GHP module is shown in Table 3.9. The actual thermal conductivity values by the GHP module were not far from the values by the thermal properties analyzer instrument with the largest difference percentage was only 1.5%.

Table 3.9 Actual thermal conductivity of MRF-132DG by GHP module

| No. | Instrument | Thermal conductivity (W/m·K) | | |
|-----|-----------------------------|------------------------------|-------|-------|
| | | 30 °C | 50 °C | 70 °C |
| 1 | Thermal properties analyzer | 0.357 | 0.383 | 0.395 |
| 2 | GHP module | 0.361 | 0.368 | 0.394 |
| | Difference (%) | 0.4 | 1.5 | 0.1 |

By including the value of ζ , Eq. (3.6) can be revised to Eq. (3.7):

$$k = \frac{0.097Ql}{A\Delta T} \quad 3.7$$

After validating the results, the GHP module was checked for its reliability. MRF-Cu5 sample was chosen for the reliability test in which the sample must be measured twice. Table 3.10 shows the two measurements of thermal conductivity for MRF-Cu5 sample in the absence of magnetic field. The table includes the recorded temperatures at T_1 and T_3 thermocouples to obtain the temperature difference. It can be observed that the thermal conductivity values of MRF-Cu5 were decreased (0.900-0.707 W/m·K) as the temperatures were increased (30-70 °C) in the first measurement.

Table 3.10 Thermal conductivity measurements of MRF-Cu5 sample in the absence of magnetic field

| Measurement | Temperature at T_1 (°C) | Temperature at T_3 (°C) | Temperature difference, ΔT (°C) | Thermal conductivity (W/m·K) |
|-------------|---------------------------|---------------------------|---|------------------------------|
| 1 | 30 | 29.00 | 1.00 | 0.900 |
| | 50 | 35.50 | 14.50 | 0.736 |
| | 70 | 42.00 | 28.00 | 0.707 |
| 2 | 30 | 29.00 | 1.00 | 0.949 |
| | 50 | 35.25 | 14.75 | 0.739 |
| | 70 | 40.75 | 29.25 | 0.681 |

The thermal conductivity values of MRF-Cu5 in the second measurement were also decreased (0.949-0.681 W/m·K) as the temperatures were increased (30-70 °C). The trend was similar for both measurements and only a slight difference of thermal conductivity at each temperature (30-70 °C). The final thermal conductivity for MRF-Cu5 was the average from the two measurements. Hence, the GHP module is reliable to be used for the measurement of MR fluid within 30-70 °C.

3.6 Determination of Magnetorheological Response

The determination of MR response in the presence of magnetic field was divided into two responses, rheological response and magnetization response. The MR fluid samples involved in the experiment were the selected category of nano metal added MR fluid sample. Similar to the investigation of thermal conductivity in the presence of magnetic field, various concentrations of nano metal additive under the selected category as in Table 3.4 were used for the investigation. The approach was to analyze the effects of the additive concentration on the rheological and magnetization behaviors. The MR response of the commercial MRF-132DG sample was used as the reference sample.

3.6.1 Rheological Response

The rheological properties involved in this research were viscosity and shear stress. To identify these properties in the selected category MR fluid samples, a rotational rheometer (Anton Paar Physica MCR302, Austria) as in Figure 3.11(a) was used. The rheometer is equipped with a parallel plate measuring system. As indicated in Figure 3.11(b), the parallel plate is the rotational upper plate while the lower plate is stationary. To perform the rheological measurement, the sample was injected at approximately 0.5 mL to entirely fill the lower plate area. Then, the parallel plate which is a part of the measuring tool was brought down at zero-gap where it touched the surface of the sample.

The viscosity and shear stress of the samples were then being measured in room temperature when the parallel plate was rotated. The measurement performed in a controlled shear rate mode in which the plate rotated under a specified shear rate range.

The shear rate range was specified at $0.1-100 \text{ s}^{-1}$ which was sufficient to analyze the rheological properties for the MR fluid samples and parallel with previous studies (Aruna, Rahman, Joladarashi, & Kumara, 2019; Thakur & Sarkar, 2020; Zhu, Dong, Huang, & Qi, 2019).

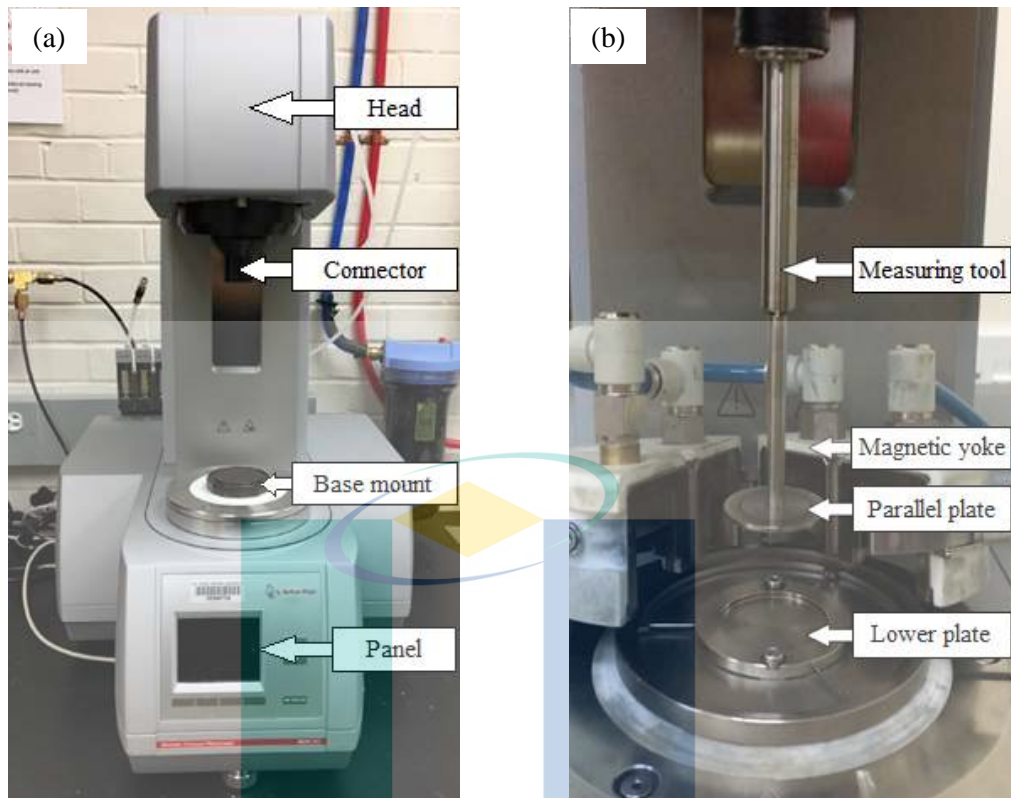


Figure 3.11 Rheological characterization by (a) MCR302 rheometer and (b) its schematic figure

The rheometer was also equipped with a standard magnetic measurement module that has built-in coils below the lower plate that can generate up to 1 Tesla. The magnetic field, controlled by the current input was generated vertically with respect to the direction of flow. For the MR fluid samples, the current inputs applied were ranged from 0-2 A to produce magnetic fields of up to 0.4 Tesla. Although the magnetic measurement module can generate up to 1 Tesla, the purpose of applying the low magnetic field range (0.4 Tesla or below) was to avoid the occurrence of viscosity instability (Ram & Bhandari, 2013; Zubarev, 2014).

Hence, after obtaining the rheological results in the absence of magnetic field, the sample was again measured in the presence of magnetic field. All measurements were carried out three times to ensure the credibility of data as shown in Figure 3.12. The complete data of each run were provided in Appendix B. From the figure, all repeated readings of viscosity and shear stress showed only small deviations between them. Hence, the viscosity and shear stress data are adequate for this study.

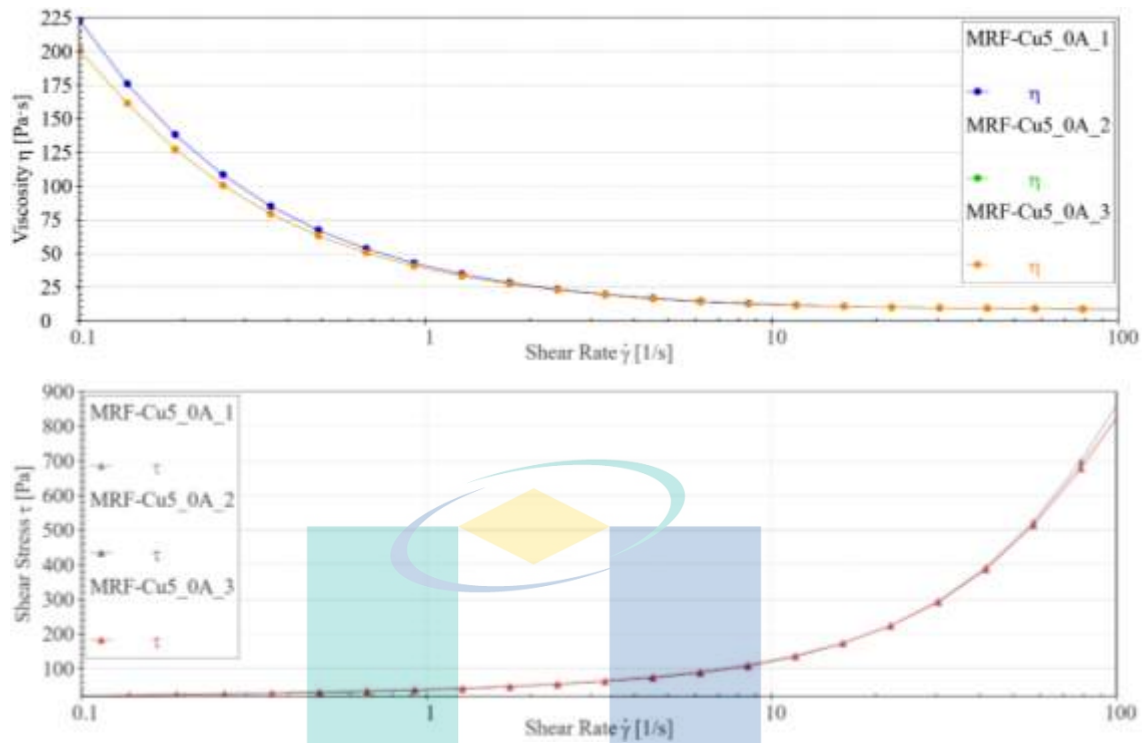


Figure 3.12 Viscosity and shear stress of MR fluid sample

3.6.2 Magnetization Response

The selected category of MR fluid samples were then being measured for their magnetization by a vibrating sample magnetometer (VSM Lakeshore 7404, USA) as shown in Figure 3.13(a). To be able to measure the samples' properties in liquid state, a liquid sample holder to contain each sample was required. The sample holder material is plastic to avoid any magnetic interference during the measurement.

Figure 3.13(b) shows an MR fluid sample contained in the liquid sample holder material. The applied magnetic field strength by the VSM was up to 1.2 Tesla (957.2 kA/m) across all samples in room temperature. The value of magnetic field strength was enough for the MR fluid samples to achieve magnetic saturation as the magnetic saturation for a typical MR fluid occurs around 300 kA/m (Kciuk & Turczyn, 2006).

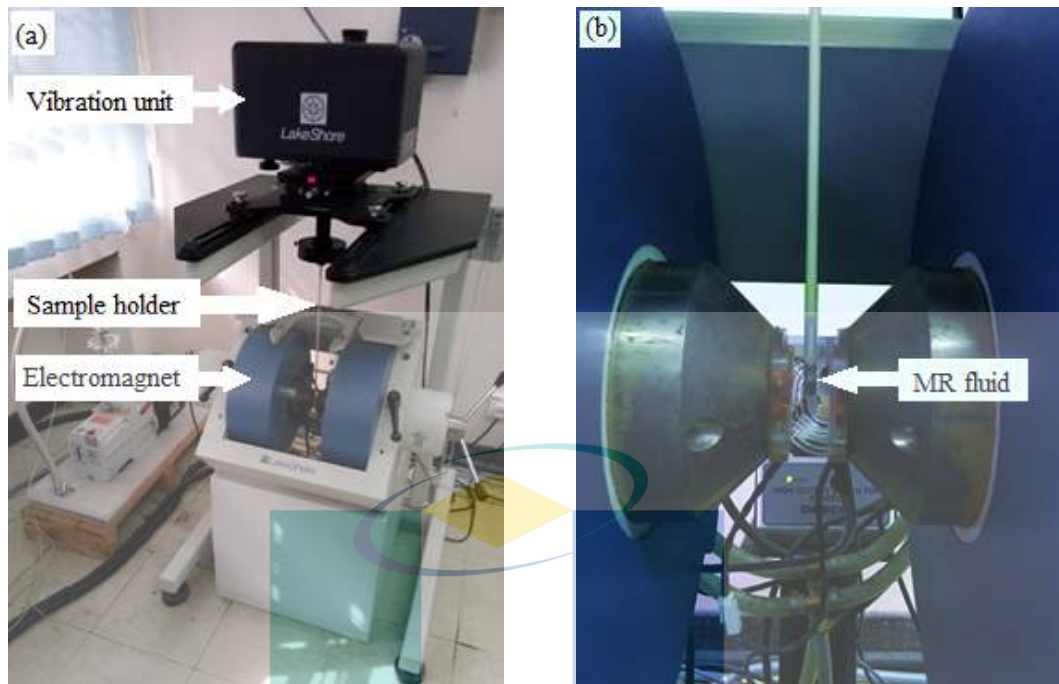


Figure 3.13 Magnetic characterization by (a) Lakeshore 7404 vibrating sample magnetometer with (b) the close-up view of MR fluid sample location

3.7 Summary

This chapter started with the development of MR fluid samples that is comprised of morphology of particles, experimental design, and synthesis of MR fluid. The involved components in MR fluid samples were CIP, HO, Cu, Al, and SiO₂. From the morphology analysis of using SEM and FESEM, all particles were spherical in shape. The particle size range of CIP was 2-5 μm while Cu, Al, and SiO₂ were 45-70 nm. In the experimental design, combined D-optimal model was used to minimize the number of MR fluid samples by strategically select the most informative combination of MR fluid components and composition. The composition of HO and CIP were set at 50-75 vol% and 20-40 vol%, respectively, while the composition of Cu, Al, and SiO₂ were 0-5 vol% each. Based on the model requirement, a total of 10 samples in three categories were synthesized namely MRF, MRF-Cu, and MRF-Al. The synthesis work was carried out by using the two-step method via mixing and ultrasonication steps.

The chapter continued with the investigation of MR fluid sedimentation ratio by visual observation method and the investigation of MR fluid apparent thermal conductivity in the absence of magnetic field by THW method. The sedimentation ratio of MR fluid samples were recorded for 28 days. Meanwhile, the thermal conductivity of

MR fluid samples was experimentally measured at 30 °C. The recorded apparent thermal conductivity values in the next chapter will be compared to the values estimated by Maxwell and Bruggeman models to ensure that the experimental apparent thermal conductivity values complied with the values projected by both models. The results from both investigations will be used for the determination of the category and optimal composition of MR fluid samples. The optimal composition will be based on MR fluid with high sedimentation ratio and high apparent thermal conductivity in the absence of magnetic field.

After that, the chapter explained on the investigation of thermal conductivity in the presence of magnetic field for the selected category of MR fluid samples. The investigation involved the development of GHP module that is capable of measuring thermal conductivity of MR fluid in the presence of magnetic field and when the magnetic flux direction is parallel with thermal gradient. Selection of suitable materials and dimensions for the GHP module have been considered. The calculation of thermal conductivity in the presence of magnetic field was based on the Fourier's law of heat conduction equation. After tested for validity and reliability, the GHP module conducted the measurement of thermal conductivity at 30-70 °C. The temperature variation was to investigate the thermal conductivity behavior of MR fluids at elevated temperature.

The chapter ended with the determination of MR response for the selected category of MR fluid samples in the presence of magnetic field. The MR response of the MR fluids was focused on the viscosity and shear stress properties under rheological response. The rheological response of the MR fluids was determined by using a rotational rheometer. The shear rate range was specified at 0.1-100 s⁻¹ and the applied magnetic field strength to magnetize the MR fluid samples was up to 0.4 Tesla in room temperature. The other MR response being investigated was the magnetization and magnetic saturation properties under magnetization response. The magnetization response of the MR fluids was determined by using a VSM. The applied magnetic field strength by the VSM was up to 1.2 Tesla in room temperature.

CHAPTER 4

RESULTS AND DISCUSSION

4.1 Introduction

This chapter presents the results and discussion of the nano metal additive enhanced MR fluid in terms of its sedimentation ratio, thermal conductivity, and magnetorheological response. The chapter starts with the discussion on sedimentation ratio of the different category of MR fluid samples. The different categories were MRF, MRF-Cu, and MRF-Al samples. The effects of the different combination of components and concentrations to the sedimentation ratio of MR fluids were analyzed.

The chapter continues with the discussion on apparent thermal conductivity behavior of the MR fluid samples in the absence of magnetic field. The thermal conductivity results were compared with two established thermal conductivity models to ensure that the experimental values complied with the projected values. The effects of the different combination of components and concentrations to the thermal conductivity of MR fluids in the absence of magnetic field were analyzed.

Next, the chapter discusses the results of optimized MR fluid configuration for both sedimentation ratio and apparent thermal conductivity properties by the combined D-optimal model. In this section, a category of nano metal added MR fluid sample was determined with optimal composition. The chapter follows with the discussion on thermal conductivity behavior of MR fluids in the presence of magnetic field. The related MR fluid samples in this section were the selected category of nano metal added MR fluids.

Finally, the chapter discusses the MR response of the selected category of nano metal added MR fluids in the presence of magnetic field. The MR response was divided into two responses namely rheological response and magnetization response. These responses were considered to determine the performance of the nano metal added MR fluids in the presence of magnetic field. The rheological response was focused on the

viscosity and shear stress properties while the magnetization response was focused on the magnetization and magnetic saturation properties.

4.2 Effect of Sedimentation Ratio

Figure 4.1 shows the sedimentation of the different category of MR fluid samples throughout the period of 14 days at room temperature. When immediately after mixed, there was no supernatant area observed in the samples. After 14 days of monitoring, supernatant can be observed in the samples which indicated that sedimentation has occurred.

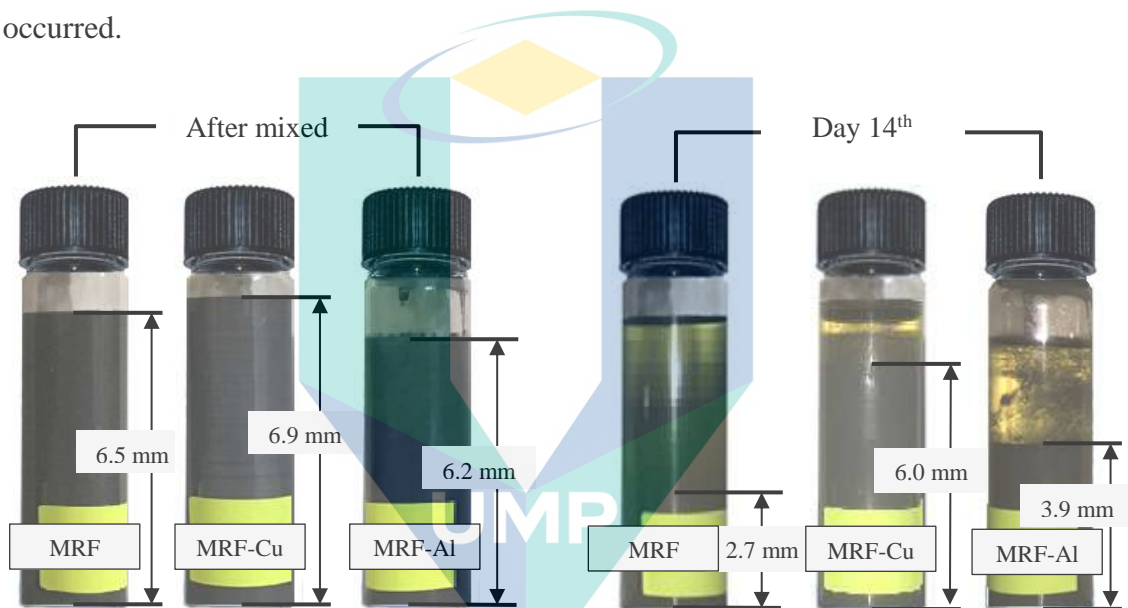


Figure 4.1 Sedimentation comparison of MR fluid samples taken when immediately after mixed and on day 14th

Table 4.1 shows the complete data of sedimentation ratio for the synthesized MR fluid samples throughout the period of 28 days. It can be seen that sedimentation occurred for all samples by the changes of sedimentation ratio values over the period. The sedimentation ratio of all samples after 28 days was used to analyze the effects of the different combination of components and concentrations in the MR fluid samples. The data were also used for the determination of the optimal composition of nano metal added MR fluid. Meanwhile, sedimentation ratio of the commercial MRF-132DG sample was also included for the purpose of comparison.

Table 4.1 Sedimentation ratio of MR fluid samples

| No. | Description | HO (vol%) | Particles (vol%) | | | | Sedimentation ratio (%) | | | | | | | | |
|-----|-------------|--------------|------------------|------|------|------------------|-------------------------|-------|-------|-------|-------|-------|-------|-------|-------|
| | | | CIP | Cu | Al | SiO ₂ | 1h | 4h | 8h | 16h | 24h | 48h | 7d | 14d | 28d |
| 1 | MRF | 75.0 | 20 | 0 | 0 | 5.00 | 95.38 | 87.69 | 75.38 | 58.46 | 52.31 | 44.62 | 43.08 | 41.54 | 41.54 |
| 2 | MRF | 60.0 | 40 | 0 | 0 | 0 | 95.65 | 91.30 | 91.30 | 82.61 | 78.26 | 73.91 | 73.91 | 69.57 | 69.57 |
| 3 | MRF-Cu2.5 | 65.0 | 30 | 2.50 | 0 | 2.50 | 98.44 | 96.88 | 96.88 | 95.31 | 93.75 | 87.50 | 67.19 | 57.81 | 57.81 |
| 4 | MRF-Cu3.75 | 57.5 | 35 | 3.75 | 0 | 3.75 | 100 | 98.44 | 98.44 | 98.44 | 98.44 | 96.88 | 87.50 | 78.13 | 78.13 |
| 5 | MRF-Cu5 | 75.0 | 20 | 5.00 | 0 | 0 | 98.44 | 96.88 | 96.88 | 93.75 | 87.50 | 76.56 | 62.50 | 57.81 | 57.81 |
| 6 | MRF-Cu5 | 50.0 | 40 | 5.00 | 0 | 5.00 | 95.65 | 95.65 | 95.65 | 95.65 | 95.65 | 94.20 | 91.30 | 86.96 | 86.96 |
| 7 | MRF-Al2.5 | 65.0 | 30 | 0 | 2.50 | 2.50 | 100 | 100 | 97.06 | 95.59 | 94.12 | 89.71 | 75.00 | 66.18 | 66.18 |
| 8 | MRF-Al3.75 | 57.5 | 35 | 0 | 3.75 | 3.75 | 100 | 100 | 100 | 97.14 | 97.14 | 94.29 | 87.14 | 78.57 | 77.14 |
| 9 | MRF-Al5 | 75.0 | 20 | 0 | 5.00 | 0 | 100 | 100 | 96.77 | 96.77 | 93.55 | 87.10 | 74.19 | 62.90 | 58.06 |
| 10 | MRF-Al5 | 50.0 | 40 | 0 | 5.00 | 5.00 | 100 | 100 | 100 | 98.57 | 98.57 | 98.57 | 95.71 | 91.43 | 88.57 |
| 11 | MRF-132DG | - | 32 | - | - | - | 100 | 97.50 | 97.00 | 96.56 | 96.25 | 95.00 | 92.50 | 87.50 | 77.50 |

The sedimentation ratio of all samples after 28 days was used to analyze the effects of MR fluid components. The related MR fluid components were CIP, SiO₂, Cu, and Al. Figure 4.2, Figure 4.3, Figure 4.4, and Figure 4.5 show the sedimentation ratio of several MR fluid samples with different concentration of MR fluid components. From the figures, it was observed that the sedimentation ratio of the samples started to decline as the time increased. The results indicated that sedimentation phenomena occurred for all samples during the period. After 336 hours (14 days), it can be seen that the sedimentation ratio of all samples became stagnant which showed that the samples were reaching full sedimentation.

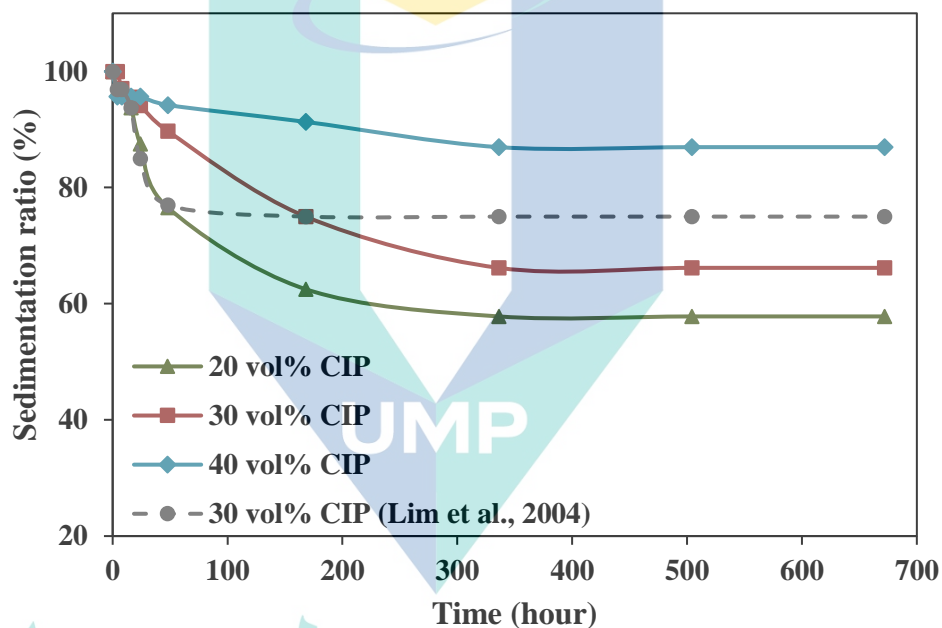


Figure 4.2 Sedimentation ratio of MR fluids at different concentration of CIP

From Figure 4.2, it was found that the sedimentation ratio of MR fluid samples was improved with increased concentration of CIP. For samples with 30 vol% CIP and below, the sedimentation ratio after 28 days was less than 70%. MR fluid sample with 40 vol% CIP showed the highest sedimentation ratio, recorded at 86.96%. The increased concentration of CIP above 30 vol% has led to the reduction of average distance between the particles and the enhancement of interaction forces between the particles. The enhanced interaction forces obstruct gravity settling and consequently improved the sedimentation ratio (Xu & Chen, 2016). The result was parallel with the previous study by Cheng et al. (2016) whereby they found that the high concentration of CIP (above 30 vol%) settle slower than the lower concentration of particles.

The results of sedimentation ratio in Figure 4.2 were also compared with the previous study by Lim et al. (2004). The sample with 30 vol% CIP from Lim et al. (2004) showed better sedimentation ratio at about 75% while the sample with 30 vol% CIP from this study was recorded at 66.18%. It was assumed that the mineral oil as the carrier fluid in the previous study has lower density mismatch with CIP that contributed to better sedimentation ratio (Niu et al., 2018). However, the sample rapidly reached full sedimentation in just about 3 days.

In the meantime, Figure 4.3 shows the sedimentation ratio of several MR fluid samples with different concentration of SiO₂. It can be seen that the sedimentation ratio of MR fluid samples was increased with the presence of SiO₂. The highest sedimentation ratio was recorded at 88.57% after 28 days by MR fluid sample with 5 vol% SiO₂. The positive result was parallel with the previous study by Lim et al. (2004). They found that the sedimentation ratio of MR fluid samples was improved with the concentration increment of SiO₂. The behavior is attributed to the high concentration of SiO₂ that formed a support structure in the MR fluid samples. The support structure was enough to hold up the whole concentration of CIP that prevented CIP from fast sedimentation (López-López et al., 2005). However, a gap in the results was observed between the sample with 2.5 vol% SiO₂ and 5 vol% SiO₂. This behavior indicated that the addition of SiO₂ in MR fluids was only effective at high concentration (5 vol%).

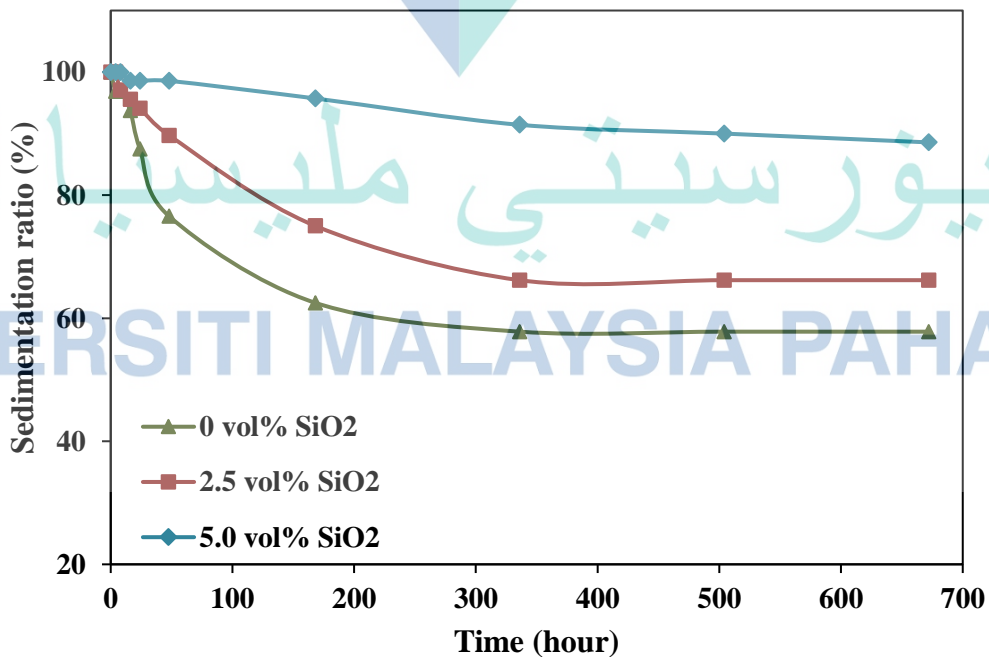


Figure 4.3 Sedimentation ratio of MR fluids at different concentration of SiO₂

Meanwhile, the sedimentation ratio of several MR fluid samples with different concentration of Cu is shown in Figure 4.4. It was observed that the sedimentation ratio of MR fluid samples was enhanced with increased concentration of Cu. The sedimentation ratio of MR fluid samples with 3.75 vol% Cu and 5 vol% Cu were recorded at 78.13% and 86.96%, respectively. A large difference of sedimentation ratio can be found between the sample with 2.5 vol% Cu and the samples with 3.75 vol% and 5 vol% Cu. It was assumed that at low concentration (2.5 vol% and below) of Cu, the nano-sized Cu particles were in Brownian motion but rapidly pulled down by the gravitational force due to its high density (8.94 g/cm^3). At higher concentration (3.75 vol% and above) of Cu, the particles were closer to each other and van der Waals forces became more dominant than the gravitational force which resulted in the aggregation of Cu particles. The formed aggregation of Cu helped to provide the support for the CIP and hence resulted in higher sedimentation ratio (Jana et al., 2007).

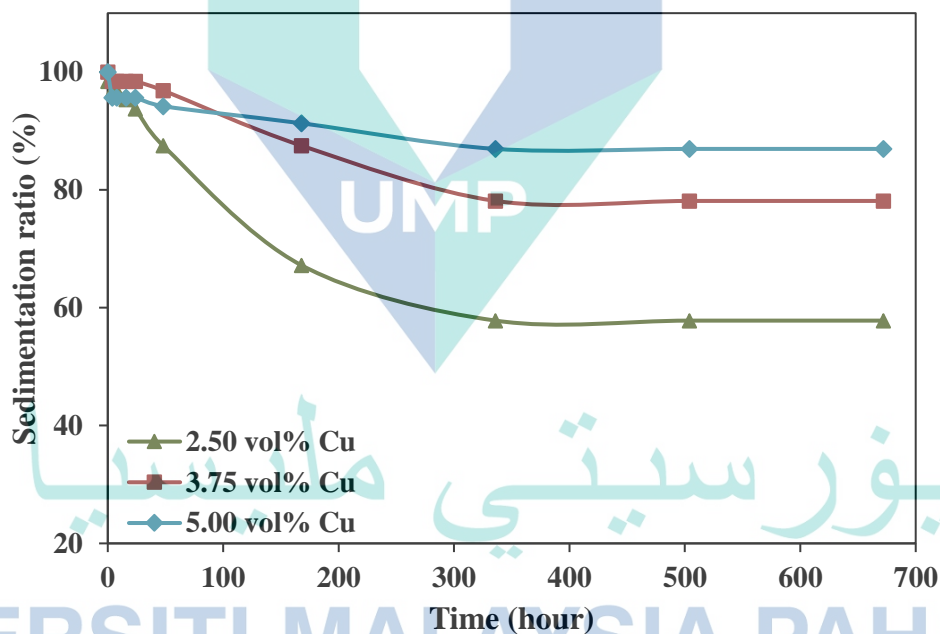


Figure 4.4 Sedimentation ratio of MR fluids at different concentration of Cu

Figure 4.5 shows the sedimentation ratio of several MR fluid samples with different concentration of Al. The increased concentration of Al has also improved the sedimentation ratio of MR fluid samples. The sedimentation ratio of MR fluid sample with 2.5 vol% Al was recorded at 66.18%. The results from MR fluid samples with 3.75 vol% and 5 vol% Al were 77.14% and 88.57%, respectively. As similar to Cu, the enhanced sedimentation ratio from MR fluid samples with Al were due to the formed

aggregations of Al that became a support for the CIP. From these aggregations, every microparticle of CIP was surrounded by the cloud of nano-sized Cu and Al particles (Hajalilou et al., 2016; Iglesias et al., 2012).

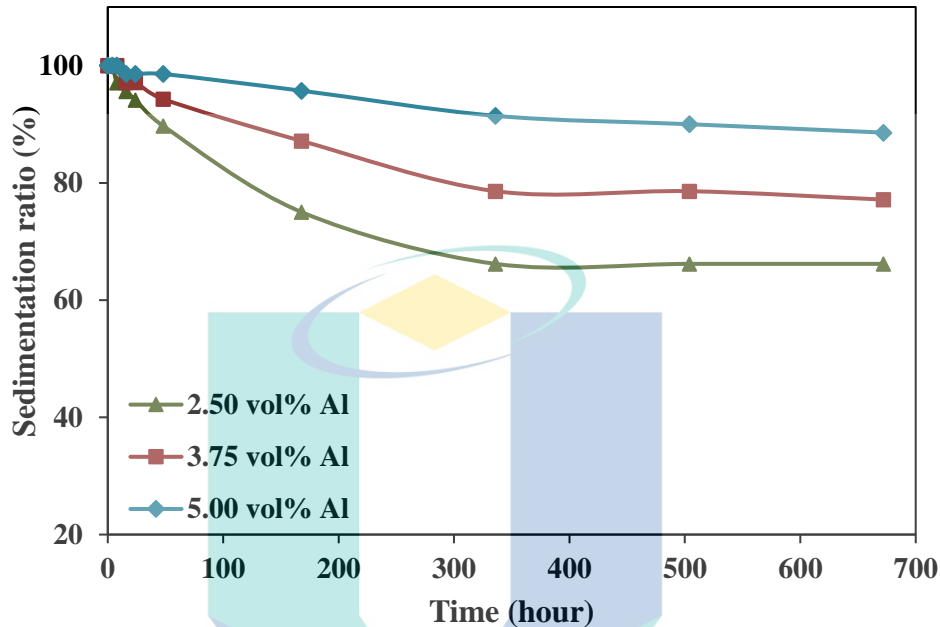


Figure 4.5 Sedimentation ratio of MR fluids at different concentration of Al

Additionally, the results in Figure 4.5 show that MR fluid samples that contained Al performed better in terms of sedimentation ratio than MR fluid samples with Cu. The MR fluid sample with 5 vol% Al recorded its sedimentation ratio at 88.57% while the MR fluid sample with 5 vol% Cu recorded at 86.96%. The difference was contributed by the smaller density of Al particles than Cu particles. Al has a density of 2.7 g/cm^3 while Cu has a density of 8.94 g/cm^3 . The smaller density of Al than Cu leads to slower rate for Al particles to sediment and thus, enabled them to be less affected by the gravitational force (Sattler, 2010).

After assessing the effect of each component in MR fluid samples as in Figure 4.2 to Figure 4.5, it was concluded that the highest concentration of CIP, SiO_2 , Cu, and Al resulted to the highest sedimentation ratio of MR fluid. From Table 4.1, there were two MR fluid samples with the highest concentration of MR fluid components namely MRF-Cu5 and MRF-Al5. The sedimentation ratio of MRF-Cu5 and MRF-Al5 samples were compared with MRF-132DG sample as shown in Figure 4.6. MRF-132DG sample recorded its sedimentation ratio at 77.5% which is lower than the recorded values by MRF-Cu5 and MRF-Al5 samples.

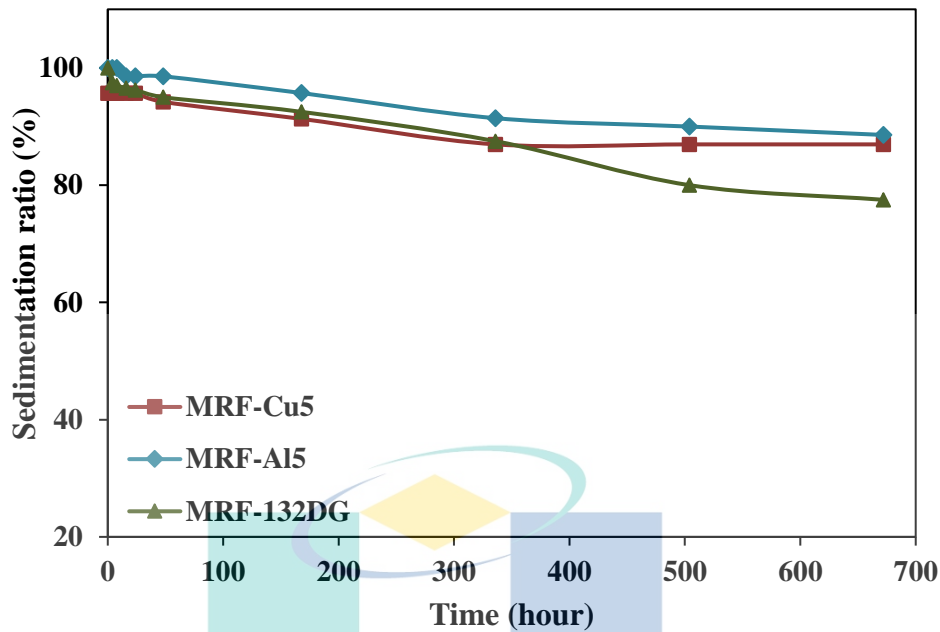


Figure 4.6 Sedimentation ratio of MR fluids and the commercial MRF-132DG

From Figure 4.6, MRF-132DG performed better than MRF-Cu5 for the first 14 days but its sedimentation ratio dropped significantly lower than MRF-Cu5 in the next 14 days. This result indicated that MRF-Cu5 has better sedimentation ratio than MRF-132DG in the longer period. It was also observed that the sedimentation ratio of MRF-Cu5 was not far off with MRF-A15. From Eq. (3.2), the sedimentation ratio enhancement for MRF-Cu5 against MRF-132DG was 12% while the sedimentation ratio enhancement for MRF-A15 against MRF-132DG was 14%.

4.3 Thermal Conductivity Behavior in the Absence of Magnetic Field

Table 4.2 shows the complete data of apparent thermal conductivity in the absence of magnetic field for the synthesized MR fluid samples. The apparent thermal conductivity values were used to analyze the effects of the different combination of components and concentrations in the MR fluid samples. The data were also used for the determination of the optimal composition of nano metal added MR fluid. Meanwhile, thermal conductivity of the commercial MRF-132DG sample was also included for the purpose of comparison.

Table 4.2 Apparent thermal conductivity of MR fluid samples in the absence of magnetic field

| No. | Description | HO (vol%) | Particle concentration (vol%) | | | | Thermal conductivity (W/m·K) |
|-----|-------------|-----------|-------------------------------|------|------|------------------|------------------------------|
| | | | CIP | Cu | Al | SiO ₂ | |
| 1 | MRF | 75.0 | 20 | 0 | 0 | 5.00 | 0.367 |
| 2 | MRF | 60.0 | 40 | 0 | 0 | 0 | 0.620 |
| 3 | MRF-Cu2.5 | 65.0 | 30 | 2.50 | 0 | 2.50 | 0.517 |
| 4 | MRF-Cu3.75 | 57.5 | 35 | 3.75 | 0 | 3.75 | 0.674 |
| 5 | MRF-Cu5 | 75.0 | 20 | 5.00 | 0 | 0 | 0.410 |
| 6 | MRF-Cu5 | 50.0 | 40 | 5.00 | 0 | 5.00 | 0.902 |
| 7 | MRF-Al2.5 | 65.0 | 30 | 0 | 2.50 | 2.50 | 0.530 |
| 8 | MRF-Al3.75 | 57.5 | 35 | 0 | 3.75 | 3.75 | 0.595 |
| 9 | MRF-Al5 | 75.0 | 20 | 0 | 5.00 | 0 | 0.305 |
| 10 | MRF-Al5 | 50.0 | 40 | 0 | 5.00 | 5.00 | 0.696 |
| 11 | MRF-132DG | - | 32 | - | - | - | 0.357 |

Before analyzing the effects of the components and concentrations in the MR fluids, the thermal conductivity of the MR fluids were compared with the estimated values obtained from Maxwell (1904) and Bruggeman (1935) models. As in Eq. (2.2) and (2.3), the estimated values were obtained by defining the particle volume fraction (ϕ), thermal conductivity of carrier fluid (k_c), and thermal conductivity of solid particles (k_p). In this study, ϕ is the volume concentration of CIP (20-40 vol%), k_c is the thermal conductivity of HO (0.156 W/m·K) and k_p is the thermal conductivity of CIP (80.4 W/m·K) (Sattler, 2010).

Figure 4.7 shows the comparison of thermal conductivity between the experimental values and the estimated values from the two models. From the figure, the characteristic trend of the thermal conductivity experimental values is very similar with the estimated values in such a way that the thermal conductivity increases as the concentration of CIP increases (Cha et al., 2010). It can be seen that the experimental values for larger concentration of CIP (30 vol% and above) were near to the predicted values by Bruggeman model. Hence, it was agreed that the experimental values followed the predicted values by Bruggeman model which is suitable for larger concentration Reinecke et al. (2008).

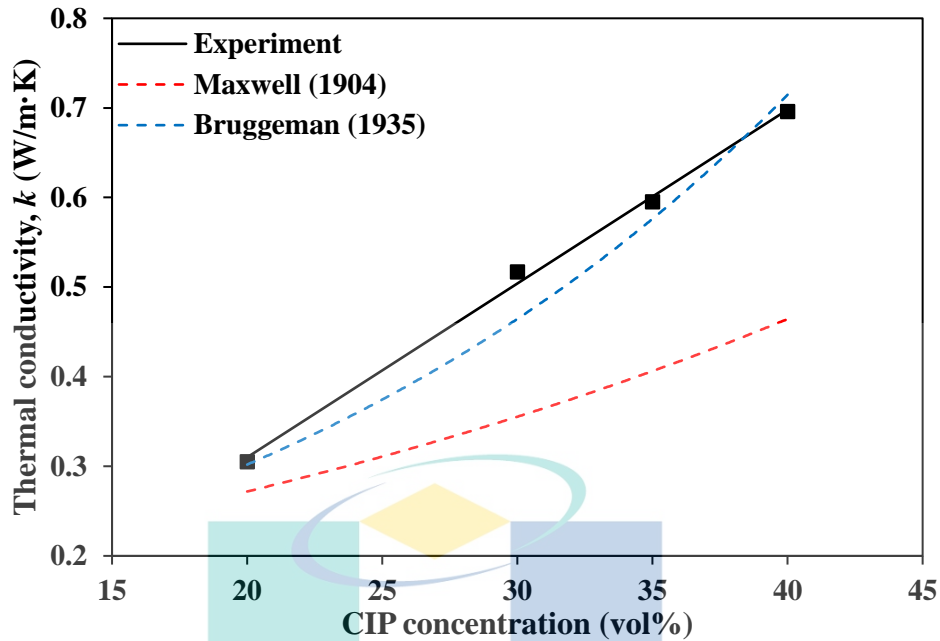


Figure 4.7 Comparison of experimental results with thermal conductivity models as a function of CIP concentration

The concentration of CIP played a major role in the thermal conductivity of MR fluids. The concentration of CIP ranged from 20-40 vol% and a substantial increase of the thermal conductivity value was clearly observed. The thermal conductivity of MR fluid sample with 20 vol% CIP was recorded at only 0.305 W/m·K while the thermal conductivity of MR fluid sample with 40 vol% CIP was recorded at 0.62 W/m·K. The significant increase was because the increased number of CIP provided additional heat conduction paths that allowed heat to be transferred more easily among the solid particles (Forero-Sandoval et al., 2017).

Then, the effects of nano metal additive components to the thermal conductivity of MR fluid samples in the absence of magnetic field was analyzed. The related nano metal additive components were Cu and Al. Figure 4.8 shows the thermal conductivity of MRF-Cu and MRF-Al samples against the different concentration of Cu and Al. For MRF-Cu samples, it was observed that the increased concentration of Cu has increased the thermal conductivity of MR fluid. The thermal conductivity of MRF-Cu2.5 was recorded at 0.517 W/m·K. The thermal conductivity values increased to 0.674 W/m·K for MRF-Cu3.75 and 0.902 W/m·K for MRF-Cu5. The increased thermal conductivity values were due to the fact that Cu is a high thermal conductivity material (401 W/m·K)

(Sattler, 2010). The increased concentration of Cu particles dissipated heat in the MR fluid at a higher rate where a larger amount of heat can be transferred in a second.

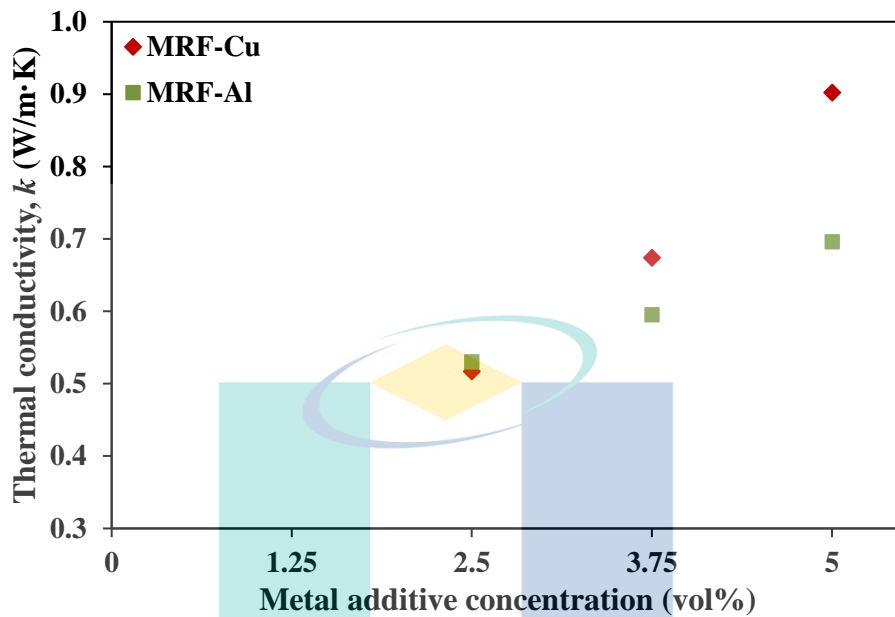


Figure 4.8 Thermal conductivity of MR fluids at different concentration of metal additive

In the meantime, it can be noticed that the increased concentration of Al has also increased the thermal conductivity of MR fluid. The thermal conductivity of MRF-Al2.5 was recorded at 0.530 W/m·K. The thermal conductivity values increased to 0.595 W/m·K for MRF-Al3.75 and 0.696 W/m·K for MRF-Al5. As similar to Cu, the enhanced thermal conductivity was due to the high thermal conductivity material of Al (237 W/m·K) (Sattler, 2010).

Another factor that contributed to the enhancement in Figure 4.8 was the particle size of Cu and Al. Both particles possessed a very high specific surface area (surface to volume ratio) due to their nano-sized form (40-60 nm) and led to a large surface area of the particle-liquid interface. Since heat transfer between particle and fluid takes place at the interface, the large interfacial area from Cu and Al particle would result in high enhancement of the thermal conductivity (Xie et al., 2002). The difference in thermal conductivity values can be observed between Cu and Al. The main cause is purely due to Cu material which has better thermal conductivity with 401 W/m·K than Al with 237 W/m·K.

After evaluating the effect of each component in MR fluid samples as in Figure 4.7 and Figure 4.8, it was concluded that the highest concentration of CIP, Cu, and Al resulted to the highest thermal conductivity of MR fluid. The thermal conductivity of MRF-Cu and MRF-Al samples were then compared with MRF-132DG sample as shown in Figure 4.9 and Figure 4.10, respectively. From Figure 4.9, every MRF-Cu sample showed enhancement of thermal conductivity against the MRF-132DG sample. By using Eq. (3.3), the least enhanced thermal conductivity against MRF-132DG was 15% by MRF-Cu5 with 20 vol% CIP while the most enhanced was 153% by MRF-Cu5 with 40 vol% CIP. The results showed the major role of CIP concentration on improving the thermal conductivity of MR fluid. Additionally, the results also indicated that the concentration of CIP and Cu should be increased simultaneously to achieve the maximum thermal conductivity of MR fluid.

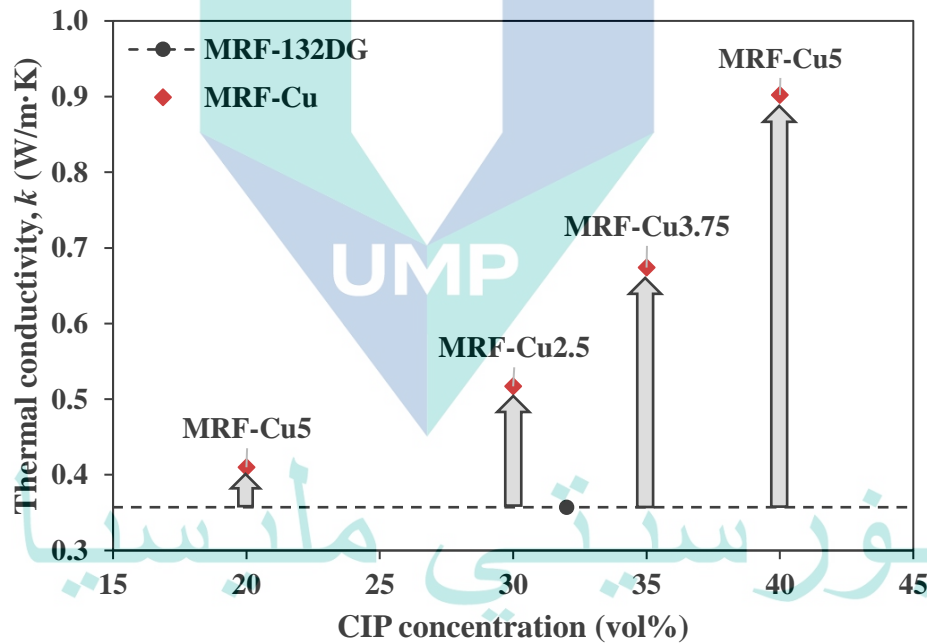


Figure 4.9 Thermal conductivity of MRF-Cu samples against MRF-132DG

Figure 4.10 shows the thermal conductivity of MRF-Al samples against the MRF-132DG sample. It can be seen that every MRF-Al sample showed enhancement of thermal conductivity against the MRF-132DG sample except MRF-Al5 with 20 vol% CIP. The MRF-Al5 (20 vol% CIP) sample recorded -15% of thermal conductivity enhancement. The result showed that the addition of Al may not necessarily enhance the thermal conductivity of MR fluid at low concentration of CIP (20 vol%). For the other MRF-Al samples, they recorded uniform enhancement of thermal conductivity with

increased concentration of CIP and Al. The highest thermal conductivity enhancement against MRF-132DG was 95% by MRF-A15 (40 vol% CIP).

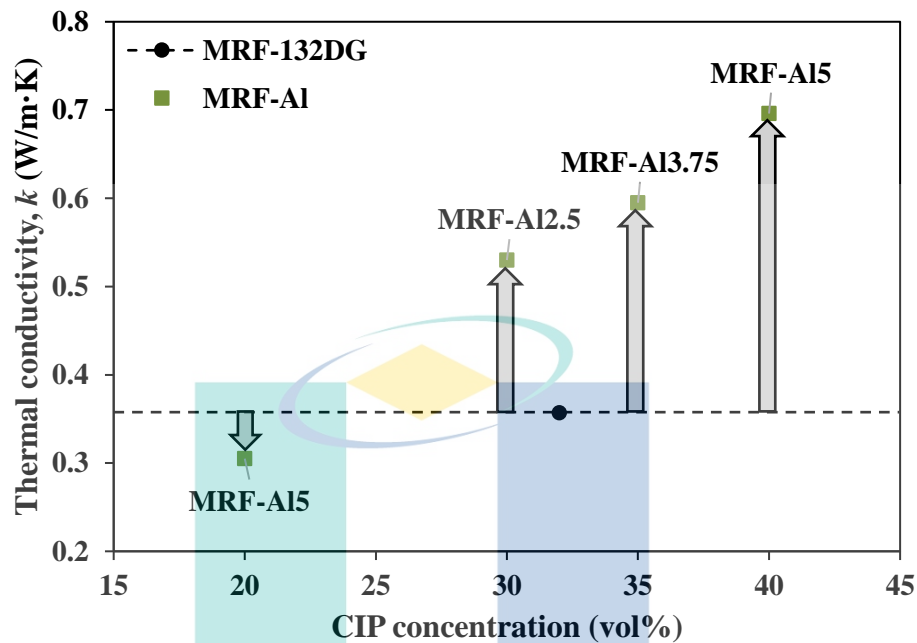


Figure 4.10 Thermal conductivity of MRF-A1 samples against MRF-132DG

4.4 Mixture Optimization by Design of Experiment

After analyzing the effects of a different combination of components and concentrations in the MR fluid samples, the combined D-optimal model was used to determine the selected category and optimal composition of nano metal added MR fluid sample. The optimal composition was to achieve high sedimentation ratio and apparent thermal conductivity properties. From the combined D-optimal model, three solutions with different optimal compositions and corresponding properties are shown in Table 4.3.

The model predicted the values of thermal conductivity and sedimentation ratio properties and provided the desirability percentage for each solution.

Table 4.3 Optimal composition solutions by combined D-optimal model

| Variables | Solution 1 | Solution 2 | Solution 3 |
|----------------------|------------|------------|------------|
| HO | 50.00 | 50.19 | 57.50 |
| CIP | 40.00 | 40.00 | 34.50 |
| SiO ₂ | 5.00 | 4.81 | 4.25 |
| Metal additive | 5.00 | 5.00 | 3.75 |
| Sedimentation ratio | 13.7 | 8.6 | 22.6 |
| Thermal conductivity | 0.881 | 0.722 | 0.668 |
| Category | MRF-Cu | MRF-Al | MRF-Cu |
| Desirability (%) | 93.4 | 86.4 | 69.4 |

From the table, it is clearly shown that only Solution 1 has the desirability with over 90%. Hence, MRF-Cu has been selected as the suitable category for an optimal MR fluid. MRF-Cu required maximum concentrations of CIP, SiO₂, and Cu because the maximum concentrations from these components contributed to high thermal conductivity and high sedimentation ratio. The predicted values of thermal conductivity and sedimentation ratio given by the combined D-optimal model were not far from the actual values. Hence, the given composition of MR fluid components were accepted as the optimal composition.

4.5 Thermal Conductivity Behavior in the Presence of Magnetic Field

From the results of mixture optimization by combined D-optimal model, MRF-Cu was selected as the suitable category for high sedimentation ratio and high thermal conductivity in the absence of magnetic field. Hence, MRF-Cu category was used for the analysis of thermal conductivity behavior in the presence of magnetic field. The analysis involved various concentrations (1, 3, and 5 vol%) of nano Cu additive as in Table 3.4 to analyze the effects of the additive concentration on the thermal conductivity behavior. The thermal conductivity of the commercial MRF-132DG sample in the presence of magnetic field was used as the reference sample.

The analysis of thermal conductivity behavior in the presence of magnetic field was conducted by the GHP module. The calculation of thermal conductivity in the presence of magnetic field by the GHP module was as shown as Eq. (3.7). Table 4.4 shows the related parameters for the calculation of thermal conductivity for MRF-Cu samples. From the table, the two parameters that contributed to the thermal conductivity difference of MRF-Cu samples were the heat flow rate (Q) and the temperature difference (ΔT) between thermocouple T_1 and thermocouple T_3 . From the table, it was observed that Q for the samples significantly increased to achieve the desired temperature at T_1 . The Q was increased from 0.33-9.32 W for MRF-Cu1, 0.35-10.61 W for MRF-Cu3, and 0.48-11.85 W for MRF-Cu5. Q was at the maximum for each sample when the temperature was at 70 °C. The result was due to the increased voltage and current supplied to the heater to achieve the required temperature of the samples.

Table 4.4 Input parameters for thermal conductivity calculation in the presence of magnetic field

| Sample | Thickness, l (m) | Surface area, A (m ²) | Heat flow rate, Q (W) | Temperature at T_1 , (°C) | Temperature difference, ΔT (°C) |
|---------|--------------------|-------------------------------------|-------------------------|-----------------------------|---|
| MRF-Cu1 | 0.03 | 0.00126 | 0.33 | 30 | 1.25 |
| | | | 4.65 | 50 | 18.00 |
| | | | 9.32 | 70 | 34.50 |
| MRF-Cu3 | 0.03 | 0.00126 | 0.35 | 30 | 1.00 |
| | | | 5.45 | 50 | 15.50 |
| | | | 10.61 | 70 | 30.25 |
| MRF-Cu5 | 0.03 | 0.00126 | 0.48 | 30 | 1.00 |
| | | | 6.38 | 50 | 13.00 |
| | | | 11.85 | 70 | 26.50 |

Meanwhile, Table 4.4 also shows that at elevated temperature, ΔT significantly decreased as the concentration of Cu increased. When T_1 is 70°C, MRF-Cu1 which has 1 vol% Cu recorded its ΔT at 34.5 °C while MRF-Cu5 recorded its ΔT at 26.5 °C. This behavior was due to the existence of more chain-like formation of structures formed from the CIP and Cu particles in MRF-Cu5 that became highly conductive “bridges” when being magnetized (Cha et al., 2010). The bridges subsequently transferred heat from T_1 to T_3 in a more efficient manner.

To demonstrate the existence effect of the chain-like structures, the results of thermal conductivity from the GHP module in the absence and the presence of magnetic field were compared. Figure 4.11 shows the comparison of thermal conductivity from MRF-Cu5 and MRF-132DG samples when being magnetized at 0.075 Tesla. It was clearly observed that the presence of magnetic field has increased the thermal conductivity in both MR fluid samples. The thermal conductivity of MRF-132DG was increased from 0.361 W/m·K to 0.464 W/m·K, an enhancement of about 29%. Meanwhile, the thermal conductivity enhancement of MRF-Cu5 was about 19% (0.925-1.102 W/m·K). The enhancement from these samples was parallel with the study by Forero-Sandoval et al. (2017). They enhanced the thermal conductivity of MR fluid at 77% (0.43-0.76 W/m·K) when being magnetized at 0.005 Tesla.

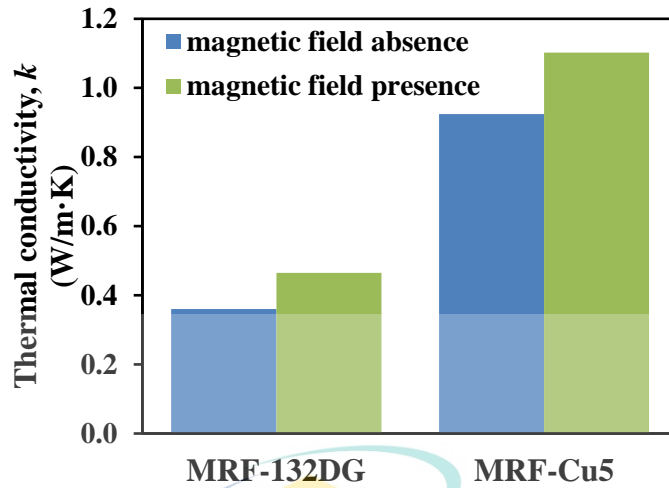


Figure 4.11 Comparison of thermal conductivity by GHP module in the absence and the presence of magnetic field

Finally, Figure 4.12 shows the thermal conductivity of MRF-Cu samples against MRF-132DG sample in the presence of magnetic field at 30 °C. The results of MRF-Cu samples at higher temperatures were given in Appendix C. It is clearly seen that every MRF-Cu sample at different temperatures showed enhancement of thermal conductivity against the MRF-132DG sample. In the presence of magnetic field, the magnetic particles in MRF-Cu samples and MRF-132DG sample developed chain-like formations in parallel with the magnetic flux that were supplied by the magnets. These formations provided high conductivity heat transfer paths.

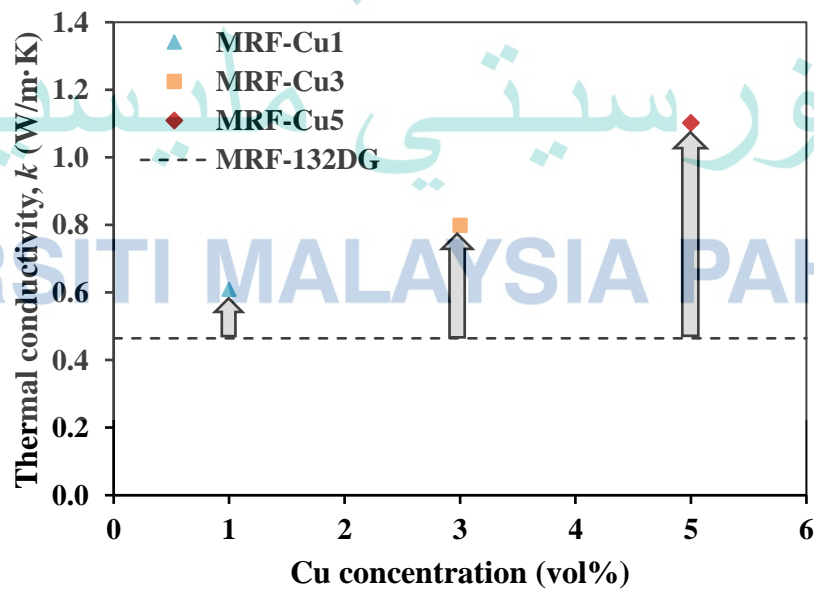


Figure 4.12 Thermal conductivity of MRF-Cu samples against MRF-132DG in the presence of magnetic field at 30 °C

Additionally, MRF-Cu1 recorded at 0.609 W/m·K of thermal conductivity and the enhancement against MRF-132DG was 31%. MRF-Cu5 recorded at 1.102 W/m·K and has the highest enhancement against MRF-132DG which was 137%. The findings showed that the maximum concentration of Cu resulted to the highest enhancement of thermal conductivity, especially in the presence of magnetic field. The result was also parallel with the study by Eastman et al. (2001) in which they increased the thermal conductivity ratio to 40% with 0.3 vol% of Cu. The increased concentration of Cu massively enhanced the thermal conductivity of MR fluid as Cu material is known to be among the highest thermal conductivity material.

4.6 Magnetorheological Response of MR Fluid

From the results of mixture optimization by combined D-optimal model, MRF-Cu was selected as the suitable category for high sedimentation ratio and high thermal conductivity in the absence of magnetic field. Hence, as similar to the analysis of thermal conductivity behavior in the presence of magnetic field, MRF-Cu category was used for the analysis of MR response in the presence of magnetic field. The analysis involved various concentrations (1, 3, and 5 vol%) of nano Cu additive as in Table 3.4 to analyze the effects of the additive concentration on the MR response. The MR response of the commercial MRF-132DG sample in the presence of magnetic field was used as the reference sample.

4.6.1 Rheological Response

Figure 4.13 shows the viscosity of MRF-Cu samples under different shear rates in the absence of magnetic field. The complete data of each run were provided in Appendix B. It is observed that the MRF-Cu samples experienced a decrease in shear viscosity as the shear rate increased. The behavior was as a result of shear-thinning characteristic of an MR fluid (Dorosti et al., 2020). The particles in the samples formed adjacent layers from the applied shear force by the rheometer. These adjacent layers made the samples to flow easily and consequently reduced the shear viscosity of the samples. The result was also parallel with the previous study by Piao et al. (2015). At 0.1 s⁻¹ of shear rate, MRF-Cu5 demonstrated the highest viscosity at 223.3 Pa·s while MRF-Cu1 has the lowest viscosity at 61.5 Pa·s. The higher viscosity in MRF-Cu5 was obviously due to the high concentration of Cu.

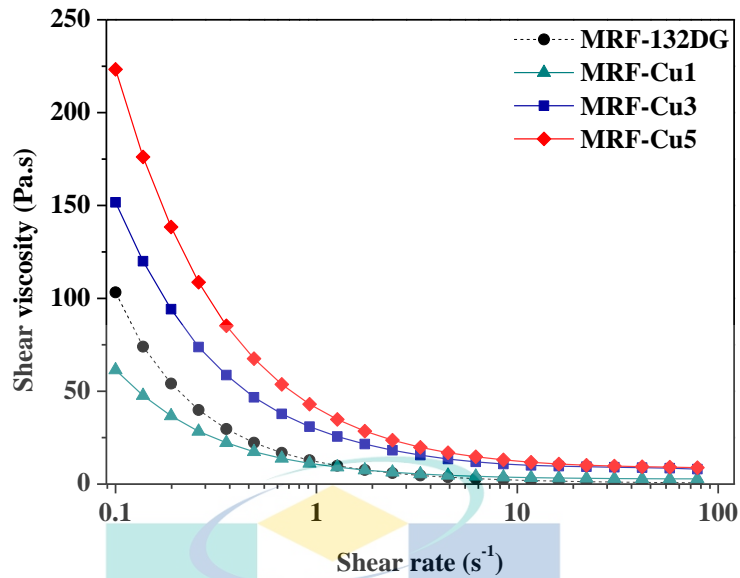


Figure 4.13 Shear viscosity of MRF-Cu samples under different shear rates in the absence of magnetic field

Figure 4.14 represents the viscosity of MRF-Cu samples under different shear rates in the presence of magnetic field (0.4 Tesla). The presence of magnetic field has led to the increment of viscosity for MRF-Cu samples. As a comparison with the result in Figure 4.13, MRF-Cu5 showed an increase of viscosity from 223.3 Pa.s to 534.2 kPa.s. The presence of magnetic field has resulted into a robust columnar structure of magnetic particles which has led to the holding of the rheometer's rotating upper plate at the given shear rate (Lim et al., 2004).

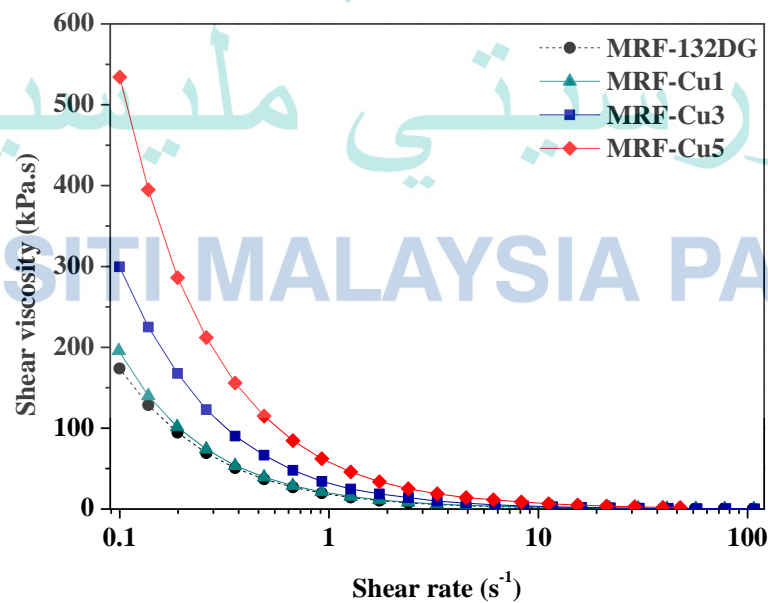


Figure 4.14 Shear viscosity of MRF-Cu samples under different shear rates in the presence of magnetic field

Furthermore, MRF-Cu1 sample that has the lowest viscosity in the absence of magnetic field has recorded higher viscosity than MRF-132DG in the presence of magnetic field. It was assumed that the presence of Cu in MRF-Cu1 contributed to the increase in viscosity. This is because the combination of nanoparticles (Cu) and microparticles (CIP) in the MRF-Cu1 created bonds between these particles (Ashtiani et al., 2015). The bonds translated to stronger chains of particles when MRF-Cu1 is being magnetized. Hence, the higher shear force needed to break the chains made MRF-Cu1 possessed a higher viscosity than MRF-132DG.

Meanwhile, the shear stress of MRF-Cu samples under different shear rates in the absence of magnetic field is shown in Figure 4.15. It was clearly seen that the shear stress for all samples was increased with increasing shear rate. The reason is that shear stress is proportional to shear rate which complies with the behavior of a Newtonian fluid (Wang, Zhao, et al., 2017). The shear stress of MRF-132DG was initially higher than MRF-Cu1 at 0.1 s^{-1} but it has decreased substantially and less than MRF-Cu1 when the shear rate was above 2 s^{-1} . The reason for this behavior was because of the shear-thinning as explained in Figure 4.13. Since viscosity is the measure of shear stress divided by the shear rate, the shear-thinning effect in MRF-132DG that significantly decreased its viscosity at higher shear rates has given lower shear stress than MRF-Cu1 (Chen, Huang, Shu, Sun, & Jian, 2013).

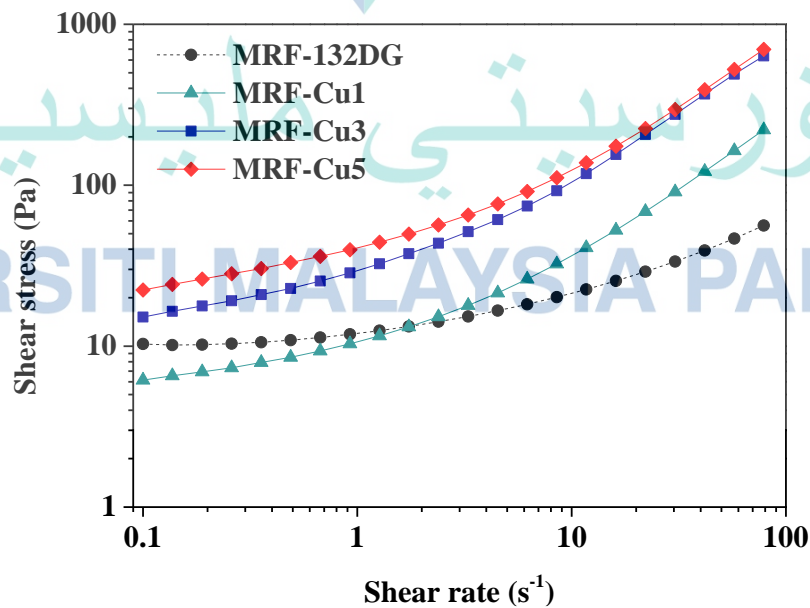


Figure 4.15 Shear stress of MRF-Cu samples under different shear rates in the absence of magnetic field

Another finding from Figure 4.15 shows that MRF-Cu5 has the highest shear stress (698.8 Pa) at the maximum shear rate. Comparing with MRF-132DG (56.1 Pa), the higher shear stress shown from MRF-Cu5 was attributed to the increased concentration of CIP (40 vol%) and the presence of Cu (5 vol%). The increased concentration of CIP and the presence of Cu has led to increased viscosity of the sample and subsequently resulted in higher shear stress.

Figure 4.16 shows the shear stress of MRF-Cu samples over different magnetic field strengths at a constant 100 s^{-1} of shear rate. From the figure, the shear stress for the samples was increased with increasing magnetic field strength. When subjected to the increased magnetic field strength, more stable chain structures of the CIP were formed in the samples (Piao et al., 2015). Due to the stronger chains, the shear stress of the samples increased.

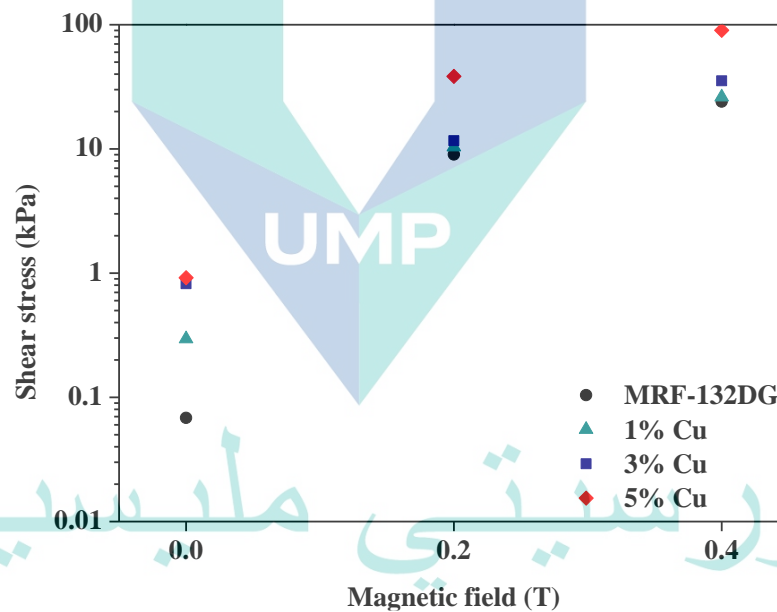


Figure 4.16 Shear stress of MRF-Cu samples under different magnetic fields

At 0.4 T, the highest shear stress recorded was from MRF-Cu5 with 90.3 kPa while the shear stress from MRF-132DG was 24 kPa. The result from MRF-Cu5 was an enhancement of over 276% when compared to MRF-132DG. The increase was achieved due to the higher number of particle chains formed from the CIP and Cu particles in the presence of magnetic field (Wang, Ma, et al., 2017; Xu & Chen, 2016).

4.6.2 Magnetization Response

Figure 4.17 shows the magnetization of MRF-Cu samples under different magnetic flux density. It is clearly seen that MRF-Cu samples have higher magnetization than MRF-132DG sample. The highest magnetization was recorded by MRF-Cu5 at 30.98 emu while the lowest magnetization was by MRF-132DG at 18.08 emu. Hence, the magnetization enhancement by MRF-Cu5 against MRF-132DG was 71%. The enhancement in MRF-Cu5 sample was due to its higher concentration of CIP (40 vol%) than MRF-132DG (32 vol%) and the strong presence of Cu (5 vol%). It was assumed that the aggregates of micron-sized CIP has hindered its magnetization ability but with the addition of Cu, the nano-sized particles avoided the formation of CIP aggregates by forming clouds around each CIP and in turn, produced more anisotropic structures (de Vicente, Klingenberg, & Hidalgo-Alvarez, 2011; Portillo & Iglesias, 2017). From the anisotropic structures, the bonds between particles were stronger and consequently resulted to improved magnetization performance in the presence of magnetic field.

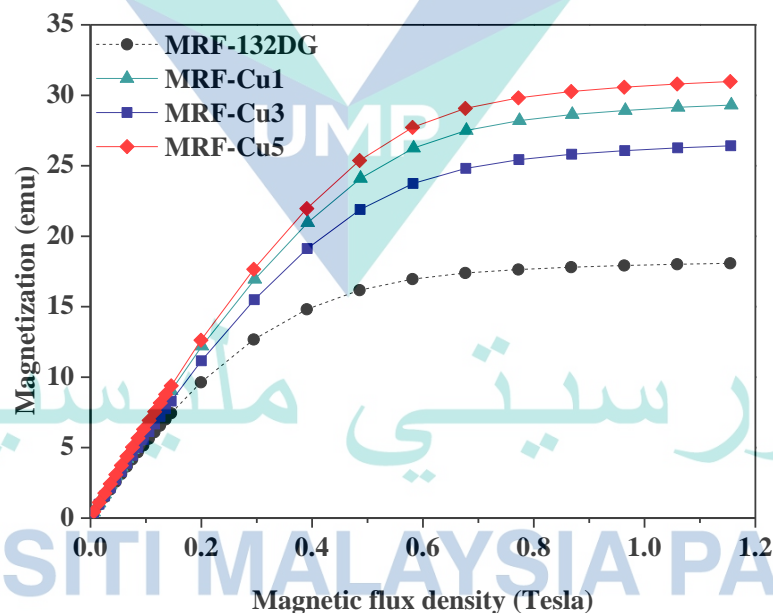


Figure 4.17 Magnetic properties of MR fluid samples under different magnetic flux density

Meanwhile, it can be observed that the magnetization in MRF-Cu samples was approaching stagnant value as the magnetic flux density was increased. When the magnetization value becomes stagnant, a further increase of magnetic flux density will not induce the magnetization anymore. The results indicated the capability of the MRF-Cu samples almost reaching their own magnetic saturation point. From the figure,

it was predicted that MRF-Cu5 has the highest magnetic saturation. The high value of magnetic saturation points to the high yield strength of MRF-Cu5 as the chain of particles will become very stiff and hard to be fragmented (Anupama et al., 2018).

4.7 Summary

This chapter started with the effect of sedimentation ratio for nano metal added MR fluid samples. The samples were divided into three categories of MRF, MRF-Cu, and MRF-Al. From the results, it was concluded that the sample with the highest concentration of CIP (40 vol%), SiO₂ (5 vol%), and nano metal (5 vol%) resulted to the highest sedimentation ratio of MR fluid. Two MR fluid samples has the highest concentration of MR fluid components namely MRF-Cu5 from the MRF-Cu category and MRF-Al5 from the MRF-Al category. The sedimentation ratio of both samples were compared with MRF-132DG sample and the enhancement against MRF-132DG was 12% for MRF-Cu5 and 14% for MRF-Al5.

The chapter continued with the apparent thermal conductivity behavior of the MR fluid samples in the absence of magnetic field. As similar to the findings of sedimentation ratio behavior, the highest concentration of CIP (40 vol%), Cu (5 vol%), and Al (5 vol%) has resulted to the highest thermal conductivity of MR fluid. The sample with the most enhanced thermal conductivity (153%) against MRF-132DG was by MRF-Cu5 (0.902 W/m·K). From the analysis, it was indicated that the concentration of CIP and Cu must be increased simultaneously to achieve the maximum thermal conductivity of MR fluid. MRF-Cu category showed superiority against MRF-Al category since the thermal conductivity enhancement against MRF-132DG by MRF-Al5 was only 95%.

Next, the chapter discussed the mixture optimization of MR fluid by the combined D-optimal model for both sedimentation ratio and apparent thermal conductivity properties. From the result, MRF-Cu was the selected category to achieve the highest sedimentation ratio and thermal conductivity while its optimal composition was 40 vol% for CIP and 5 vol% for each additive (Cu and SiO₂). MRF-Cu category was then used for the analysis of thermal conductivity behavior in the presence of magnetic field and MR response. MRF-Cu samples with various concentrations of Cu (1, 3, and 5 vol%) were used for the analyses to investigate the effects of Cu concentration.

The chapter followed with the thermal conductivity behavior of MRF-Cu samples in the presence of magnetic field. By using the GHP module, the thermal conductivity of MRF-Cu5 was increased from 0.925 W/m·K in the absence of magnetic field to 1.102 W/m·K in the presence of magnetic field. The result was from the effect of the chain-like structures formed by the particles in MRF-Cu5 when experiencing magnetization. MRF-Cu5 recorded at 1.102 W/m·K and has the highest enhancement against MRF-132DG at 137%. The result indicated that the maximum concentration of Cu resulted to the highest enhancement of thermal conductivity, especially in the presence of magnetic field.

Finally, the chapter ended with the MR response of MRF-Cu samples in the presence of magnetic field. The presence of magnetic field has led to the increment of viscosity and shear stress for MRF-Cu samples. MRF-Cu5 has the highest shear stress (90.3 kPa) with 276% enhancement against MRF-132DG due to the higher number of particle chains formed from CIP and Cu particles in the presence of magnetic field. Meanwhile, MRF-Cu5 recorded the highest magnetization (30.98 emu) and magnetic saturation with 71% enhancement against MRF-132DG. The addition of nano-sized Cu has avoided the formation of CIP aggregates by forming clouds around each CIP and resulted to stronger bonds between the particles.

اونيورسيتي ملايسيا قهغ

UNIVERSITI MALAYSIA PAHANG

CHAPTER 5

CONCLUSION

5.1 Summary of Findings

This thesis has developed a new formulation of MR fluid with nano metal additive. The new formulation focused on the best composition of MR fluid components to simultaneously achieve high sedimentation ratio and enhanced thermophysical property. The combined D-optimal model which is new in the field of MR fluid synthesization was introduced to identify the best composition. From the findings, the new formulation of MR fluid was from MRF-Cu5 with 50 vol% HO, 40 vol% CIP, 5 vol% SiO₂, and 5 vol% nano metal Cu. With high sedimentation ratio and high thermal conductivity properties, the nano metal added MR fluid has potential as the candidate for elevated temperature applications.

The nano metal added MR fluid was analyzed for enhanced thermophysical property in the presence of magnetic field. A module based on the GHP method was developed to determine the thermal conductivity of the nano metal added MR fluid in the presence of magnetic field. Thermal conductivity of MRF-Cu5 was recorded at 1.102 W/m·K and has the highest enhancement against MRF-132DG at 137%. The findings indicated that the maximum concentration of Cu resulted to the highest enhancement of thermal conductivity in the presence of magnetic field.

The effects of nano metal added MR fluid on MR response were evaluated in the presence of magnetic field. The recorded shear stress (90.3 kPa) from MRF-Cu5 almost reached the maximum yield stress (100 kPa) of a typical MR fluid. MRF-Cu5 only needed 2 A to achieve the desired shear stress. The small amount of current required is beneficial in terms of energy-saving for MR devices. The low current would inhibit significant increase in the devices' operating temperature and avoid the adverse effects on their performance. MRF-Cu5 is thought to be very suitable in elevated temperature applications with direct-shear mode such as MR clutch and MR brake.

5.2 Recommendation for Future Works

As a whole, the objectives of this research have been achieved. The findings in this work provide a good platform for improving the thermophysical property of MR fluids. Following these investigations, several extensions to this research could be conducted to strengthen or expand the outcomes. Thus, the recommendations for future works are as follows:

- i. Investigation of redispersibility for the nano metal added MR fluid. The study on the redispersibility is part of the stability performance of an MR fluid. It is crucial particularly for the highly concentrated MR fluid to determine its ability to redisperse after reaching full sedimentation and after being magnetized.
- ii. Investigation of other thermophysical properties such as specific heat for the nano metal added MR fluid. While the enhanced nano metal added MR fluid has the ability to efficiently transfer heat by conduction, the investigation of its specific heat is also important to measure its temperature stability especially at high temperature state.
- iii. Modification of GHP module that is equipped with magnetic field from induced current. From this modification, the intensity of magnetic field in the module can be varied to analyze the effects on MR fluid. This extension of study can replicate most MR devices that have the ability to control magnetic field strength.
- iv. Development of a prototype of direct-shear mode MR device such as MR brake. From the prototype, the new nano metal added MR fluid can be utilized to analyze its effects on the device performance. Monitoring of temperature in the device can also be conducted to determine the impact of using the high thermal conductivity MR fluid.

REFERENCES

- Acharya, S., Tak, R. S. S., Singh, S. B., & Kumar, H. (2020). Characterization of magnetorheological brake utilizing synthesized and commercial fluids. *Materials Today: Proceedings*.
- Agromayor, R., Cabaleiro, D., Pardinas, A. A., Vallejo, J. P., Fernandez-Seara, J., & Lugo, L. (2016). Heat transfer performance of functionalized graphene nanoplatelet aqueous nanofluids. *Materials*, 9(6), 455.
- Alves, S., Alcantara, M. R., & Neto, A. M. F. (2009). The effect of hydrophobic and hydrophilic fumed silica on the rheology of magnetorheological suspensions. *Journal of Rheology*, 53(3), 651-662.
- Anupama, A. V., Kumaran, V., & Sahoo, B. (2018). Application of monodisperse Fe₃O₄ submicrospheres in magnetorheological fluids. *Journal of Industrial and Engineering Chemistry*, 67, 347-357.
- Aruna, M. N., Rahman, M. R., Joladarashi, S., & Kumara, H. (2019). Investigating Sedimentation and Rheological properties of Magnetorheological Fluids using various carrier fluids. *IOP Conference Series: Materials Science and Engineering*, 577, 012049.
- Ashtiani, M., Hashemabadi, S., & Ghaffari, A. (2015). A review on the magnetorheological fluid preparation and stabilization. *Journal of Magnetism and Magnetic Materials*, 374, 716-730.
- ASTM. (2014). *Standard test method for determination of thermal conductivity of soil and soft rock by thermal needle probe procedure*. (ASTM D5334-14). Retrieved from <http://www.astm.org/cgi-bin/resolver.cgi?D5334-14>
- Bae, D. H., Choi, H. J., Choi, K., Nam, J. D., Islam, M. S., & Kao, N. (2017). Microcrystalline cellulose added carbonyl iron suspension and its magnetorheology. *Colloids and Surfaces A: Physicochemical and Engineering Aspects*, 514, 161-167.
- Bagheli, S., Fadafan, H. K., Orimi, R. L., & Ghaemi, M. (2015). Synthesis and experimental investigation of the electrical conductivity of water based magnetite nanofluids. *Powder Technology*, 274, 426-430.
- Bateer, B., Qu, Y., Tian, C., Du, S., Ren, Z., Wang, R., . . . Fu, H. (2014). Facile synthesis of stable magnetic fluid using size-controlled Fe₃O₄ nanoparticles. *Materials Research Bulletin*, 56, 34-38.
- Bica, I., Liu, Y. D., & Choi, H. J. (2013). Physical characteristics of magnetorheological suspensions and their applications. *Journal of Industrial and Engineering Chemistry*, 19(2), 394-406.

- Bomberg, M., & Solvason, K. (1981). *Precision and accuracy of guarded hot plate method*. Paper presented at the 17th International Thermal Conductivity Conference, Gaithersburg, Maryland.
- Bossis, G., Kuzhir, P., Lopez-Lopez, M., Meunier, A., & Magnet, C. (2013). Importance of Interparticle Friction and Rotational Diffusion to Explain Recent Experimental Results in the Rheology of Magnetic Suspensions. *Magnetorheology: Advances and Applications*, 1.
- Bruggeman, D. (1935). The prediction of the thermal conductivity of heterogeneous mixtures. *Annals of Physics*, 24, 636-664.
- Carlson, J., Catanzarite, D., & Clair, K. S. (1996). Commercial magneto-rheological fluid device. *International Journal of Modern Physics B*, 10(23-24), 2857-2865.
- Cha, G., Ju, Y. S., Ahur , L. A., & Wereley, N. M. (2010). Experimental characterization of thermal conductance switching in magnetorheological fluids. *Journal of Applied Physics*, 107(9), 09B505.
- Chae, H., Piao, S., Maity, A., & Choi, H. (2015). Additive role of attapulgite nanoclay on carbonyl iron-based magnetorheological suspension. *Colloid and Polymer Science*, 293(1), 89-95.
- Chen, S., Huang, J., Jian, K., & Ding, J. (2015). Analysis of influence of temperature on magnetorheological fluid and transmission performance. *Advances in Materials Science and Engineering*, 2015, 1-7.
- Chen, S., Huang, J., Shu, H., Sun, T., & Jian, K. (2013). Analysis and testing of chain characteristics and rheological properties for magnetorheological fluid. *Advances in Materials Science and Engineering*, 2013, 1-6.
- Cheng, H., Hong, W., & Liu, C. (2014). Study on preparation and thermal conductivity of high stability magnetorheological fluids. *Journal of the Chinese Advanced Materials Society*, 2(2), 130-137.
- Cheng, H., Wang, M., Liu, C., & Wereley, N. M. (2018). Improving sedimentation stability of magnetorheological fluids using an organic molecular particle coating. *Smart Materials and Structures*, 27(7), 075030.
- Cheng, H., Zhang, X., Liu, G., Ma, W., & Wereley, N. M. (2016). Measuring the sedimentation rate in a magnetorheological fluid column via thermal conductivity monitoring. *Smart Materials and Structures*, 25(5), 055007.
- Cheng, X., McCoy, J. H., Israelachvili, J. N., & Cohen, I. (2011). Imaging the microscopic structure of shear thinning and thickening colloidal suspensions. *Science*, 333(6047), 1276-1279.
- Cho, M. S., Lim, S. T., Jang, I. B., Choi, H. J., & Jhon, M. S. (2004). Encapsulation of spherical iron-particle with PMMA and its magnetorheological particles. *IEEE Transactions on Magnetics*, 40(4), 3036-3038.

- Chon, C. H., Kihm, K. D., Lee, S. P., & Choi, S. U. S. (2005). Empirical correlation finding the role of temperature and particle size for nanofluid (Al_2O_3) thermal conductivity enhancement. *Applied Physics Letters*, 87(15), 1531071-1531073.
- Cruze, D., Hemalatha, G., Jebadurai, S. V. S., Sarala, L., Tensing, D., & Christy, S. J. E. (2018). A review on the magnetorheological fluid, damper and its applications for seismic mitigation. *Civil Engineering Journal*, 4(12), 3058-3074.
- Cvek, M., Mrlik, M., Moucka, R., & Sedlacik, M. (2018). A systematical study of the overall influence of carbon allotrope additives on performance, stability and redispersibility of magnetorheological fluids. *Colloids and Surfaces A: Physicochemical and Engineering Aspects*, 543, 83-92.
- Das, P. K. (2017). A review based on the effect and mechanism of thermal conductivity of normal nanofluids and hybrid nanofluids. *Journal of Molecular Liquids*, 240, 420-446.
- de Vicente, J., Klingenberg, D. J., & Hidalgo-Alvarez, R. (2011). Magnetorheological fluids: a review. *Soft Matter*, 7(8), 3701-3710.
- Diaz-Bleis, D., Vales-Pinzón, C., Freile-Pelegrián, Y., & Alvarado-Gil, J. J. (2014). Thermal characterization of magnetically aligned carbonyl iron/agar composites. *Carbohydrate Polymers*, 99(0), 84-90.
- Dimitrakis, B., & Profilet, R. (2008). Go with the flow in selecting the right liquid. Retrieved from <https://www.hydraulicspneumatics.com/technologies/hydraulic-fluids/article/21883713/go-with-the-flow-in-selecting-the-right-fluid>
- Dipalkumar, M. P., & Upadhyay, R. V. (2018). Predicting the thermal sensitivity of MR damper performance based on thermo-rheological properties. *Materials Research Express*, 6(1), 015707.
- Dixit, R. K., & Buckner, G. D. (2005). Sliding mode observation and control for semiactive vehicle suspensions. *Vehicle System Dynamics*, 43(2), 83-105.
- Dorosti, A. H., Ghatee, M., & Norouzi, M. (2020). Preparation and characterization of water-based magnetorheological fluid using wormlike surfactant micelles. *Journal of Magnetism and Magnetic Materials*, 498, 166193.
- Eastman, J. A., Choi, S. U. S., Li, S., Yu, W., & Thompson, L. J. (2001). Anomalously increased effective thermal conductivities of ethylene glycol-based nanofluids containing copper nanoparticles. *Applied Physics Letters*, 78(6), 718-720.
- Eriksson, L. (2001). Design of Experiments, Principles and Applications. *Journal of Chemometrics*, 15(5), 495-496.
- Esfe, M. H., Firouzi, M., & Afrand, M. (2018). Experimental and theoretical investigation of thermal conductivity of ethylene glycol containing functionalized single walled carbon nanotubes. *Physica E: Low-dimensional Systems and Nanostructures*, 95, 71-77.

- Esfe, M. H., Rostamian, H., & Shabani-samghabadi, A. (2017). Application of three-level general factorial design approach for thermal conductivity of MgO/water nanofluids. *Applied Thermal Engineering*, 127, 1194-1199.
- Esfe, M. H., Saedodin, S., Biglari, M., & Rostamian, H. (2015). Experimental investigation of thermal conductivity of CNTs-Al₂O₃/water: A statistical approach. *International Communications in Heat and Mass Transfer*, 69, 29-33.
- Esmailnezhad, E., Jin Choi, H., Schaffie, M., Gholizadeh, M., Ranjbar, M., & Hyuk Kwon, S. (2017). Rheological analysis of magnetite added carbonyl iron based magnetorheological fluid. *Journal of Magnetism and Magnetic Materials*, 444(Supplement C), 161-167.
- Fang, F. F., Choi, H. J., & Seo, Y. (2010). Sequential coating of magnetic carbonyliron particles with polystyrene and multiwalled carbon nanotubes and its effect on their magnetorheology. *ACS Applied Materials & Interfaces*, 2(1), 54-60.
- Fang, F. F., Liu, Y. D., & Choi, H. J. (2009). Fabrication of carbonyl iron embedded polycarbonate composite particles and magnetorheological characterization. *IEEE Transactions on Magnetics*, 45(6), 2507-2510.
- Farjoud, A., Vahdati, N., & Fah, Y. F. (2008). MR-fluid yield surface determination in disc-type MR rotary brakes. *Smart Materials and Structures*, 17(3), 035021.
- Fei, C., Zuzhi, T., Xiangfan, W., Shuyou, W., & Hao, L. (2018). Research on preparation and characteristics of a novel transmission magnetorheological fluid. *Journal of Magnetism*, 23(1), 99-105.
- Fonseca, H., Gonzalez, E., Restrepo, J., Parra, C., & Ortiz, C. (2016). *Magnetic effect in viscosity of magnetorheological fluids*. Paper presented at the Journal of Physics: Conference Series.
- Forero-Sandoval, I. Y., Vega-Flick, A., Alvarado-Gil, J. J., & Medina-Esquivel, R. A. (2017). Study of thermal conductivity of magnetorheological fluids using the thermal-wave resonant cavity and its relationship with the viscosity. *Smart Materials and Structures*, 26(2), 025010.
- Gao, C. Y., Lu, Q., & Choi, H. J. (2018). Effect of magnetic nanoparticle additive on viscoelastic behaviors of carbonyl iron-based magnetorheological suspension. *IEEE Transactions on Magnetics*, 54(11), 1-4.
- Gavili, A., Zabihi, F., Isfahani, T. D., & Sabbaghzadeh, J. (2012). The thermal conductivity of water base ferrofluids under magnetic field. *Experimental Thermal and Fluid Science*, 41(0), 94-98.
- Genc, S., & Derin, B. (2014). Synthesis and rheology of ferrofluids: a review. *Current Opinion in Chemical Engineering*, 3, 118-124.
- Goharkhah, M., Salarian, A., Ashjaee, M., & Shahabadi, M. (2015). Convective heat transfer characteristics of magnetite nanofluid under the influence of constant and alternating magnetic field. *Powder Technology*, 274, 258-267.

- Hajalilou, A., Mazlan, S. A., Lavvafi, H., & Shameli, K. (2016). *Field responsive fluids as smart materials* (1st ed.): Springer Singapore.
- Heine, M. C., de Vicente, J., & Klingenberg, D. J. (2006). Thermal transport in sheared electro- and magnetorheological fluids. *Physics of Fluids*, 18(2), 023301.
- IEEE. (1981). *IEEE guide for soil thermal resistivity measurements*. (IEEE 442-1981). Retrieved from <https://standards.ieee.org/standard/442-1981.html>
- Iglesias, G. R., López-López, M. T., Durán, J. D. G., González-Caballero, F., & Delgado, A. V. (2012). Dynamic characterization of extremely bidisperse magnetorheological fluids. *Journal of Colloid and Interface Science*, 377(1), 153-159.
- ISO. (1991). *Thermal insulation - determination of steady-state thermal resistance and related properties - heat flow meter apparatus*. (ISO 8301:1991). Retrieved from <https://www.iso.org/standard/15421.html>
- Jana, S., Salehi-Khojin, A., & Zhong, W.-H. (2007). Enhancement of fluid thermal conductivity by the addition of single and hybrid nano-additives. *Thermochimica Acta*, 462(1-2), 45-55.
- Jiang, W., Zhang, Y., Xuan, S., Guo, C., & Gong, X. (2011). Dimorphic magnetorheological fluid with improved rheological properties. *Journal of Magnetism and Magnetic Materials*, 323(24), 3246-3250.
- Jiang, Z., & Christenson, R. (2012). A fully dynamic magneto-rheological fluid damper model. *Smart Materials and Structures*, 21(6), 065002.
- Jolly, M. R., Bender, J. W., & Carlson, J. D. (1999). Properties and applications of commercial magnetorheological fluids. *Journal of Intelligent Material Systems and Structures*, 10(1), 5-13.
- Katiyar, A., Dhar, P., Nandi, T., & Das, S. K. (2016). Enhanced heat conduction characteristics of Fe, Ni and Co nanofluids influenced by magnetic field. *Experimental Thermal and Fluid Science*, 78, 345-353.
- Kciuk, M., & Turczyn, R. (2006). Properties and application of magnetorheological fluids. *Journal of Achievements in Materials and Manufacturing Engineering*, 18(1-2), 127-130.
- Khdher, A. M., Sidik, N. A. C., Hamzah, W. A. W., & Mamat, R. (2016). An experimental determination of thermal conductivity and electrical conductivity of bio glycol based Al₂O₃ nanofluids and development of new correlation. *International Communications in Heat and Mass Transfer*, 73, 75-83.
- Kim, S. Y., Kwon, S. H., Liu, Y. D., Lee, J.-S., You, C.-Y., & Choi, H. J. (2014). Core-shell-structured cross-linked poly(glycidyl methacrylate)-coated carbonyl iron microspheres and their magnetorheology. *Journal of Materials Science*, 49(3), 1345-1352. doi:10.1007/s10853-013-7818-3

- Kumar, A., & Subudhi, S. (2018). Preparation, characteristics, convection and applications of magnetic nanofluids: A review. *Heat and Mass Transfer*, 54(2), 241-265.
- Kumbhar, B. K., Patil, S. R., & Sawant, S. M. (2015). Synthesis and characterization of magneto-rheological (MR) fluids for MR brake application. *Engineering Science and Technology, an International Journal*, 18(3), 432-438.
- Lee, J. H., & Choi, H. J. (2018). Synthesis of core-shell formed carbonyl iron/polydiphenylamine particles and their rheological response under applied magnetic fields. *Colloid and Polymer Science*, 296(11), 1857-1865.
- Lee, R., Kim, J. B., Qin, C., Lee, H., Lee, B. J., & Jung, G. Y. (2020). Synthesis of Thermanol-based plasmonic nanofluids with core/shell nanoparticles and characterization of their absorption/scattering coefficients. *Solar Energy Materials and Solar Cells*, 209, 110442.
- Li, F., Li, L., Zhong, G., Zhai, Y., & Li, Z. (2019). Effects of ultrasonic time, size of aggregates and temperature on the stability and viscosity of Cu-ethylene glycol (EG) nanofluids. *International Journal of Heat and Mass Transfer*, 129, 278-286.
- Li, Q., Xuan, Y., & Wang, J. (2005). Experimental investigations on transport properties of magnetic fluids. *Experimental Thermal and Fluid Science*, 30(2), 109-116.
- Li, W., & Du, H. (2003). Design and experimental evaluation of a magnetorheological brake. *The International Journal of Advanced Manufacturing Technology*, 21(7), 508-515.
- Lim, S. T., Cho, M. S., Jang, I. B., & Choi, H. J. (2004). Magnetorheological characterization of carbonyl iron based suspension stabilized by fumed silica. *Journal of Magnetism and Magnetic Materials*, 282, 170-173.
- Lin, Y., Jia, Y., Alva, G., & Fang, G. (2018). Review on thermal conductivity enhancement, thermal properties and applications of phase change materials in thermal energy storage. *Renewable and Sustainable Energy Reviews*, 82, 2730-2742.
- Liu, Y., Fang, F., & Choi, H. (2011). Core-shell-structured silica-coated magnetic carbonyl iron microbead and its magnetorheology with anti-acidic characteristics. *Colloid and Polymer Science*, 289(11), 1295-1298.
- López-López, M. T., de Vicente, J., González-Caballero, F., & Durán, J. D. G. (2005). Stability of magnetizable colloidal suspensions by addition of oleic acid and silica nanoparticles. *Colloids and Surfaces A: Physicochemical and Engineering Aspects*, 264(1-3), 75-81.
- Maroofi, J., & Hashemabadi, S. H. (2019). Experimental and numerical investigation of parameters influencing anisotropic thermal conductivity of magnetorheological fluids. *Heat and Mass Transfer*, 55(10), 2751-2767.

- Maxwell, J. C. (1904). *A Treatise on Electricity and Magnetism* (2nd ed.). Cambridge, UK: Oxford University Press.
- Min, T. H., Choi, H. J., Kim, N.-H., Park, K., & You, C.-Y. (2017). Effects of surface treatment on magnetic carbonyl iron/polyaniline microspheres and their magnetorheological study. *Colloids and Surfaces A: Physicochemical and Engineering Aspects*, 531, 48-55.
- Mishra, A. K., Lahiri, B., & Philip, J. (2018). Thermal conductivity enhancement in organic phase change material (phenol-water system) upon addition of Al₂O₃, SiO₂ and TiO₂ nano-inclusions. *Journal of Molecular Liquids*, 269, 47-63.
- Mistik, S. I., Shah, T., Hadimani, R. L., & Siores, E. (2012). Compression and thermal conductivity characteristics of magnetorheological fluid-spacer fabric smart structures. *Journal of Intelligent Material Systems and Structures*, 23(11), 1277.
- Mrlík, M., Ilčíková, M., Pavlínek, V., Mosnáček, J., Peer, P., & Filip, P. (2013). Improved thermooxidation and sedimentation stability of covalently-coated carbonyl iron particles with cholesteryl groups and their influence on magnetorheology. *Journal of Colloid and Interface Science*, 396, 146-151.
- Nabil, M. F., Hamzah, W. A. W., Hamid, K. A., Mamat, R., & Hagos, F. Y. (2017). An experimental study on the thermal conductivity and dynamic viscosity of TiO₂-SiO₂ nanofluids in water: Ethylene glycol mixture. *International Communications in Heat and Mass Transfer*, 86, 181-189.
- Ngatu, G. T., & Wereley, N. M. (2007). Viscometric and sedimentation characterization of bidisperse magnetorheological fluids. *IEEE Transactions on Magnetics*, 43(6), 2474-2476.
- Niu, F.-H., Hu, Z.-D., Yan, H., Yang, J.-J., & Zhang, H.-S. (2018). Rheological response of magnetorheological suspensions sediments and its implications for redispersibility. *Journal of Magnetism and Magnetic Materials*, 465, 421-429.
- Nollet, L. M., & Toldrá, F. (2015). *Handbook of Food Analysis-Two Volume Set*: CRC Press.
- Olabi, A. G., & Grunwald, A. (2007). Design and application of magneto-rheological fluid. *Materials & Design*, 28(10), 2658-2664.
- Park, B., Fang, F., Zhang, K., & Choi, H. (2010). Polymer-coated magnetic carbonyl iron microparticles and their magnetorheological characteristics. *Korean Journal of Chemical Engineering*, 27(2), 716-722.
- Park, I. H., & Choi, H. J. (2018). Fabrication of p-aminobenzoic acid grafted carbonyl iron/polyindole composite particles and their magnetorheological response. *Journal of Industrial and Engineering Chemistry*, 64, 102-106.
- Patel, H., Sundararajan, T., & Das, S. (2010). An experimental investigation into the thermal conductivity enhancement in oxide and metallic nanofluids. *Journal of Nanoparticle Research*, 12(3), 1015-1031.

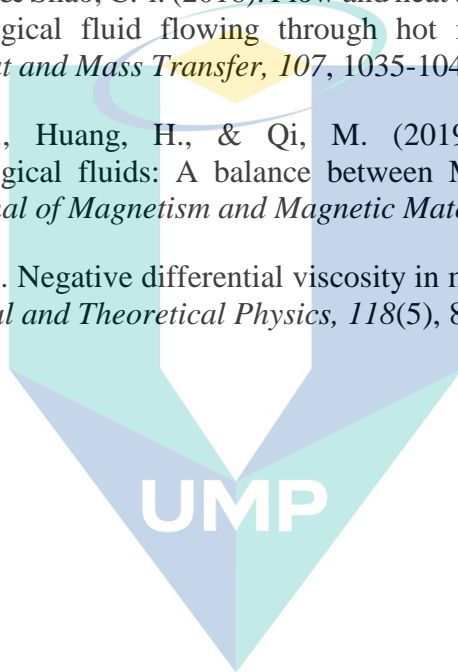
- Patil, S. R., Powar, K. P., & Sawant, S. M. (2016). Thermal analysis of magnetorheological brake for automotive application. *Applied Thermal Engineering*, 98, 238-245.
- Paul, G., Chopkar, M., Manna, I., & Das, P. K. (2010). Techniques for measuring the thermal conductivity of nanofluids: A review. *Renewable and Sustainable Energy Reviews*, 14(7), 1913-1924.
- Paval, K. L., & Patil, S. R. (2015). Synthesis and characterization of high yield stress smart fluids with no sedimentation—A review. *Journal of Material Science and Mechanical Engineering*, 2(3), 254-259.
- Phulé, P. P. (2001). Magnetorheological (MR) fluids: principles and applications. *Smart Materials Bulletin*, 2001(2), 7-10.
- Piao, S. H., Chae, H. S., & Choi, H. J. (2015). Carbonyl iron suspension with core-shell structured Fe₃O₄@SiO₂ nanoparticle additives and its magnetorheological property. *IEEE Transactions on Magnetics*, 51(11), 1-4.
- Plachy, T., Kutalkova, E., Sedlacik, M., Vesel, A., Masar, M., & Kuritka, I. (2018). Impact of corrosion process of carbonyl iron particles on magnetorheological behavior of their suspensions. *Journal of Industrial and Engineering Chemistry*, 66, 362-369.
- Portillo, M. A., & Iglesias, G. (2017). Magnetic nanoparticles as a redispersing additive in magnetorheological fluid. *Journal of Nanomaterials*, 2017.
- Prekas, K., Shah, T., Soin, N., Rangoussi, M., Vassiliadis, S., & Siores, E. (2013). Sedimentation behaviour in electrorheological fluids based on suspensions of zeolite particles in silicone oil. *Journal of Colloid and Interface Science*, 401, 58-64.
- Price, D. M., & Jarratt, M. (2002). Thermal conductivity of PTFE and PTFE composites. *Thermochimica Acta*, 392, 231-236.
- Ram, P., & Bhandari, A. (2013). Negative viscosity effects on ferrofluid flow due to a rotating disk. *International Journal of Applied Electromagnetics and Mechanics*, 41(4), 467-478.
- Reinecke, B. N., Shan, J. W., Suabedissen, K. K., & Cherkasova, A. S. (2008). On the anisotropic thermal conductivity of magnetorheological suspensions. *Journal of Applied Physics*, 104(2), 1-7.
- Rodríguez-Arco, L., López-López, M. T., Kuzhir, P., & Durán, J. D. (2013). Steady state rheological behaviour of multi-component magnetic suspensions. *Soft Matter*, 9(24), 5726-5737.
- Sarkar, C., & Hirani, H. (2015). Synthesis and characterisation of nano silver particle-based magnetorheological fluids for brakes. *Defence Science Journal*, 65(3), 252-258.

- Sattler, K. D. (2010). *Handbook of Nanophysics: Nanoparticles and Quantum Dots*: Taylor and Francis.
- Shah, K., Choi, S.-B., & Choi, H. J. (2015). Thermorheological properties of nano-magnetorheological fluid in dynamic mode: experimental investigation. *Smart Materials and Structures*, 24(5), 057001.
- Shahsavari, A., Saghafian, M., Salimpour, M. R., & Shafii, M. B. (2015). Effect of temperature and concentration on thermal conductivity and viscosity of ferrofluid loaded with carbon nanotubes. *Heat and Mass Transfer*, 1-9.
- Shahsavari, A., Salimpour, M. R., Saghafian, M., & Shafii, M. (2016). Effect of magnetic field on thermal conductivity and viscosity of a magnetic nanofluid loaded with carbon nanotubes. *Journal of Mechanical Science and Technology*, 30(2), 809-815.
- Sharif, M. Z., Hamzah, W. A. W., Redhwan, A. A. M., & Mamat, R. (2016). Investigation of thermal conductivity and viscosity of Al₂O₃/PAG nanolubricant for application in automotive air conditioning system. *International Journal of Refrigeration*, 70, 93-102.
- Sherman, S. G., Becnel, A. C., & Wereley, N. M. (2015). Relating Mason number to Bingham number in magnetorheological fluids. *Journal of Magnetism and Magnetic Materials*, 380, 98-104.
- Siginer, D. A., De Kee, D., & Chhabra, R. P. (1999). *Advances in the flow and rheology of non-Newtonian fluids* (Vol. 8): Elsevier.
- Simpson, M., & Janna, W. (2008). *Newtonian and non-newtonian fluids: Velocity profiles, viscosity data, and laminar flow friction factor equations for flow in a circular duct*. Paper presented at the ASME International Mechanical Engineering Congress and Exposition.
- Spaggiari, A. (2012). Properties and applications of magnetorheological fluids. *Fracture and Structural Integrity*, 7(23), 48-61.
- Steinhaus, T. (1999). *Evaluation of the thermophysical properties of poly (methylmethacrylate): A reference material for the development of a flammability test for micro-gravity environments*.
- Sung, H. W. F., & Rudowicz, C. (2003). Physics behind the magnetic hysteresis loop—a survey of misconceptions in magnetism literature. *Journal of Magnetism and Magnetic Materials*, 260(1), 250-260.
- Susan-Resiga, D., & Vékás, L. (2014). Yield stress and flow behavior of concentrated ferrofluid-based magnetorheological fluids: the influence of composition. *Rheologica Acta*, 53(8), 645-653.
- Tao, R. (2001). Super-strong magnetorheological fluids. *Journal of Physics: Condensed Matter*, 13(50), R979.

- Teng, T.-P., Hung, Y.-H., Teng, T.-C., Mo, H.-E., & Hsu, H.-G. (2010). The effect of alumina/water nanofluid particle size on thermal conductivity. *Applied Thermal Engineering*, 30(14), 2213-2218.
- Thakur, M. K., & Sarkar, C. (2020). Influence of graphite flakes on the strength of magnetorheological fluids at high temperature and its rheology. *IEEE Transactions on Magnetics*, 1-1.
- Triefenbach, F. (2008). *Design of experiments: the D-optimal approach and its implementation as a computer algorithm*. (Bachelor's Thesis in Information and Communication Technology), South Westphalia University of Applied Sciences, Meschede.
- Tritt, T. M. (2005). *Thermal conductivity: theory, properties, and applications*: Springer Science & Business Media.
- Varley, J. (2003). HEAT TRANSFER METHODS. In B. Caballero (Ed.), *Encyclopedia of Food Sciences and Nutrition (Second Edition)* (pp. 3029-3034). Oxford: Academic Press.
- Wang, D., Hou, Y., & Tian, Z. (2013). A novel high-torque magnetorheological brake with a water cooling method for heat dissipation. *Smart Materials and Structures*, 22(2), 025019.
- Wang, D., Hou, Y., Tian, Z., Meng, Q., & Taylor, J. (2015). Temperature rise characteristic of MR fluid in a multi-disc MR clutch under slip condition. *Industrial Lubrication and Tribology*, 67(2), 85-92.
- Wang, D., Zi, B., Zeng, Y., Hou, Y., & Meng, Q. (2014). Temperature-dependent material properties of the components of magnetorheological fluids. *Journal of Materials Science*, 49(24), 8459-8470.
- Wang, D., Zi, B., Zeng, Y., Xie, F., & Hou, Y. (2015). An investigation of thermal characteristics of a liquid-cooled magnetorheological fluid-based clutch. *Smart Materials and Structures*, 24(5), 055020.
- Wang, G., Ma, Y., Li, M., Cui, G., Che, H., Mu, J., . . . Dong, X. (2017). Magnesium ferrite nanocrystal clusters for magnetorheological fluid with enhanced sedimentation stability. *Solid State Sciences*, 63, 70-75.
- Wang, G., Zhao, D., Ma, Y., Zhang, Z., Che, H., Mu, J., . . . Dong, X. (2017). Synthesis of calcium ferrite nanocrystal clusters for magnetorheological fluid with enhanced sedimentation stability. *Powder Technology*, 322, 47-53.
- Wang, G., Zhou, F., Lu, Z., Ma, Y., Li, X., Tong, Y., & Dong, X. (2019). Controlled synthesis of CoFe₂O₄/MoS₂ nanocomposites with excellent sedimentation stability for magnetorheological fluid. *Journal of Industrial and Engineering Chemistry*, 70, 439-446.

- Wang, L., Wang, Y., Yan, X., Wang, X., & Feng, B. (2016). Investigation on viscosity of Fe₃O₄ nanofluid under magnetic field. *International Communications in Heat and Mass Transfer*, 72, 23-28.
- Wang, N., Liu, X., Sun, S., Królczyk, G., Li, Z., & Li, W. (2020). Microscopic characteristics of magnetorheological fluids subjected to magnetic fields. *Journal of Magnetism and Magnetic Materials*, 501, 166443.
- Weiss, K. D., & Duclos, T. G. (1994). Controllable fluids: the temperature dependence of post-yield properties. *International Journal of Modern Physics B*, 8, 3015-3032.
- Wereley, N., Chaudhuri, A., Yoo, J.-H., John, S., Kotha, S., Suggs, A., . . . Sudarshan, T. (2006). Bidisperse magnetorheological fluids using Fe particles at nanometer and micron scale. *Journal of Intelligent Material Systems and Structures*, 17(5), 393-401.
- Xiao, D., Lu, T., Zeng, R., & Bi, Y. (2016). Preparation and highlighted applications of magnetic microparticles and nanoparticles: a review on recent advances. *Microchimica Acta*, 1-21.
- Xie, H., Wang, J., Xi, T., Liu, Y., Ai, F., & Wu, Q. (2002). Thermal conductivity enhancement of suspensions containing nanosized alumina particles. *Journal of Applied Physics*, 91(7), 4568-4572.
- Xu, Y., Gong, X., Xuan, S., Zhang, W., & Fan, Y. (2011). A high-performance magnetorheological material: preparation, characterization and magnetic-mechanic coupling properties. *Soft Matter*, 7(11), 5246-5254.
- Xu, Z.-D., & Chen, B.-B. (2016). Experimental and numerical study on magnetorheological fluids based on mixing coated magnetic particles. *Journal of Materials in Civil Engineering*, 28(5), 04015198.
- Yang, J., Yan, H., Hu, Z., & Ding, D. (2016). Viscosity and sedimentation behaviors of the magnetorheological suspensions with oleic acid/dimer acid as surfactants. *Journal of Magnetism and Magnetic Materials*, 417, 214-221.
- Yaojung, S., Quang-Anh, N., & Zhengyang, Z. (2015). Design and experiment of a new magnetorheological brake. *International Journal of Applied Electromagnetics & Mechanics*, 48(4), 309-326.
- Yildirim, G., & Genc, S. (2013). Experimental study on heat transfer of the magnetorheological fluids. *Smart Materials and Structures*, 22(8), 1-8.
- You, H., Chen, Y., Liu, P., & Jia, X. (2014). Combined D-optimal design and generalized regression neural network for modeling of plasma etching rate. *International Journal of Metrology and Quality Engineering*, 5(1).
- Yu, G., Du, C., & Sun, T. (2015). Thermodynamic behaviors of a kind of self-decoupling magnetorheological damper. *Shock and Vibration*, 501, 502747.

- Yüksel, N. (2016). The review of some commonly used methods and techniques to measure the thermal conductivity of insulation materials *Insulation Materials in Context of Sustainability*: InTech.
- Zhang, Y., Li, D., Cui, H., & Yang, J. (2020). A new modified model for the rheological properties of magnetorheological fluids based on different magnetic field. *Journal of Magnetism and Magnetic Materials*, 500, 166377.
- Zhao, D., Qian, X., Gu, X., Jajja, S. A., & Yang, R. (2016). Measurement techniques for thermal conductivity and interfacial thermal conductance of bulk and thin film materials. *Journal of Electronic Packaging*, 138(4), 040802.
- Zhou, J.-f., Zhang, H., & Shao, C.-l. (2016). Flow and heat transfer performances of dilute magnetorheological fluid flowing through hot micro channel. *International Journal of Heat and Mass Transfer*, 107, 1035-1043.
- Zhu, W., Dong, X., Huang, H., & Qi, M. (2019). Iron nanoparticles-based magnetorheological fluids: A balance between MR effect and sedimentation stability. *Journal of Magnetism and Magnetic Materials*, 491, 165556.
- Zubarev, A. Y. (2014). Negative differential viscosity in magnetic suspensions. *Journal of Experimental and Theoretical Physics*, 118(5), 814-821.



اونيورسيتي ملايسيا قهغ

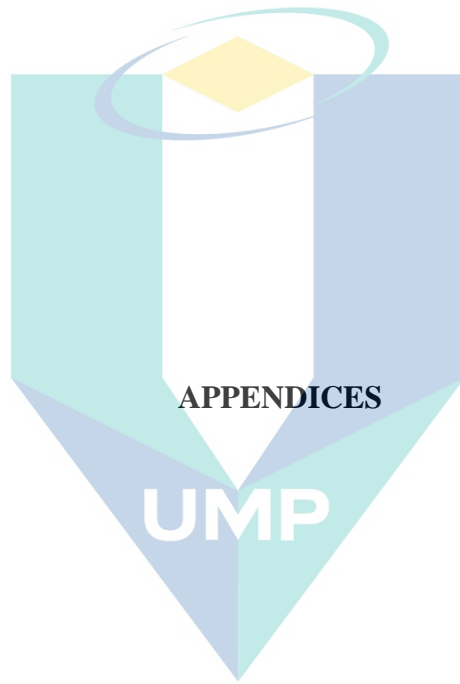
UNIVERSITI MALAYSIA PAHANG

LIST OF PUBLICATIONS

- Rahim, M. S. A., Ismail, I., & Aqida, S. N. (2017). Effects of nano copper additive on thermal conductivity of magnetorheological fluid at different environment temperature. *Materials Science Forum*, 890, 108-111.
- Rahim, M. S. A., Ismail, I., Choi, S. B., Hamzah, W. A. W., & Aqida, S. N. (2017). Thermal conductivity enhancement and sedimentation reduction of magnetorheological fluids with nano-sized Cu and Al additives. *Smart Materials and Structures*, 26(11), 115009.
- Rahim, M. S. A., Ismail, I., Wahid, S. A., Aid, S., & Aqida, S. N. (2017). Magnetic field simulation of a thermal conductivity measurement instrument for magnetorheological fluid. *MATEC Web of Conferences*, 90, 01061.
- Rahim, M. S. A., & Ismail, I. (2015). Review of magnetorheological fluids and nanofluids thermal behaviour. *IOP Conference Series: Materials Science and Engineering*, 100(1), 012040.
- Wahid, S. A., Ismail, I., Aid, S., & Rahim, M. S. A. (2016). Magneto-rheological defects and failures: A review. *IOP Conference Series: Materials Science and Engineering*, 114(1), 012101.

اونيورسيتي ملايسيا قهغ

UNIVERSITI MALAYSIA PAHANG



اونيورسيتي ملايسيا قهغ

UNIVERSITI MALAYSIA PAHANG

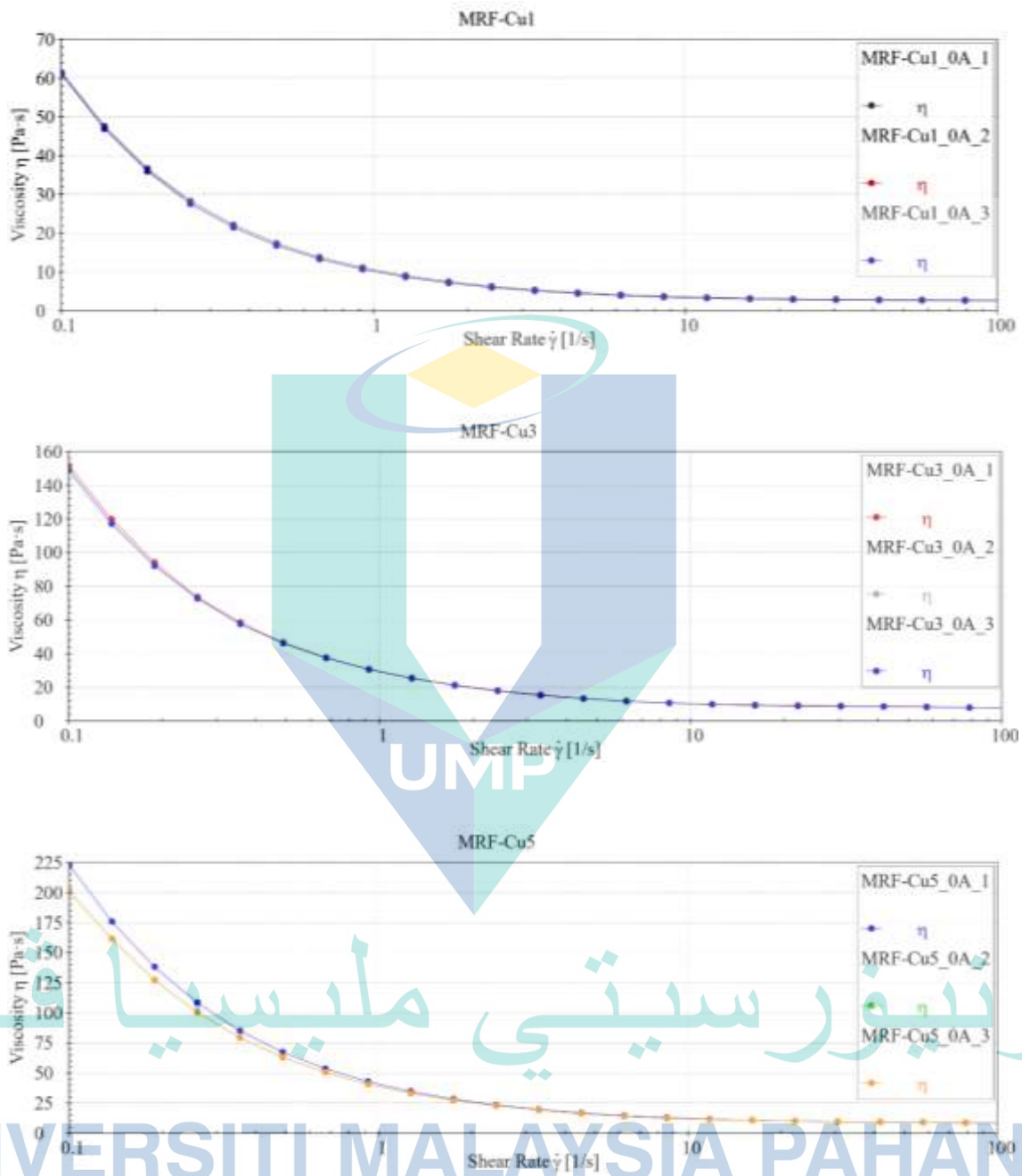
Appendix A: Thermal conductivity of MR fluid samples by thermal properties analyzer instrument

| No. | Description | HO (vol%) | Particle concentration (vol%) | | | | k (W/m·K) | Ave. k (W/m·K) |
|-----|-------------|-----------|-------------------------------|------|------|------------------|-------------------------|------------------|
| | | | CIP | Cu | Al | SiO ₂ | | |
| 1 | MRF | 75.0 | 20 | 0 | 0 | 5 | 0.367 0.366 0.369 | 0.367 |
| 2 | MRF | 60.0 | 40 | 0 | 0 | 0 | 0.618 0.619 0.622 | 0.620 |
| 3 | MRF-Cu2.5 | 65.0 | 30 | 2.50 | 0 | 2.50 | 0.525 0.513 0.513 | 0.517 |
| 4 | MRF-Cu3.75 | 57.5 | 35 | 3.75 | 0 | 3.75 | 0.672 0.680 0.671 | 0.674 |
| 5 | MRF-Cu5 | 75.0 | 20 | 5.00 | 0 | 0 | 0.407 0.412 0.411 | 0.410 |
| 6 | MRF-Cu5 | 50.0 | 40 | 5.00 | 0 | 5.00 | 0.904 0.902 0.901 | 0.902 |
| 7 | MRF-Al2.5 | 65.0 | 30 | 0 | 2.50 | 2.50 | 0.534 0.529 0.526 | 0.530 |
| 8 | MRF-Al3.75 | 57.5 | 35 | 0 | 3.75 | 3.75 | 0.566 0.596 0.624 | 0.595 |
| 9 | MRF-Al5 | 75.0 | 20 | 0 | 5.00 | 0 | 0.295 0.307 0.312 | 0.305 |
| 10 | MRF-Al5 | 50.0 | 40 | 0 | 5.00 | 5.00 | 0.682 0.692 0.713 | 0.696 |
| 11 | MRF-132DG | - | 32 | - | - | - | 0.354 0.359 0.357 | 0.357 |

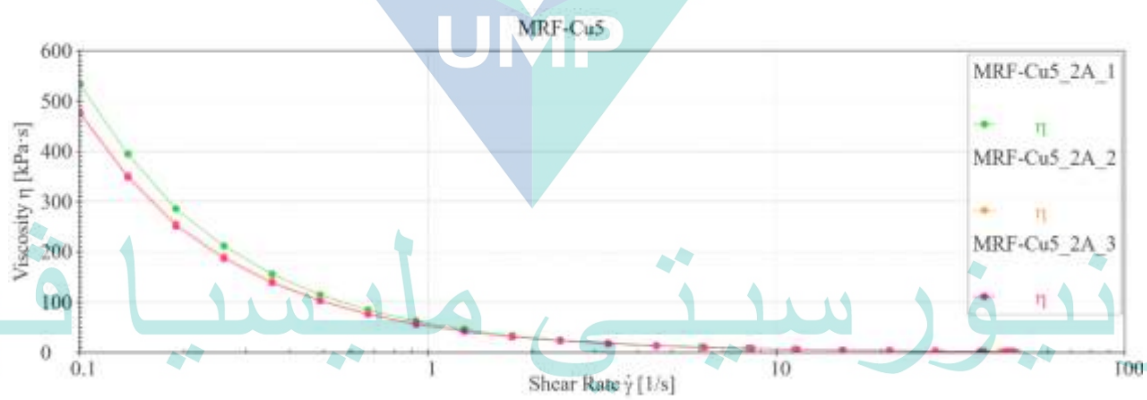
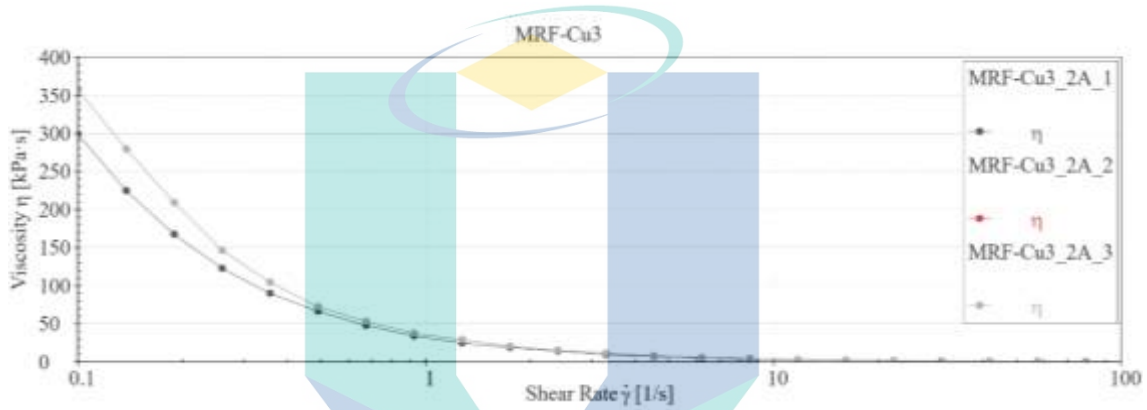
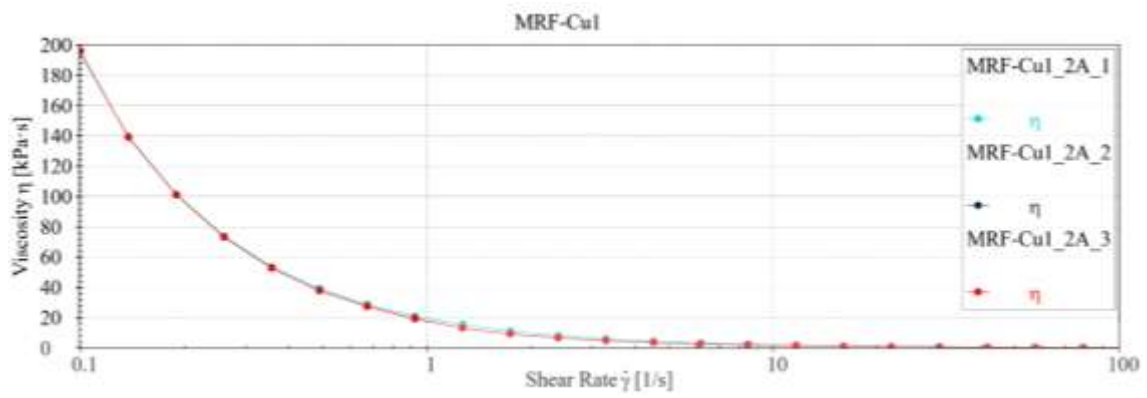
اونيفرسيتي ملايسيا فاهغ

UNIVERSITI MALAYSIA PAHANG

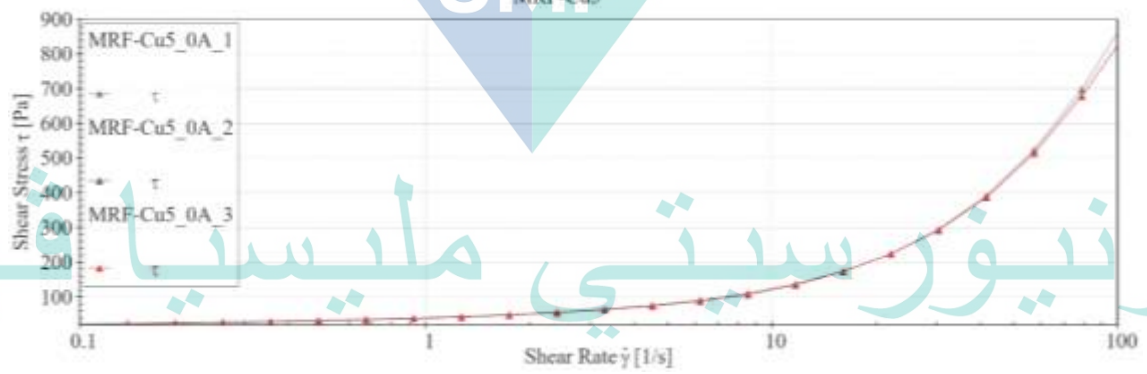
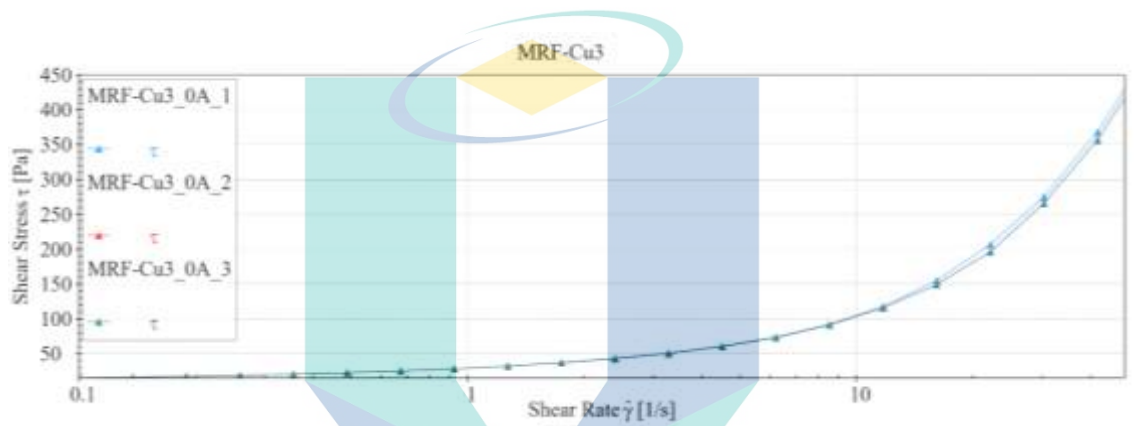
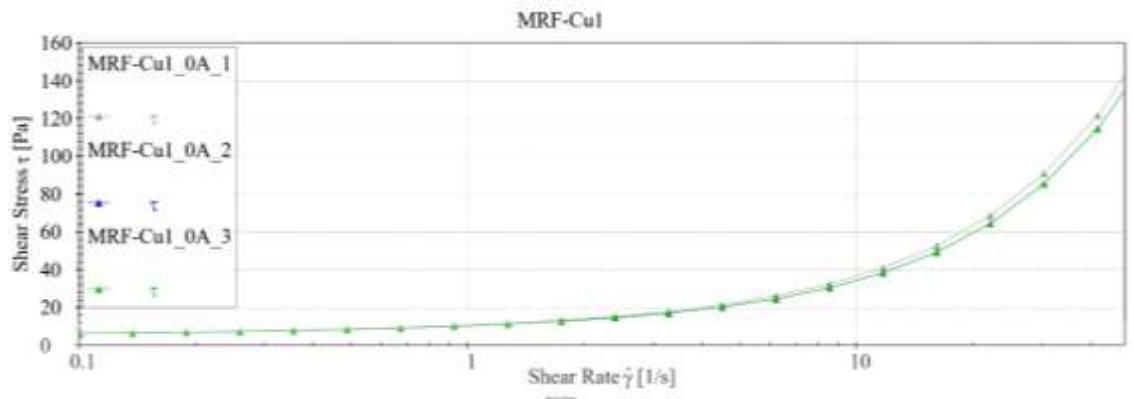
Appendix B: Viscosity and shear stress against shear rate of MRF-Cu samples



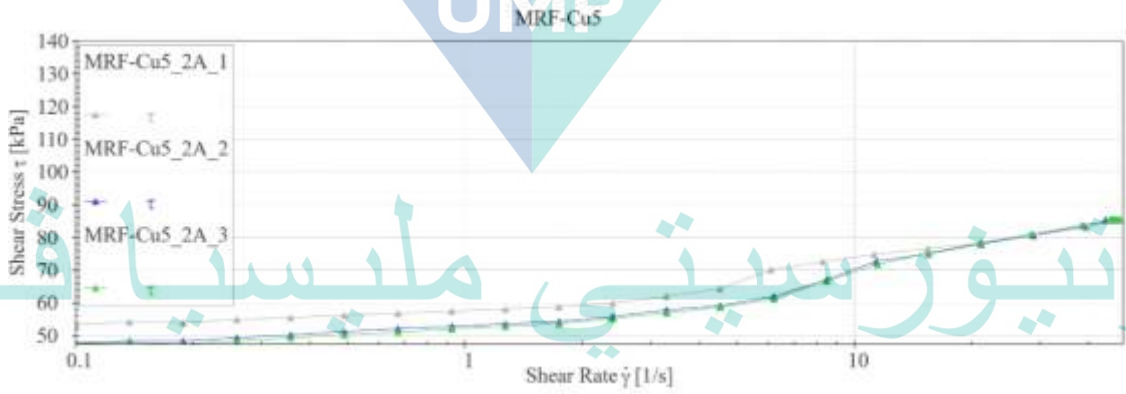
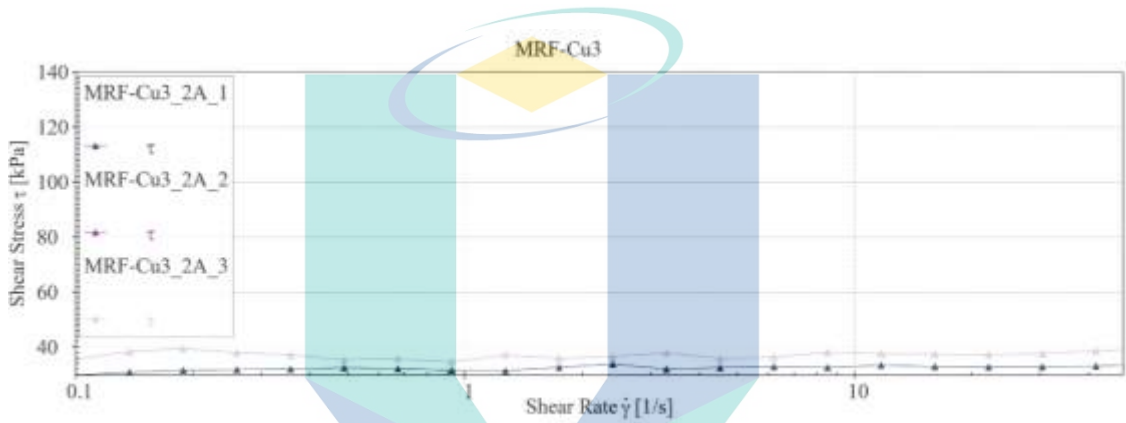
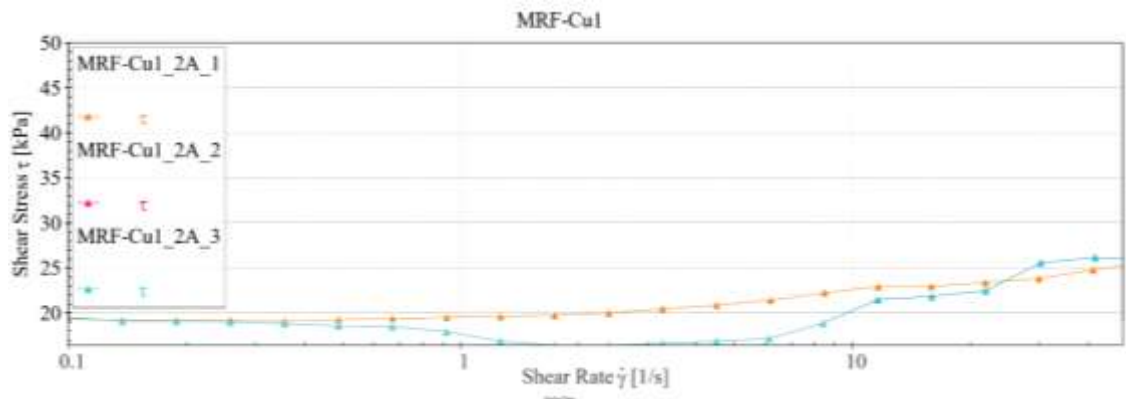
Appendix B1 Shear viscosity of MRF-Cu samples in the absence of magnetic field



Appendix B2 Shear viscosity of MRF-Cu samples in the presence of magnetic field



Appendix B3 Shear stress of MRF-Cu samples in the absence of magnetic field

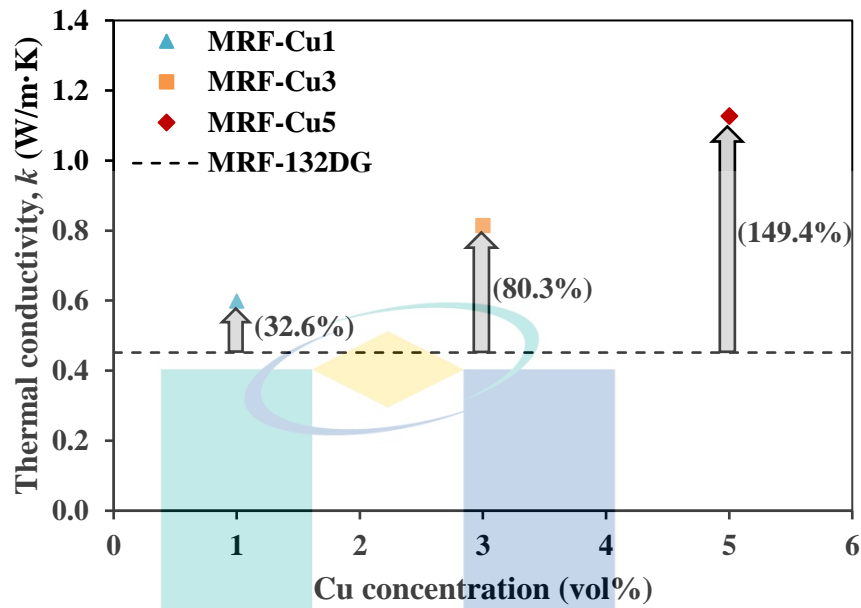


اوبیورسیٹی ملیسیا مالیزیا

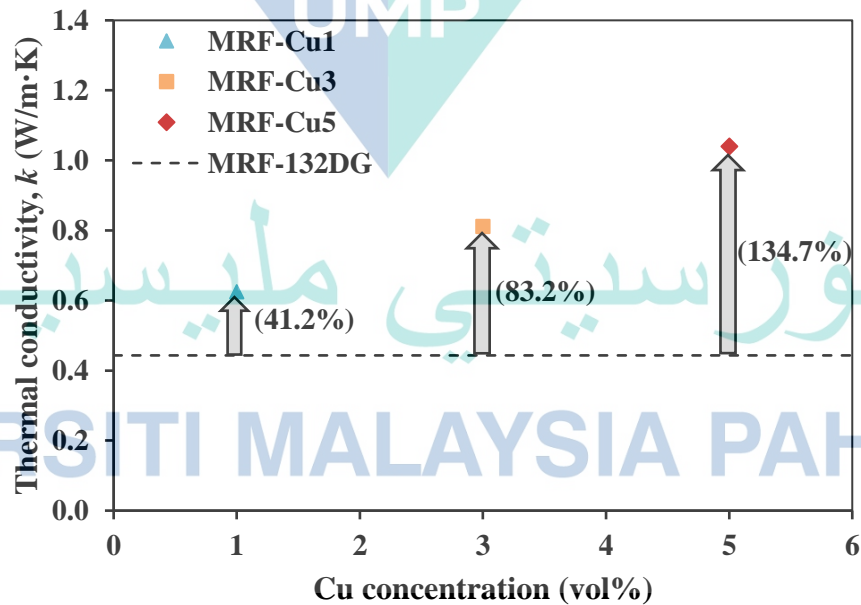
UNIVERSITI MALAYSIA PAHANG

Appendix B4 Shear stress of MRF-Cu samples in the presence of magnetic field

Appendix C: Thermal conductivity of MRF-Cu samples against MRF-132DG in the presence of magnetic field at higher temperatures



Appendix C1 Thermal conductivity enhancement (in %) of MRF-Cu samples against MRF-132DG in the presence of magnetic field at 50 °C



Appendix C2 Thermal conductivity enhancement (in %) of MRF-Cu samples against MRF-132DG in the presence of magnetic field at 70 °C